AD NUMBER

AD876337

NEW LIMITATION CHANGE

TO

Approved for public release, distribution unlimited

FROM

Distribution authorized to U.S. Gov't. agencies and their contractors; Critical Technology; 26 JUN 1970. Other requests shall be referred to Naval Electronics Laboratory Center, San Diego, CA 92152.

AUTHORITY

USNELC ltr, 22 AUg 1974

NELC / TR 1718

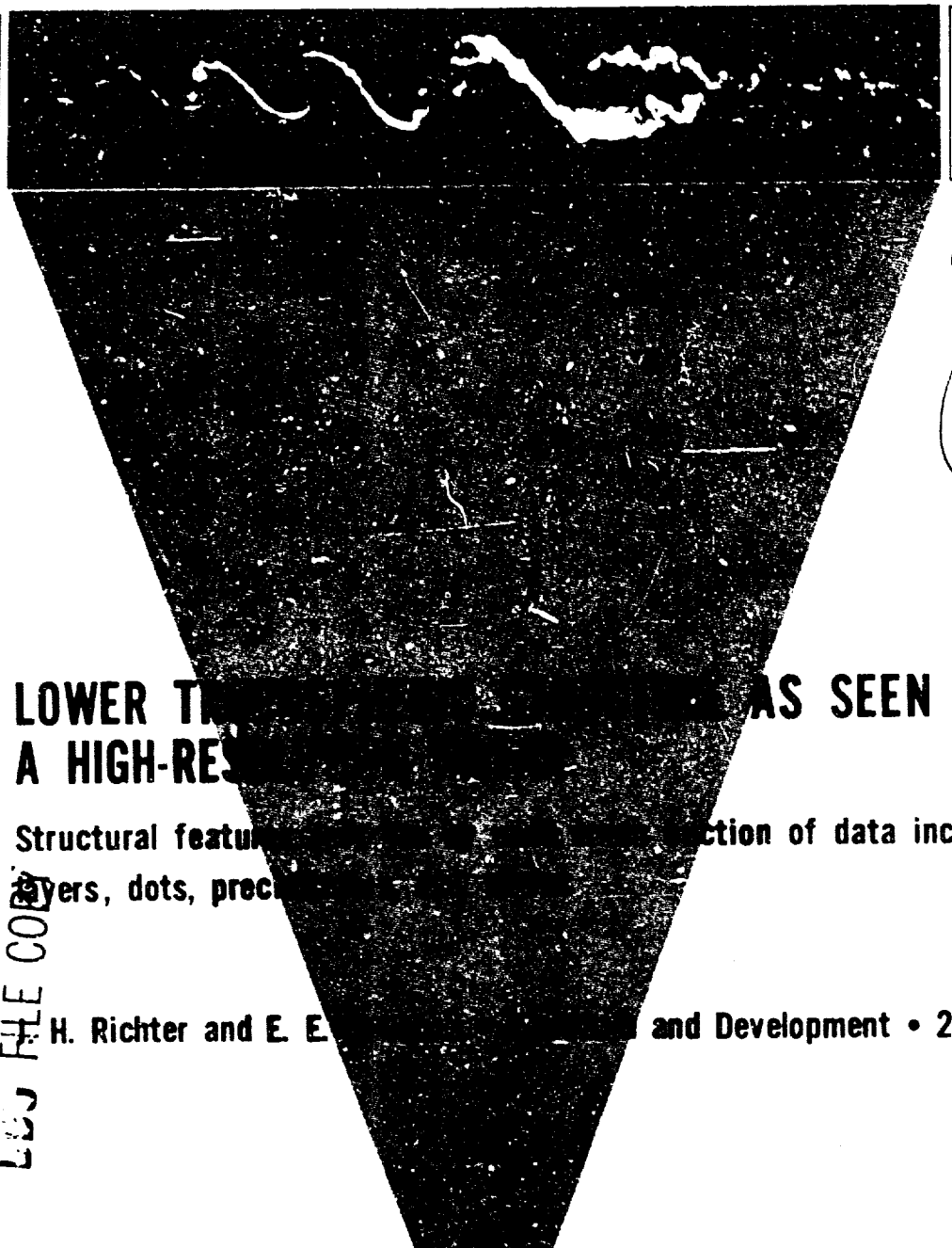

LOWER T... AS SEEN BY A HIGH-RE...

Structural featu... ction of data include layers, dots, prec...

H. Richter and E. E... and Development • 26 June 1970

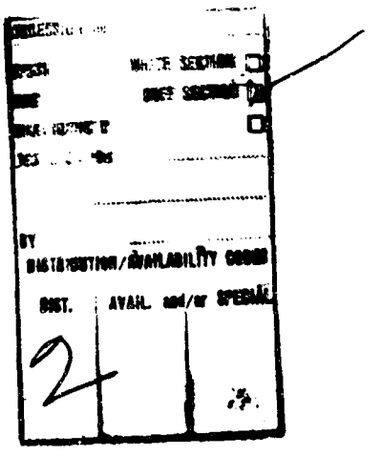

PROBLEM

Provide a sounding system by means of a vertically directed radar and obtain continuous information concerning time and space behavior of tropospheric discontinuities in the height from about 100 to 3000 meters.

RESULTS

1. A high-sensitivity FM/cw radar has been built for the study of the refractive index structure in the troposphere. Design considerations and performance characteristics are given.

2. Recordings obtained with the sounder are presented and discussed; simultaneous radar and radiosonde sounding is described.

3. Specific tropospheric structural features including layers, dots, precipitation, and waves are discussed.

RECOMMENDATIONS

1. Study the mechanism responsible for the reflection of electromagnetic energy; employ direct measurement of refractive index fluctuation.

2. Continue the study of atmospheric mesoscale structure, emphasizing wave phenomena.

3. Improve and extend sounder hardware and technology; for example, consider the use of magnetic-tape recording and digital processing for the analysis of data from a wider height range.

4. Study the feasibility of a second-generation FM/cw radar sounder for mobile use with a single antenna.

ADMINISTRATIVE INFORMATION

Work was performed under XR 008 01 01, Task 7031 (NELC M103), by the Propagation Technology Division. The report covers work performed from January through December 1969 and was approved for publication 26 June 1970.

The assistance of D. W. Truax, W. K. Horner, and L. D. Duncan, of the same division, with radar, meteorological observation, and analysis of results is acknowledged. Professor D. Atlas, of the University of Chicago, provided stimulating discussions and suggestions.

CONTENTS

APPROACH

RADAR

For the study of the fine-scale refractive index structure in the troposphere we need a radar sounder that combines the properties of high range resolution, high sensitivity, and close minimum range without clutter. The requirement of high-range-resolution capability would suggest the use of pulse compression techniques. However, this approach would make it difficult to meet the additional requirement of close minimum range. This is due to the fact that during the transmission of the uncompressed pulse (and usually several pulsewidths after) no signal can be received. The reason that the minimum range is such an important factor for the sounder is that low-level inversions frequently produce scatter layers in the lowest 300 meters of the atmosphere, and it is these which can be studied most effectively by simultaneous meteorological observations by tower and tethered-balloon instruments.

FM/cw RADAR

A radar that does not have the minimum-range restriction and that allows high range resolution is an FM/cw radar. It has the additional advantage of a peak-power-to-average-power ratio of unity, which is very desirable from a technological viewpoint. It also permits a change of resolution without affecting the transmitted energy (which is not the case for pulse radars).

The principle of its operation is given briefly in figure 1. The top portion shows a linear ramp (solid line) which is transmitted during T_M (modulation time) and a reflected ramp (dashed line) which is delayed by Δt according to the distance of the reflecting object. The two ramps are mixed instantaneously to yield a difference or beat frequency f_b. The middle portion of figure 1 shows this beat frequency and the lower part its frequency spectrum. In the case of multiple targets, reflected waves will arrive at different time intervals and cause different beat frequencies to be superimposed. A spectrum analysis of the beat frequencies allows the different targets to be resolved according to range. The amplitudes of the different beat frequencies are a measure of the reflection coefficients of the targets. For this kind of radar, range resolution means the ability to separate adjacent spectral lines of the kind shown in the lower portion of figure 1. The minimum resolvable distance h is given by

$$h = c/kF \qquad (1)$$

where F is frequency excursion, c is velocity of propagation, and k is a constant whose value depends on the criterion used to define 'separation' of two spectral lines. (E.g., $k = 1$ for $\Delta f = 2/T_M$ and $k = 2$ for $\Delta f = 1/T_M$, where Δf is the frequency separation between two spectra.) Equation (1) is essentially the same formula as that used for pulse radars and shows that resolution is only dependent on the frequency excursion or bandwidth of the transmitted signal.

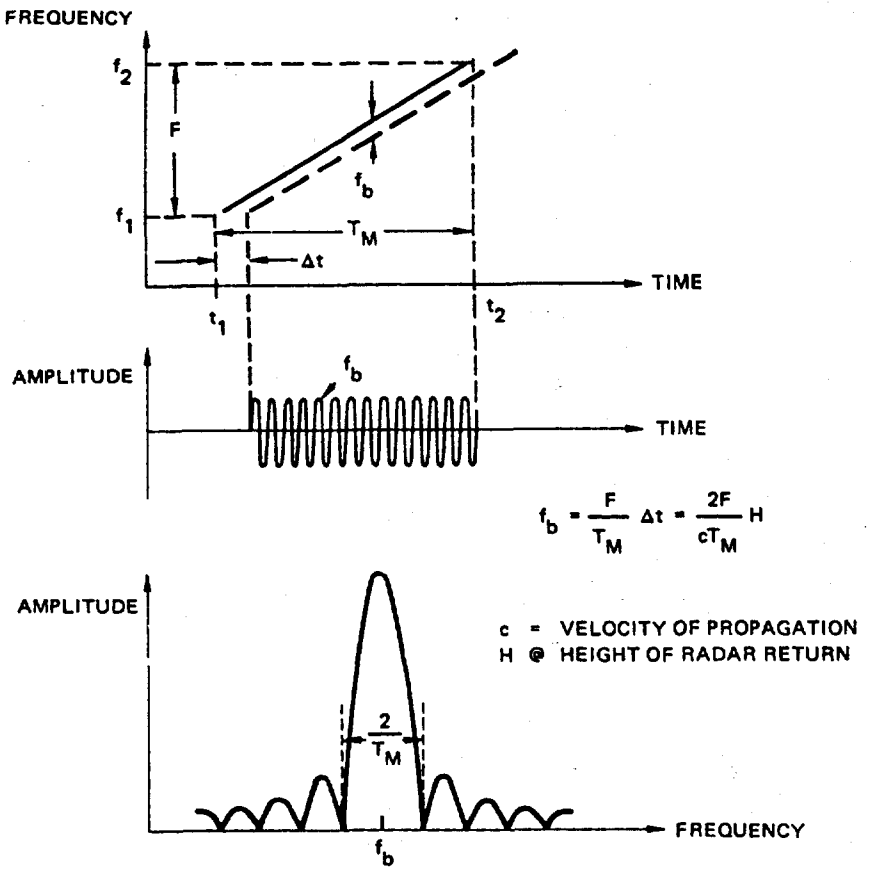

Figure 1. Principle of FM/cw radar using linear frequency modulation. The sinusoidal beat frequency f_b is generated by instantaneous mixing of the transmitted and the received ramp.

RADAR DESIGN

The frequency of the radar was chosen to be around 3 GHz as a compromise between higher and lower frequencies each of which would have been desirable for different reasons. Thus, to achieve a narrow antenna beam with a small antenna diameter, it would have been better to select a higher frequency. However, we must also consider the reflectivity-wavelength dependence of the scattering volume. For specular surfaces, the power reflection coefficient increases as the thickness in wavelengths of the transition zone decreases, and we should thus want to use the largest possible wavelength. On the other hand, the preponderance of the evidence available suggests that clear-air-scatter layers are comprised of inhomogeneities in refractivity, producing a reflectivity (η)-wavelength dependence of about $\lambda^{-1/3}$ [Atlas and Hardy, 1966; Hardy et al., 1966; Hardy and Katz, 1969].[2-4] Although this wavelength dependence is small, it suggests using the shortest wavelength, provided that it does not approach the limiting microscale (ℓ_m) of the refractivity perturbations. Atlas and Hardy [1966]

therefore suggest an optimum wavelength of about five times the limiting microscale. In weakly turbulent conditions, ℓ_m is of the order of 1 to 2 cm, and so a λ of 5 to 10 cm seemed optimum.

By means of theoretical calculations and experimental data (Saxton et al., 1964)[5], we decided that with an equivalent pulse length, h = 1 meter, and antenna gain of 35 decibels, a ratio of 190 decibels between average transmitted and received power should be adequate to detect most scatter layers in the lowest 2 km. The actual sensitivity is discussed below.

With the above radar parameters determined, our search was then directed toward a suitable FM generator. It is possible to achieve 3-meter resolution at 100-MHz frequency excursion with a commercial microwave sweep generator that uses a backward-wave oscillator. The difficulty with this kind of FM generator is that, even after compensating for the nonlinear modulation characteristic, fine-grain variations exist that are due to imperfections of the helix. We then had to find a suitable part of the frequency range of an individual tube. During the course of these investigations a new device became available that consists of a transistor oscillator that is tuned in frequency by changing the magnetic field of an yttrium iron garnet sphere. The tuning linearity of this device is much higher than that previously attainable, and it also does not exhibit the fine-grain variations of backward-wave oscillators. The Watkins-Johnson YIG-tuned transistor oscillator that we used in the radar sounder has deviation of less than 0.001 percent from straight-line tuning over a frequency range of 200 MHz (2.9 GHz center frequency). Power output is 12 mW and tuning sensitivity 3.6 MHz/mA. The high tuning sensitivity necessitates a very linear, low-noise, low-ripple sweeping current supply.

The spectrum analysis of the beat frequencies has to be performed in real time, and this is done with a Ubiquitous spectrum analyzer from Federal Scientific Corporation. The analyzer 'time compresses' the signal and performs a scanning analysis on the speeded-up and stored signal. The 10-kHz analysis band has a 20-Hz bandwidth and can be positioned anywhere from 0 to 1 MHz. It takes 50 msec to fill the memory, and this time determines the modulation time T_M. During T_M the memory is updated, and the analysis starts at the end of T_M, when the memory is put into 'hold.' The input signal is time-compressed by a factor of 500, which enables the scanning spectrum analysis to be completed in 50 msec. After this time, a new modulation cycle starts. In other words, the entire cycle of frequency sweeping, signal storage, and frequency-spectrum analysis is repeated 10 times per second. The output of the spectrum analyzer is multiplied by a sine-squared weighting function which suppresses the sidelobes of the $|(\sin x)/x|$ spectrum shown in figure 1. The resulting spectrum is somewhat broadened, and the resolution bandwidth is about 30 Hz.

The mixer used for the radar sounder is a balanced mixer using backward diodes with a matched low-noise preamplifier. The noise figure of this combination is 13 decibels at 10 kHz. The incoming rf signal passes through a low-noise traveling-wave-tube amplifier with a noise figure of 4.8 decibels and 30-decibel gain. The overall noise figure of the entire receiver is, therefore, only about 5 decibels. A simplified block diagram of the sounder is shown in figure 2, and the hardware involved is shown in figure 3. The linear

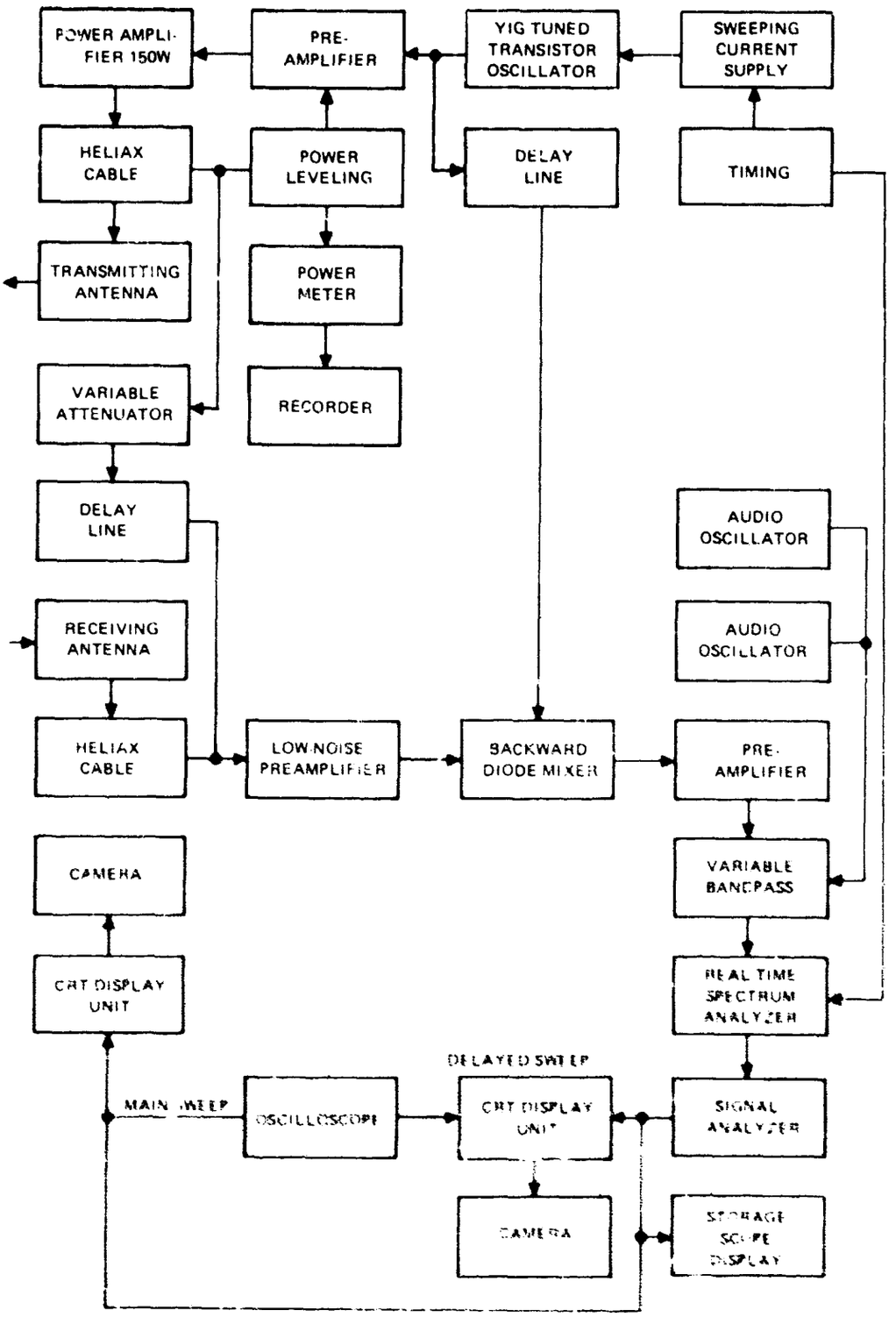

Figure 1. Block diagram of the system

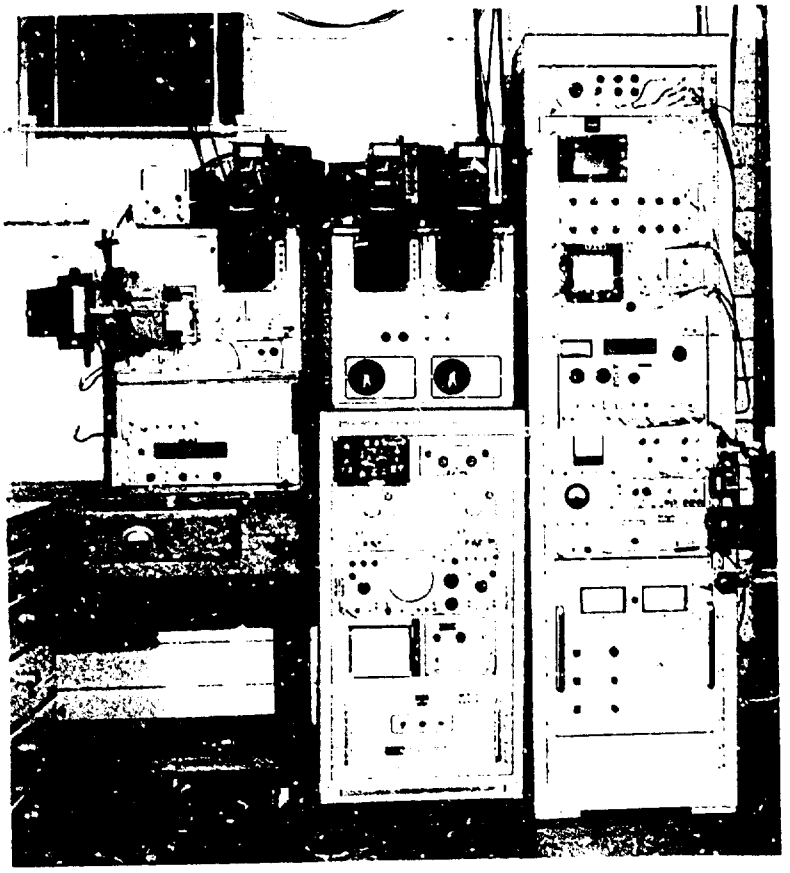

Figure 3. Sounder hardware.

FM is generated with the YIG-tuned transistor oscillator, amplified to a maximum power of 150 watts and radiated by the transmitting antenna. Transmitting and receiving antennas are shown in figure 4. Part of the transmitted power is delayed and coupled into the backward diode mixer, where it is mixed instantaneously with the signal that is received by the receiving antenna and amplified by a low-noise TWT amplifier. The reason for the delay of the transmitted portion of the signal is to compensate for delays created by the preamplifiers, the power amplifier, and the cables to and from the antennas. The delay line is exactly long enough to produce a zero beat frequency with the signal that is created by coupling between the transmitting and receiving antennas. The second delay line that couples part of the transmitted energy into the low-noise preamplifier serves as a monitor for the entire system. The length is equivalent to a radar return from a height of 167 meters. The reference-signal amplitude created in this manner is a check of all the active components of the system, gives a height calibration, and provides a check of range resolution in connection with another short delay line. The output of the spectrum analyzer is further processed in a signal analyzer that averages consecutive sweeps. The number of sweeps averaged can be selected, thus determining the time constant introduced to the signal. The signals are then displayed on cathode ray tubes in an A-scope

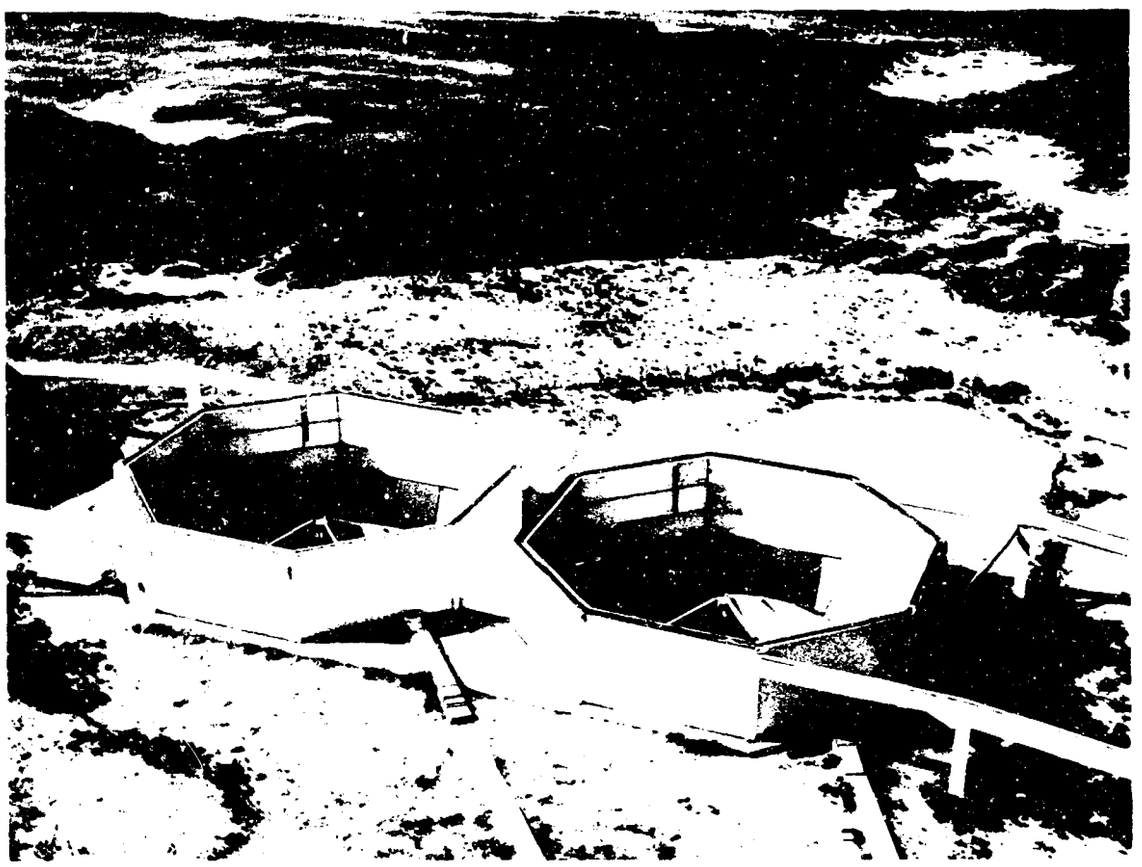

Figure 4. Sounder antennas.

presentation, or an intensity modulation, or in a combination of both amplitude and intensity modulation (or A-I scope), which is described below. The horizontal sweep for the display units is provided by an oscilloscope having a delayed sweep, which allows simultaneous viewing of the entire analysis band and any enlarged portion. The two audio oscillators provide variable height markings. The data are recorded by 35-mm, shutterless movie cameras with film speeds ranging from 1 cm/hr to 0.5 cm/sec. This recording procedure gives high-quality data but has the disadvantage of providing the time history of the data only after the films have been developed. To alleviate this problem, a storage scope display was adopted which permits real-time display of the time history of the data up to 1 hour. An example of the storage scope display and the same data recorded from a conventional scope with a 35-mm camera is shown for comparison in figure 5. In the right-hand frame a time interval of 30 minutes is stored on the storage scope and photographed with a Polaroid camera; in the left-hand frame the same segment is recorded on a conventional scope with 35-mm film enlarged to the same height scale as the Polaroid picture. Even though the storage scope display does not have the dynamic range of the conventional scope, it is sufficient to enable viewing the immediate time history of the data without the need for a

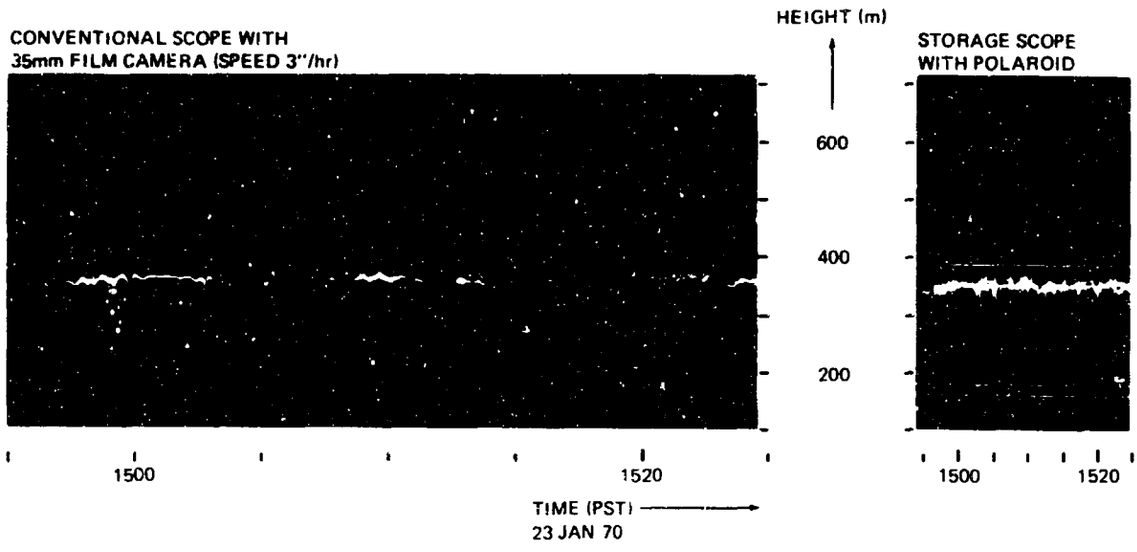

Figure 5. Example of 35-mm film and storage scope recording.

developing process. This is of particular importance when, for instance, meteorological support measurements (such as the timing of the launch of a sounding balloon) are to be coordinated with selected radar data.

The antennas, shown in figure 4, consist of two parabolic dishes, 3 meters in diameter, with waveguide feeds. For good isolation, the antennas were located in pits, an arrangement that had been used successfully before (Fehlhaber and Grosskopf, 1965).[6] At least 60 decibels' isolation is necessary to avoid saturation of the preamplifier. The insides of the pits are lined with microwave absorbers to suppress reflections. The absorbing screens are also required to suppress echoes from nearby ground targets. The antennas are steerable within a limited degree ($\pm 2.5^\circ$) to optimize the common volume for a given height.

PERFORMANCE CHARACTERISTICS

The performance characteristics of the radar are compiled in table 1. The basic components of the radar system allow operation in the entire 2-4-GHz range. The restriction to the narrower range around 2.9 GHz is determined by the standing wave ratio of the antenna feed and the balanced mixer. The variable range resolution is an important feature of the radar. In the case of volume scattering, signal amplitude changes continuously with resolution, thereby permitting significant conclusions to be drawn. The maximum range resolution of about 1 meter was determined experimentally. The spectra of two targets 93 cm apart (simulated by delay lines) were separable by choosing F = 219 MHz frequency excursion.

TABLE 1. PERFORMANCE CHARACTERISTICS OF THE RADAR SOUNDER.

Parameter	Value	Remarks
Power	150 watts	
Center frequency	2.8 to 3.1 GHz	
Frequency excursion	Variable	Linear modulation
Range resolution	Variable	Maximum resolution 1 meter for 200-MHz frequency excursion
Sweep duration	50 msec	Ten sweeps/sec
Receiver noise figure	5 dB	
Minimum detectable signal	- 150 dBm	
Antenna gain	35 dB	
Antenna beamwidth	2.3 degrees	
Isolation between antennas	105 dB	
Minimum detectable cross section at 1 km	$\simeq 3.7 \cdot 10^{-6}$ cm^2	
Minimum detectable reflectivity at 1 km	$\simeq 4.2 \cdot 10^{-15}$ cm^{-1}	For 1-meter range resolution

The values for computing minimum detectable cross section and minimum detectable reflectivity are based on a minimum detectable signal of - 150 dBm. This minimum detectable signal was determined by using a delay line with a delay time equivalent to that of a target at a height of 167 meters. The receiving antenna was disconnected for this measurement. When connected, the baseline noise of the A-scope, presumably due to nearby ground-clutter echoes, increases the minimum discernible signal (measured with the delay line target at the fixed range of 167 meters) by some 10 decibels. However, typical atmospheric echoes undulate in range and so can commonly be discerned at lower signal levels than indicated by calibration measurements with the antenna connected. Thus, a minimum detectable signal of - 150 dBm is thought to be a reasonable estimate.

The sensitivity of the radar for a point target is given by

$$\sigma_{min} = 3.7\ 10^{-6}\ r^4 \qquad (2)$$

where σ_{min} is the minimum detectable cross section in cm^2, and r is the distance of the target in kilometers. Typical insects with cross sections of 10^{-3} (Hardy and Katz, 1969) can, therefore, cause dot echoes 24 decibels above noise at 1-km height. For distributed targets the minimum detectable reflectivity, η_{min}, in cm^{-1} is

$$\eta_{min} = 4.2 \cdot 10^{-15}\ r^2/h \qquad (3)$$

where r is distance in kilometers, and h is range resolution in meters. Typical values of η for a 10-cm wavelength are 10^{-16} 10^{-14} cm^{-1} as given by Hardy et al. (1966), Atlas and Hardy (1966), and Hardy and Katz (1969). It can be seen from equation (3) that even for the highest range resolution of

1 meter, returns can be expected from as high as 1 km. To detect the weaker scattering regions at greater ranges, we should have to increase the effective pulse depth or resolution, provided of course that the scatter regions are thicker than the effective pulse.

By way of comparison, the powerful 10.7-cm radar used by Hardy et al. (1966) at Wallops Island has a sensitivity equation of $\eta_{min} \simeq 6 \times 10^{-17}$ r^2/h (same units as equation (3)) for beam-filling distributed targets. Although the Wallops 10.7-cm radar thus appears to be 18 decibels more sensitive than our radar, this is true only for scattering regions having a range extent 300 times as great (at maximum resolution) because their pulse length in space is 300 meters. Since we shall see that some scatter layers have thickness of only a meter or less, the Wallops radar would produce signals comparable to those of the FM/cw radar for such thin layers. Moreover, the absence of appreciable ground clutter permits us to measure at ranges 20 to 100 times as small as those at Wallops Island, thus providing greatly enhanced signals.

Even though there is no basic minimum-range restriction inherent in this kind of radar, some practical limitations (which could be overcome if necessary) reduce the sensitivity of the radar for targets closer than 50 meters to the antennas. Reflections from an adjacent building give permanent returns for the first 50 meters in height; therefore, targets must be capable of providing stronger returns or must change their position in order to be discernible. Also, the separation of the two antennas imposes a minimum height range for beam intersection. The antennas are separated by 5 meters, and their beams intersect within 50 meters above the ground. The general location of the sounding facility is shown in figure 6. To the left of the building the sounder antennas are visible. The radome on top of the building houses a radiosonde tracking antenna whose purpose is described in the following paragraphs.

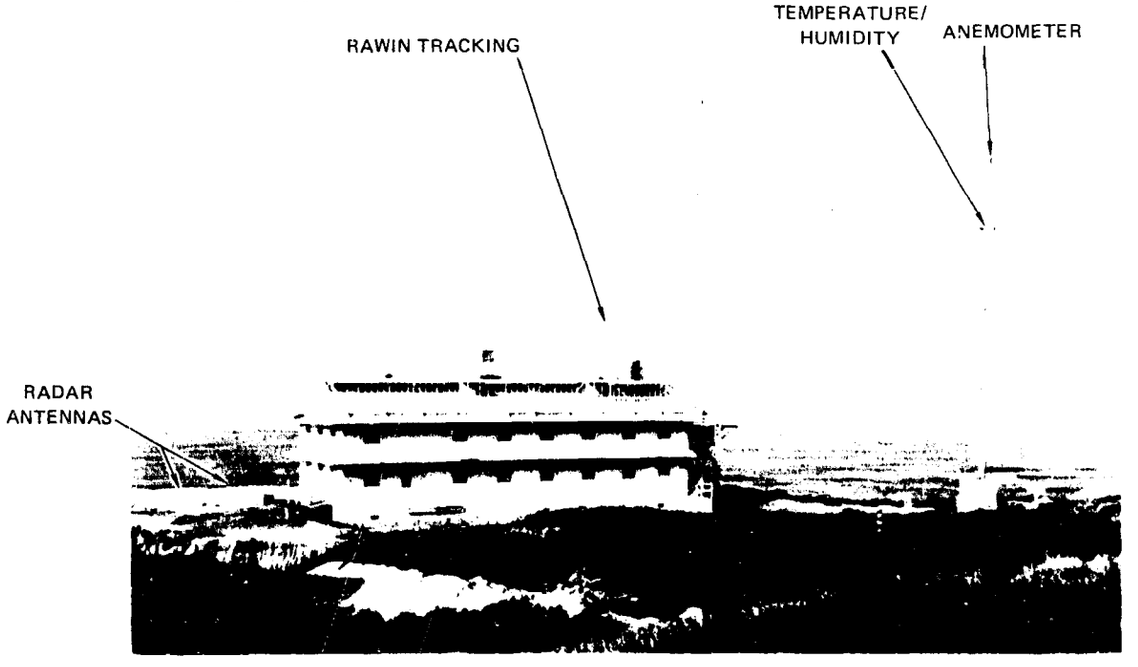

Figure 6. Sounder location.

METEOROLOGICAL SUPPORT MEASUREMENTS

The meteorological support measurements used in conjunction with the radar sounder consist mainly of RAWINSONDES and continuous surface measurements of wind, pressure, temperature, and humidity.

SURFACE MEASUREMENTS

Wind speed and velocity are obtained from a UMQ-5 wind-measuring set. The vane is located on top of the pole on the right-hand side of figure 6, 55 meters above mean sea level. The circuitry of the recording system is shown in figure 7. The voltage proportional to the wind speed is obtained directly from the Wind Indicator Set. Wind direction is obtained by mounting a single-turn precision potentiometer on the UMQ-5 indicator synchro with the connections shown in figure 7. For both wind speed and direction, time constants of 10, 25, or 50 sec can be selected in order to suppress higher-frequency fluctuations. A high-resistance network is used to produce these time constants. The high resistance values require a high-input-impedance network which is realized with a hybrid FET operational amplifier (ADO-29B Fairchild) in a noninverting feedback configuration. The input impedance of the amplifiers is 10^{11} ohms.

A Vibrotron (United Control Corporation) pressure transducer is used to measure the surface pressure. The transducer consists of a tungsten wire tensioned in a magnetic field between an anchor point and a diaphragm. An oscillator circuit is formed with an external amplifier so that the frequency is determined by the natural frequency of the tungsten wire. A digital counter is used to measure the period of the oscillations and a digital-to-analog converter to display the counter readings on a recorder. This arrangement permits recording absolute pressure in analog form with accuracy of 0.01 mb. The pressure sensors are 31 meters above sea level. The frequency of the Vibrotron oscillator is approximately 10 kHz (for sea level pressure) and changes linearly at the rate of 1.17 Hz/mb. For high resolution, 100 000 periods (10 sec) are averaged, and the period is measured rather than frequency. For the surface pressure range encountered, the error introduced by measuring period instead of frequency is negligible. Wind speed, wind direction, and absolute pressure are displayed on an eight-channel Speedomax recorder. On other channels of the same recorder, continuous recordings are made of temperature, relative humidity, and pressure measured with a T21B microbarograph system described by Johnson and Chiles (1957).[7] The rack housing this equipment is shown in figure 8. The cabinet on the left side contains the pressure transducers, which are embedded in styrofoam to avoid contamination of pressure changes by temperature changes. Timing marks are made simultaneously on the radar records and on the Speedomax recorder to ensure exact time correlation of radar and meteorological data.

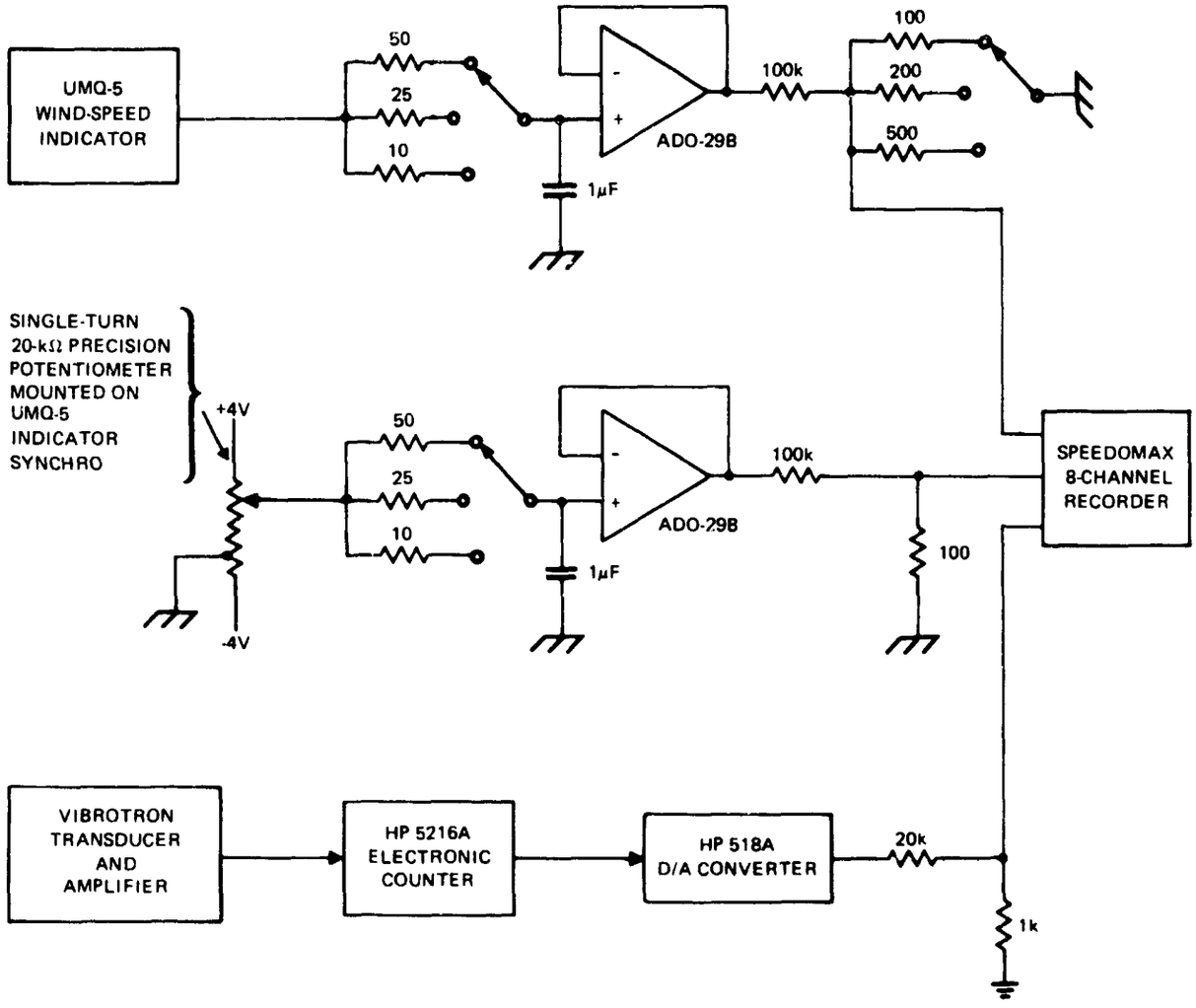

Figure 7. Surface wind and pressure recording system.

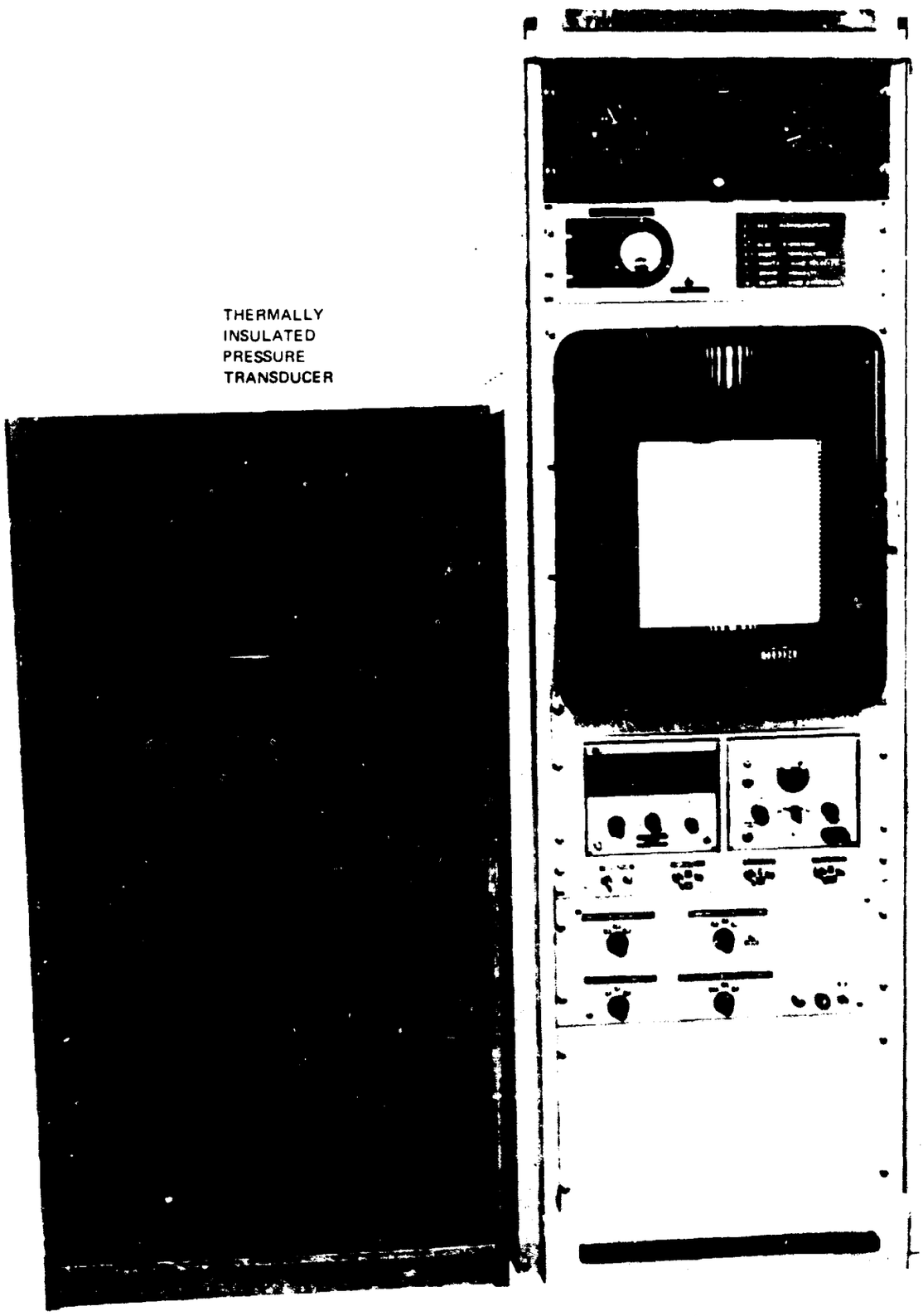

Figure 8. Recording system for surface meteorological data.

RADIOSONDE MEASUREMENTS

The most important support measurements for interpretation of the radar data are height profiles of wind, temperature, and humidity measured by balloon sounding. AMT-11B transmitters were used in making the profiles until December 1969. The balloon carried two modified AMT-11B transmitters, as shown in figure 9, one of which measured temperature continuously and the other humidity continuously. Pressure height was obtained from the usual radiosonde commutator contacts. There was no switching of elements; the commutator contacts merely caused a 'spike' to appear on the records. In the unaltered version of the transmitter, leads go from the two relay contacts to the temperature sensor and the humidity sensor, respectively. In the modification the two leads are connected. Ground is removed from the element during switching times, causing short spikes. High and low reference contacts were disconnected in the humidity transmitter. The high reference contacts were left in the temperature transmitter; the low reference contacts were modified so that the trace was shifted during the low reference condition but still gave temperature readings. The rf frequencies of the two transmitters were separated by about

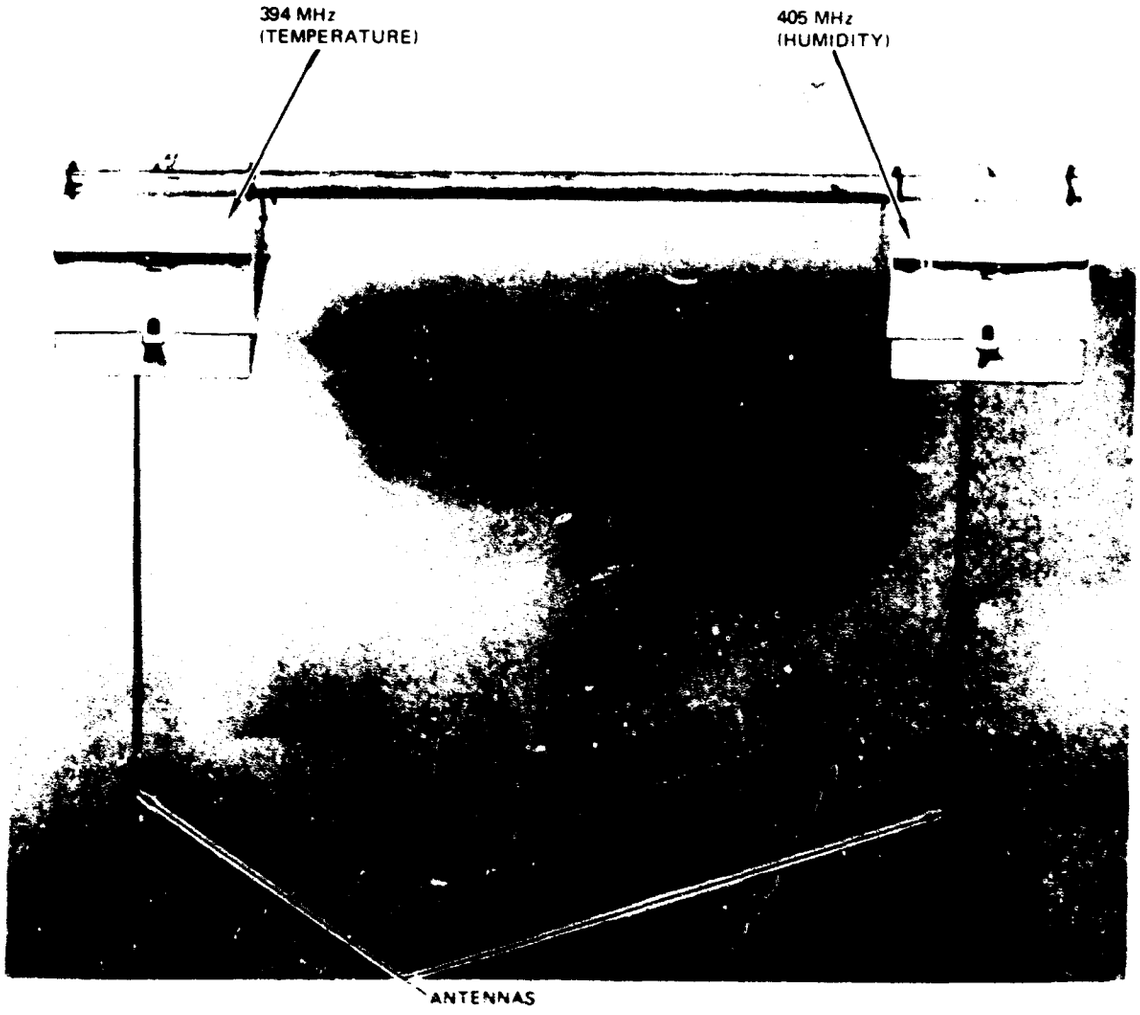

Figure 9. Modified AMT-11B radiosonde transmitters for continuous fast-response temperature and humidity measurements.

5 MHz, which is sufficient to prevent interference between the two. The two transmitters were physically separated by about 1 meter to prevent mutual pulling of their blocking frequencies. A carbon element was used to provide fast-response humidity readings. This required changing some electronic components and resulted in the humidity-deflection curve shown in figure 10 for the SMQ-3 radiosonde receiver records. The rate of rise sought for the balloons was 100 meters per minute in order to achieve the same height resolution as the radar. Tethered Kytoons were used for soundings up to 300-meter height. The arrangement of the transmitter for this purpose is shown in figure 11. Temperature and humidity sensors were aspirated by small battery-driven fans to guarantee fast response even at slow vertical ascent rates. Originally the wind data were obtained by optical tracking of the balloon with theodolite readings taken every 10 seconds. To avoid the shortcomings of optical tracking - in particular the visibility limitation of cloud cover - an automatic tracking system was installed and became operational in December 1969. All wind data after this time were obtained with a GMD-1A automatic tracking system using AMT-4 transmitters. (The tracking antenna is under the radome shown in figure 6.) The continuous humidity trace is obtained from the AMT-4 transmitter and the continuous temperature trace from an AMT-11B transmitter with the previously described modifications.

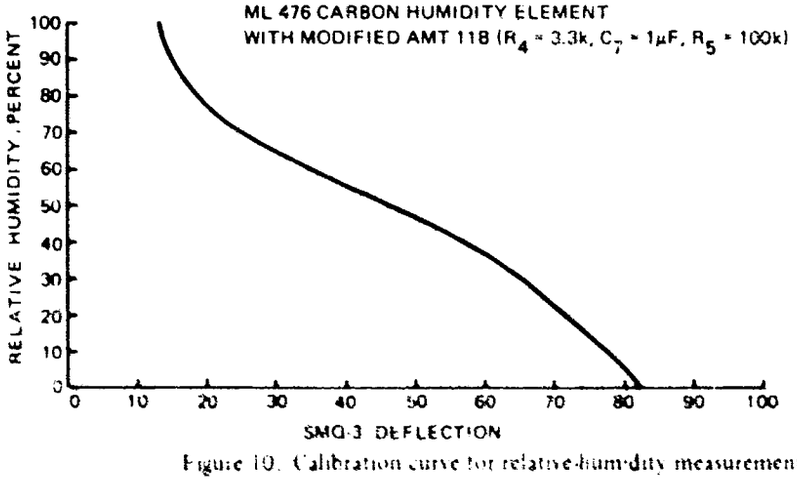

Figure 10. Calibration curve for relative-humidity measurements.

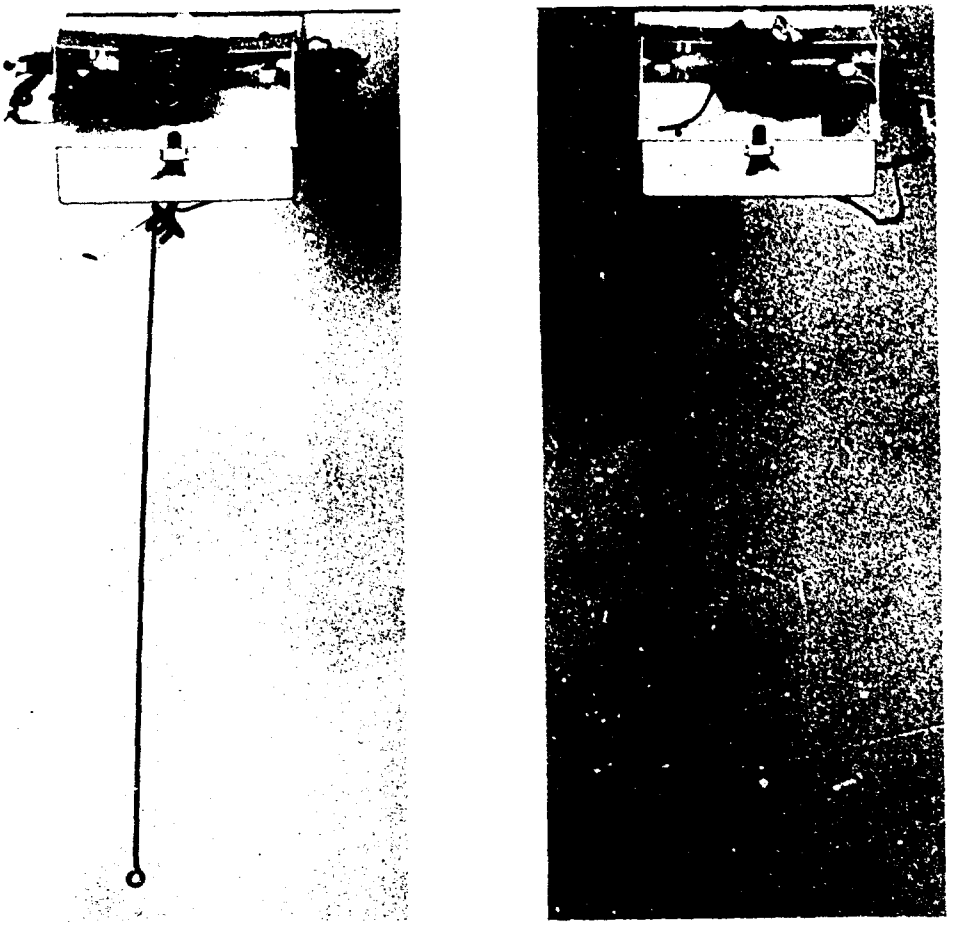

Figure 11. Aspirated AMT-11B transmitters for tethered soundings.

RESULTS

LAYER STRUCTURES

Figures 12 and 13 illustrate some of the features of thin scatter layers that are depicted by this radar system.

Figure 12 is a 45-minute section of an intensity-modulated trace recorded January 7, 1969, during a weather condition locally called a Santa Ana, which was observed continuously for 3 days. (The Santa Ana is a downslope wind flow from the higher desert area east of San Diego. It produces a subsidence inversion leading to dry, warm air aloft and providing large contrast in humidity and temperature with the marine air next to the sea surface.) The refractive index profile computed from a radiosonde flight at the radar site is shown at the right. (A modified radiosonde system is employed that uses two transmitters on one balloon to provide continuous,

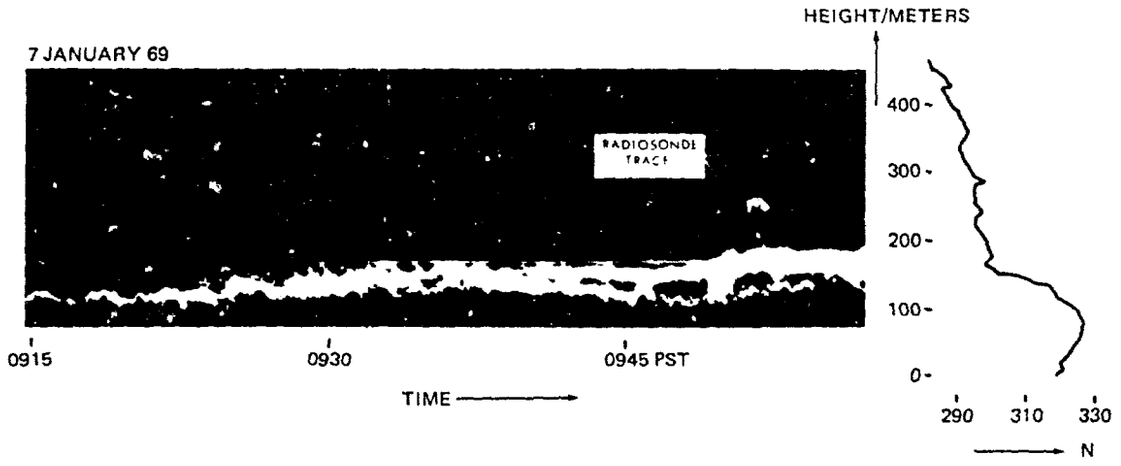

Figure 12. Typical echo layers as seen with low time resolution and corresponding temperature and modified refractive index profiles. $N = (n-1)\ 10^6$ where n is refractive index (height in meters).

fast-response temperature and humidity readings.) Note that the echo from the sonde is seen on the radar record, thus permitting close correlation of the two records. Clearly, there are two predominant echo layers, although three are noticeable at about 0935 PST (Pacific Standard Time). Both the echo layers and the atmospheric strata undulate. At the time of the radiosonde transmissions the bottom echo layer was very close to the height of the sharpest refractive (N) gradient at 136 meters, while the upper thick layer was collocated with the top of the N gradient stratum centered at 167 meters. While the lower echo occurred at the base of the major temperature inversion, the upper one occurred at the point of changing slope in the temperature trace below the top of the inversion. This seems to be a characteristic feature. In other words, the base of the inversion is detected routinely, whereas the top is not. Clearly, there is close association between the heights at which the vertical N gradient changes sharply and the echo layers.

The thickness of the echo strata is seen in figure 12 to vary from about 1 meter, the maximum resolution (comparable with the thickness of the 167-meter height marker), to about 30 meters. But the 30-meter thickness of the upper layer at 0955 PST is due to a combination of blooming of the display and rapid oscillations in layer height which are apparent under close scrutiny at about 0944 PST. A 10-to-15-meter thickness is more representative of both layers.

Figure 13 illustrates the combined amplitude-intensity (A-I) display recorded on its typically expanded time basis. Each vertical trace on the record is a running average of the signals on the previous 32 frequency sweeps with an exponential weighting function and a time constant of 3.2 sec. However, only every sixteenth trace is displayed, so that the record shows

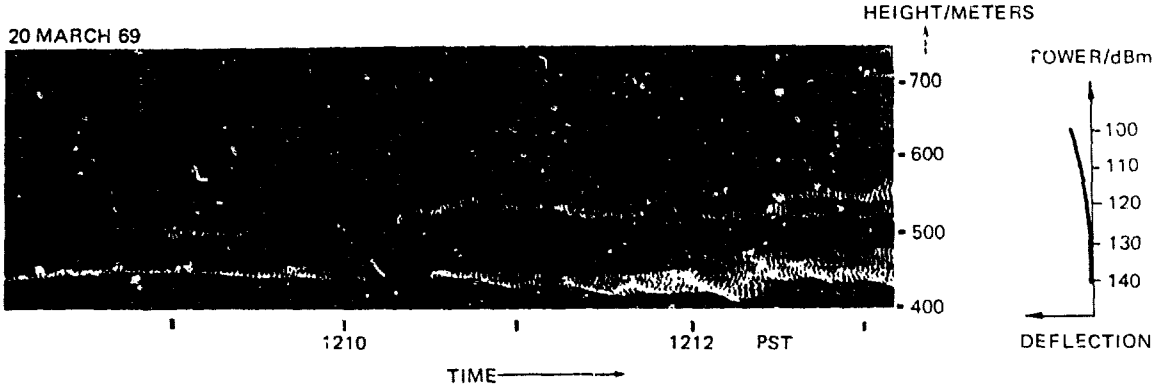

Figure 13. Multiple layers on amplitude-intensity (A-I) display with 32-sweep averaging and display of one trace in 16 (height in meters).

37.5 sweeps per minute. It is only in this way that the signal amplitudes can be read quantitatively without excessive overlap of adjacent traces. By using the signals themselves to provide simultaneous intensity modulation, the record is shaded so that the brightest echoes are also the strongest. The signal intensities can be scaled off quantitatively from the calibration curve on the right. Because both the fine structure of the layers and their intensity can be obtained from the A-I display, it is especially valuable for this kind of work.

Although no radiosonde record is shown to correspond with figure 13, the two predominant layers were found close to the base and the top of the major gradient of refractivity. Close examination of the record shows that the bottom layer thickens progressively with time from about 5 meters at the start to a maximum of about 35 meters at about 1213 PST. In fact, the apparent broadening of the stratum just after 1212 PST appears to be due to a jump in layer height. Careful scrutiny shows that the lower layer has two well defined intensity peaks at about 1209 PST that are separated by about 5 to 10 meters. Thus, the lower layer may actually be comprised of two undulating bands also, each having thickness of 10 to 25 meters and occasionally blending to form one apparent, thick layer.

It will be seen that the signal intensity of the lower layer increases to a maximum of about -102 dBm just after 1212 PST. At the corresponding range of 430 meters, this signal corresponds to a volume reflectivity of about 5×10^{-11} cm^{-1}. Although the accuracy is no better than about ±5 decibels at this stage, the indicated reflectivity is more than 1000 times the maximum reported by Atlas and Hardy (1966) and Hardy and Katz (1969) at a 10-cm

wavelength. If we can assume that the scattering is from refractive inhomogeneities, this suggests that the inhomogeneities observed with our high-resolution radar are indeed much stronger than inhomogeneities previously observed either by radar or by refractometers. In fact, this would have to be the case; if the Wallops 10-cm radar reports a reflectivity of 10^{-14} cm^{-1} when only 1 percent of its scatter volume is filled, then the actual reflectivity would be 100 times as great. Therefore, the reality of such high localized reflectivities can hardly be questioned.

The temporal continuity of the radar observation technique may be used for presentations of the kind shown in figure 14. It is hand-drawn to achieve the time compression necessary for the figure. It shows height and thickness of the layer for a 2-day time period of which figure 12 was one part. No simple diurnal behavior of layer structure has been established so far, even though continuous observations for as long as 4 weeks have been studied. This may be due to superposition of other meteorological factors on a diurnal effect. It is also difficult in the case of multiple-layer structures to objectively identify and connect strata with strong fading characteristics which alternately appear and disappear.

An excellent example of a multiple-layer structure is presented in figure 15. Several distinct strata of various vertical thicknesses and temporal behavior can be seen; superimposed is the refractive index profile obtained from a radiosonde sounding at 1238 PST. Remarkable is the agreement of backscatter zones and refractive index gradients. The significance of this

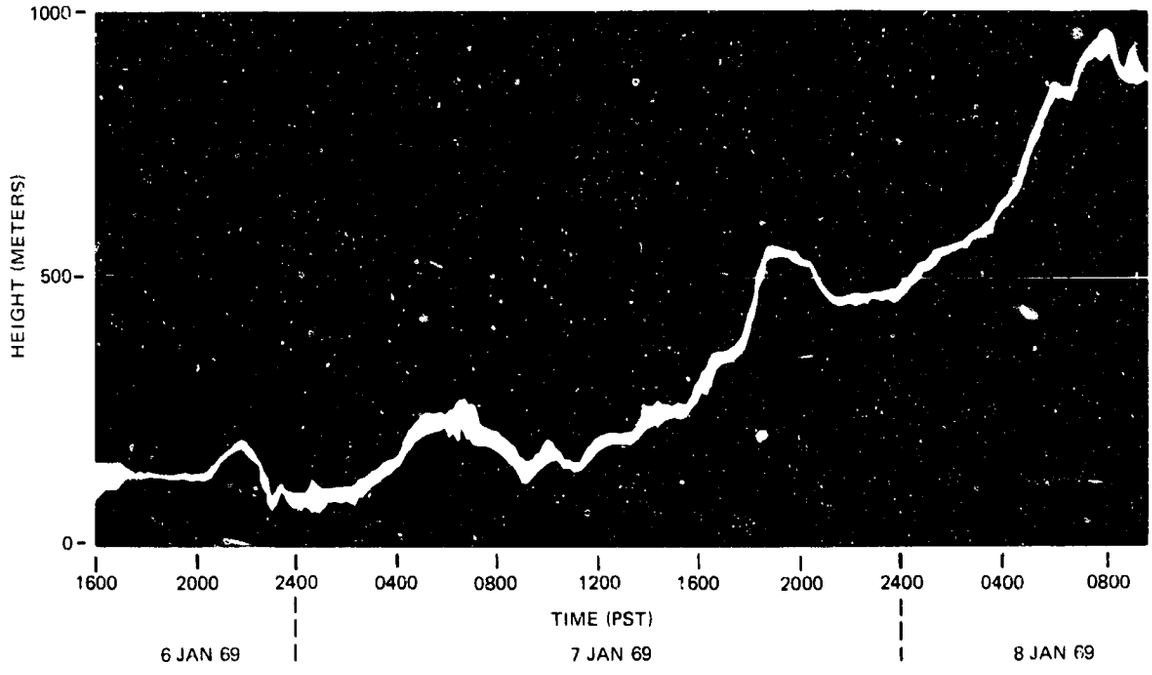

Figure 14. Approximate height and thickness of layer structure observed continuously from 6-8 January 1969.

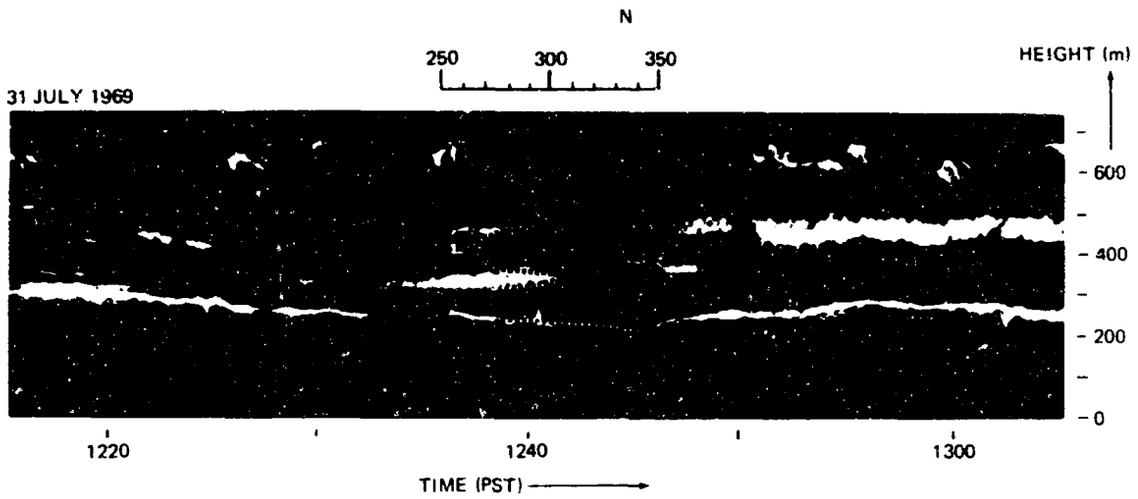

Figure 15. Multiple-layer structure. The dashed curve is the refractive index profile measured with a sounding balloon.

layer structure on radar coverage is illustrated in figure 16, in which a transmitter at a height of 100 feet is assumed. The earth is drawn flat, which gives a straight ray an upward bend. From the ray trace picture we should expect a hole in coverage at a range of around 25 nautical miles. We also see from the ray trace picture that only the layer belonging to the steepest gradient influences the coverage significantly. This layer changed about 80 meters in height between 1220 and 1240 PST, which could influence an accurate coverage prediction. This example emphasizes the need for precise and continuous knowledge of the refractive index structure if accurate coverage predictions are required. Another example of multiple layers is shown in figure 17. Up to 10 distinct layers can be distinguished; the vertical thicknesses of some approach the resolution of the radar (2 meters in this case). Many more examples of layer structures with radiosonde sounding data are presented in the appendix.

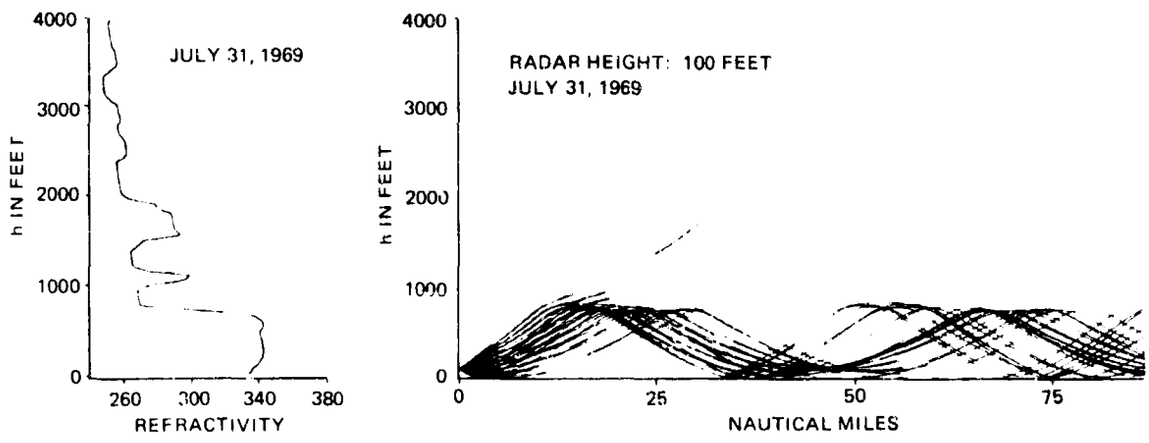

Figure 16. Ray trace for the refractive index profile and layer structure of figure 15.

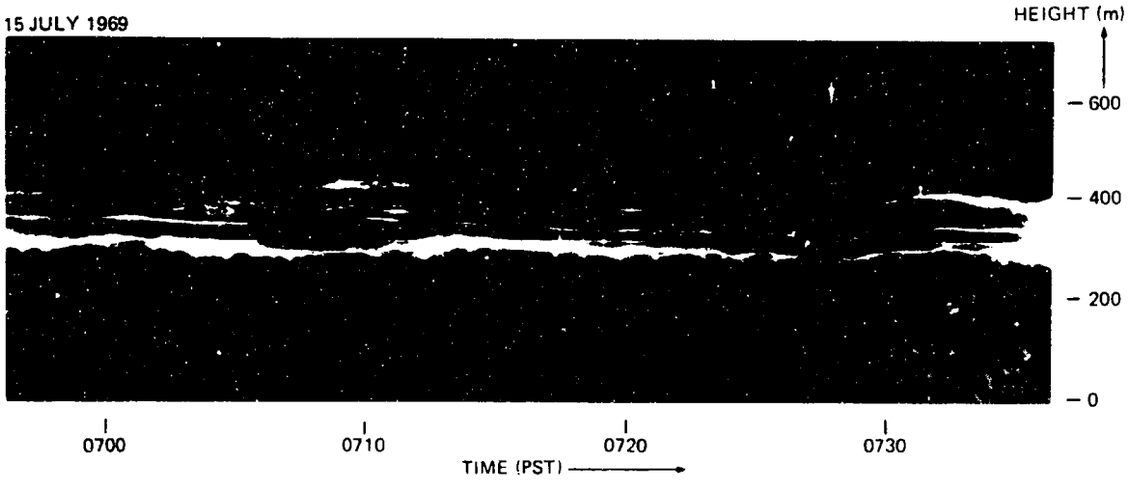

Figure 17. Multiple-layer structure.

DOT ECHOES

The radar records almost always contain dot echoes; some of them are due to birds, but most of them are believed to be caused by insects, as the signal strength of the dot echoes usually agrees with the backscatter to be expected from commonly occurring insects. Particularly during the summer months, there is also a diurnal cycle in the occurrence of dot echoes. The cycle consists of a sudden and strong onset of echoes around sunset and a disappearance at dawn. The insects in this case are nocturnal moths and small butterflies which are quite common and noticeable in the area in which the sounder is located.

There are several cases of descending 'swarms' of dot echoes. One example is shown in figure 18. The two radar records show the same event recorded with different film speeds. Meteorological surface observations are also given. A discussion of the meteorological data and a conjecture on what may have caused the descent are given by Atlas, Richter, and Gossard (1969)[8] and are not repeated here. The only point that should be mentioned is that the intensity of the dot echoes is consistent with insect cross sections. On several other occasions similar descents were recorded in which signal strength was several orders of magnitude higher than could be accounted for by the largest insects. Because of the slow rates of descent, birds seem to be excluded as a possible source. In one case which occurred during daylight and under clear skies, a visual observation failed to detect any particulate matter. Further observations will be necessary to interpret this phenomenon. Under certain circumstances insect echoes may provide additional information of motion in the atmosphere. An analysis and a detailed discussion of this possibility are given by Atlas, Harris, and Richter (1970).[9]

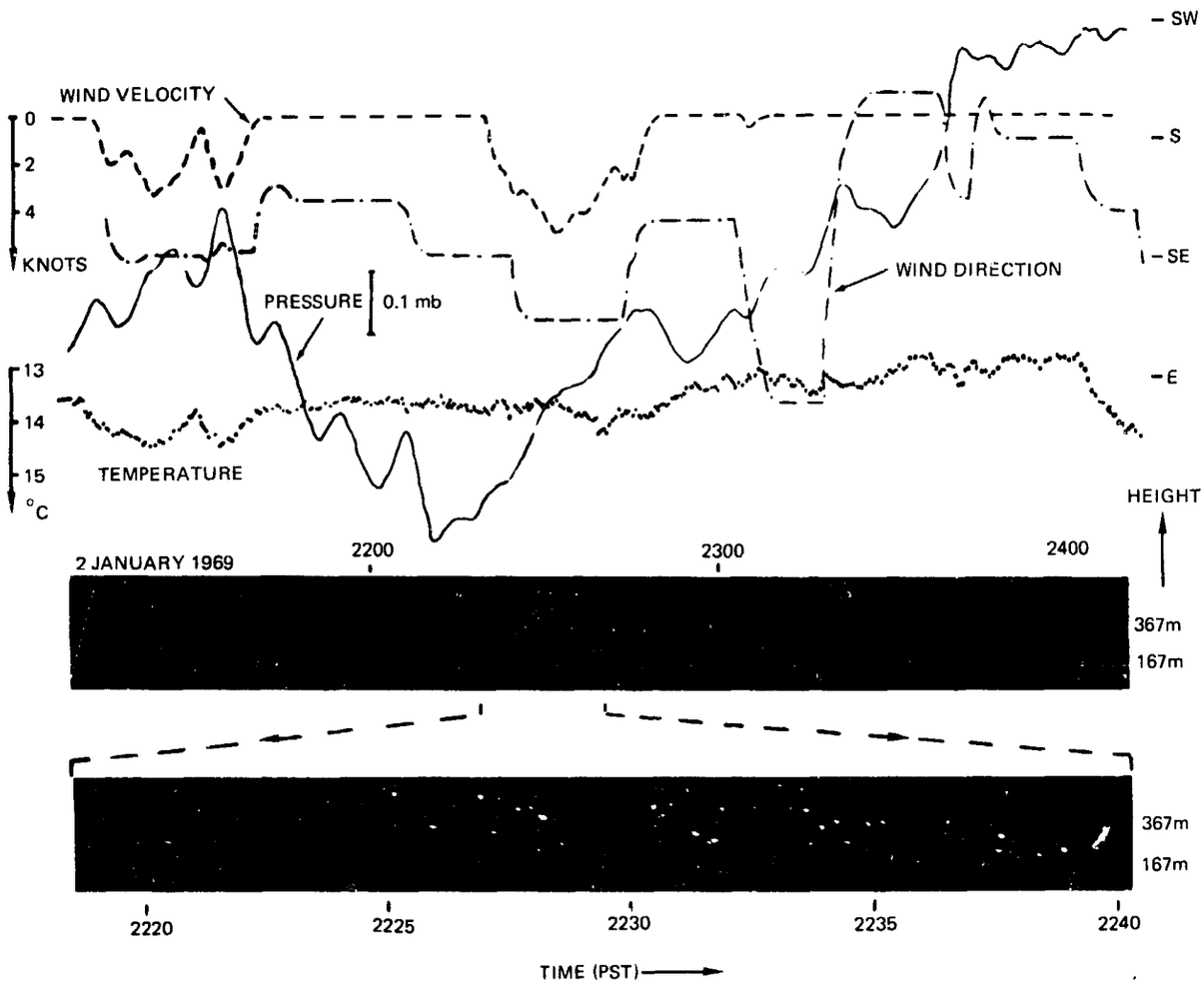

Figure 18. Descending swarms of dot echoes.

RAIN

The radar backscatter properties of water droplets (and, therefore, of rain) are well known. What is not well known is the fine-scale structure of rainfall, and the radar sounder offers itself as a powerful tool for studying it. This possibility has not been fully exploited in San Diego for two reasons. First, it is not associated with the purpose for which the sounder was built; and, second, San Diego has yearly average rainfall of only 10 inches, which is not enough for extensive study. Figure 19 illustrates the capability of the sounder with respect to rain. The upper portion of this figure is the intensity-modulated radar record of a multiple-layer structure with intermittent rain showers starting at 1152 PST and 1222 PST. The echo intensity of the rain overexposed the intensity-modulated record. The A-I record of the time interval from 1151-1158 PST is shown in the lower part of figure 19. In this presentation structural details of the rain shower are evident. The

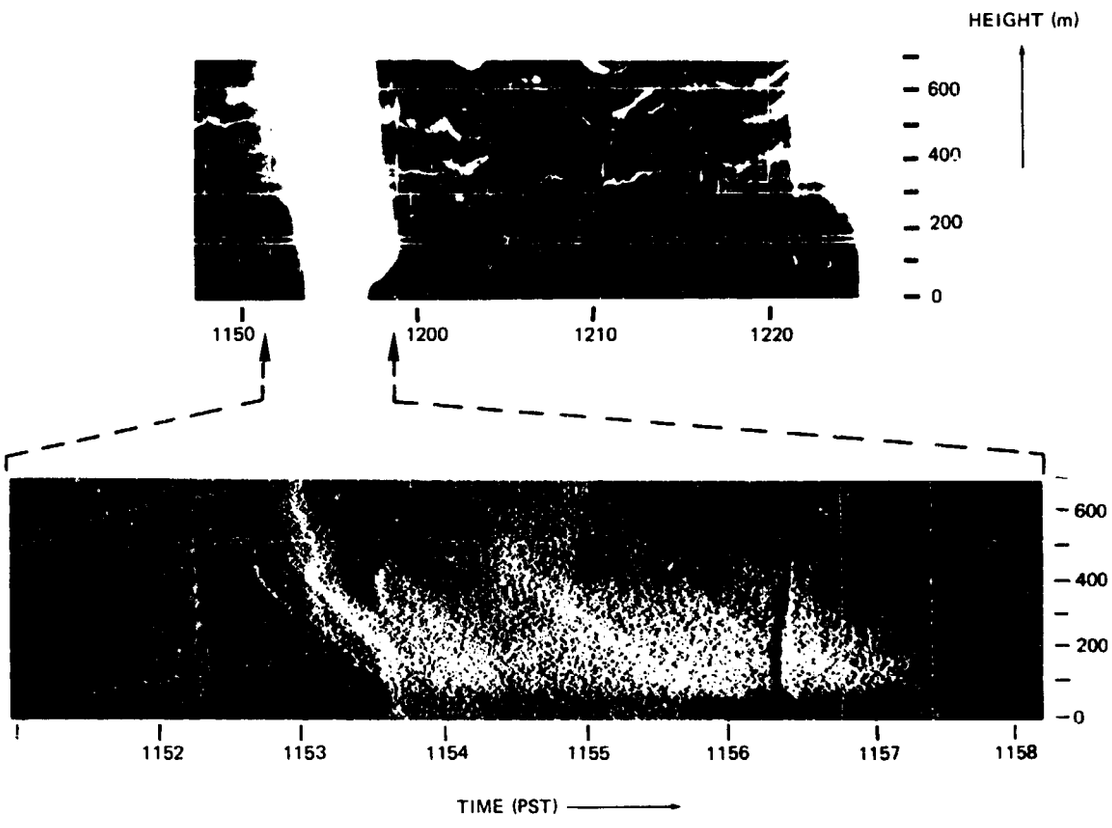

Figure 19. Structure of rain. Between 1156 and 1157 receiver was momentarily overdriven producing vertical streak.

intensity of the rain with respect to time varies, leading to different 'streaks.' The streaks do not always have a constant slope. This gives immediately the fall velocity. The deviations from a constant slope must be due to wind shear. The gap in the record between 1156 and 1157 PST stems from a baseline shift which is caused by a strong echo (probably bird or airplane) overdriving the radar receiver. Figure 19 is one example of what can be studied with the sounder. Other recordings exist in which rain evaporates before it reaches the ground. Atlas has suggested (private communication) that the ice-water transition is another problem that could be studied, as the scatter properties of ice crystals are different from those of raindrops.

WAVE MOTIONS

Perhaps the most exciting observations made with the radar sounder concern the detailed structure of wave motions in the troposphere. The presence of such waves had been known (Gossard and Munk, 1954),[10] and

they have been recorded by other radars on rare occasions when the size scales and amplitudes were large enough for their much coarser resolution. The present sounder showed that the waves are ubiquitous, and occur with vertical amplitudes of as little as some 10 meters. It also revealed details of wave motions which had never been observed before. The development of the sounder coincided with a renaissance of interest in the field of wave motions in gases and fluids. Consequently, many presentations and interpretations of wave motions observed with the sounder have already been done and are not repeated here (Gossard, Richter, Atlas, 1970; Atlas, Metcalf, Richter, Gossard 1970; Gossard, Richter, 1970).[11-13] A number of additional wave pictures recorded with the radar sounder are shown in this report in order to give a more complete cross section of this phenomenon and to provide material for further interpretation and discussion.

A good example of wave patterns is shown in figure 20. It shows the same recording three times, each time enlarged differently. Two different types of wave motion are clearly distinguishable: long-period (5-10 minutes or longer) internal waves, and much shorter-period Kelvin-Helmholtz (K-H) wave instability structures sometimes superimposed on the longer-period waves. The enlargements in the middle and lower part of figure 20 permit us to recognize short-period and small-amplitude K-H waves which show clear evidence of breaking. The most perfect sequence of a K-H wave recorded to date is shown in figure 21. The wave builds up until it overturns and breaks, and the air masses at the interface become mixed. Figure 22 shows a section of the same event but in A-I presentation. This kind of presentation shows particularly clearly the sharp boundaries and the small vertical extent of the zones from which the electromagnetic energy is returned.

Another wave train which occurred on the same day 2 hours earlier is shown in figure 23. It is similar to the previous picture but has a 'braided' appearance commonly observed. The fact that the wavetrain of figure 23 is close in time to the one of figure 21 is not coincidental. Frequently these wave trains occur sequentially and an example of such repetition is shown in figure 24.

Figure 25 shows splitting of one layer into two layers with a wave instability structure originating between the two new layers. This is not an isolated occurrence.

Cases in which the radar illuminates the wave structure through considerable depth are of special interest because they can reveal details of the region where true wave motion couples with the instability structures at the critical level. This requires radar returns from multiple layers over considerable depth. Figure 26 is such a case; unfortunately, no layer structure below the wave train is visible. In figure 27 there are layers above and below the major wave train located between 400 and 500 meters. The major wave train perturbs the upper stable layers but has no apparent effect on the layers below, which, themselves, tend to consist of independent, breaking wave trains. The vertical structures between 100 and 170 meters are caused by convection in the marine layer below the stable region.

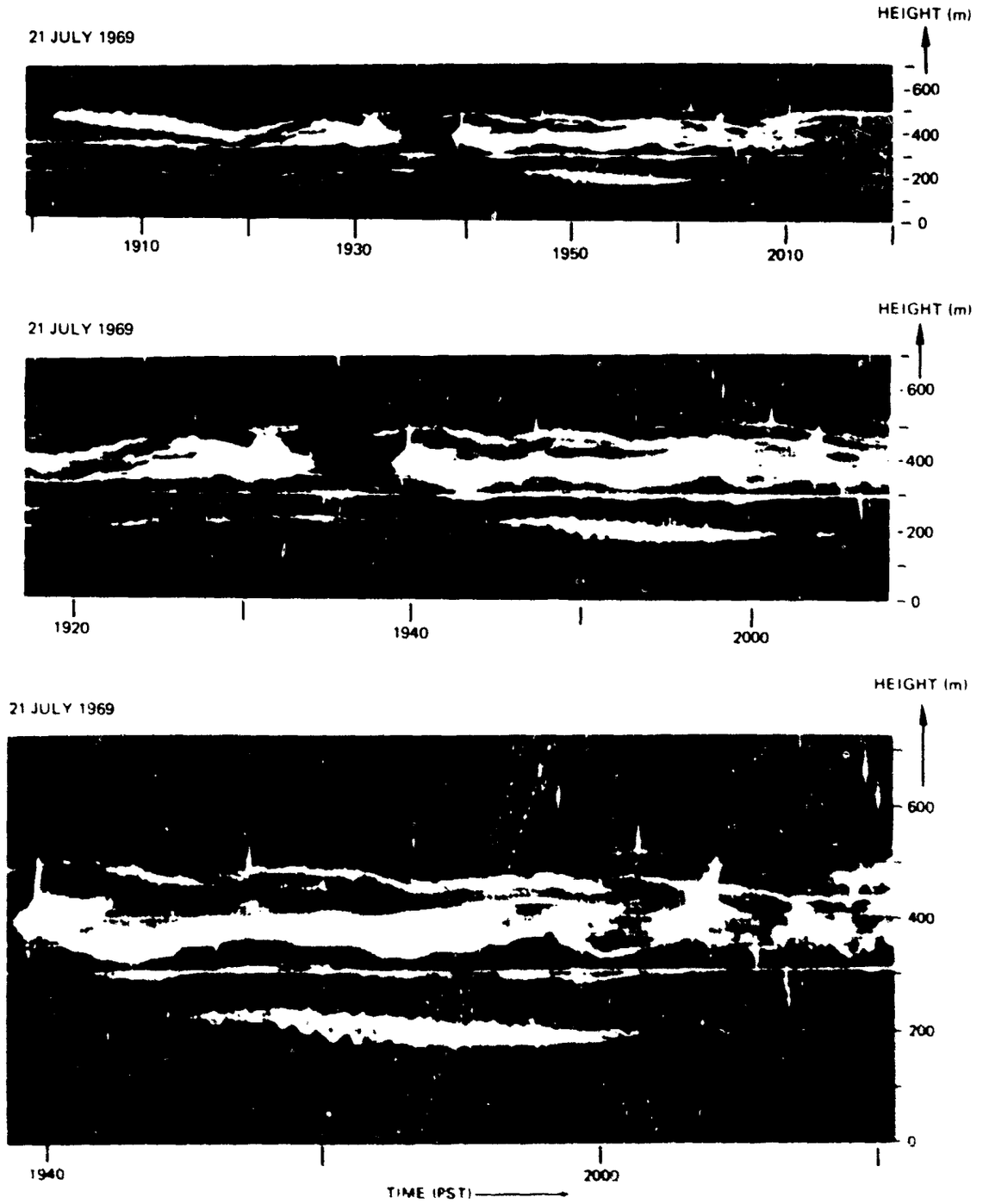

Figure 20 Wave patterns

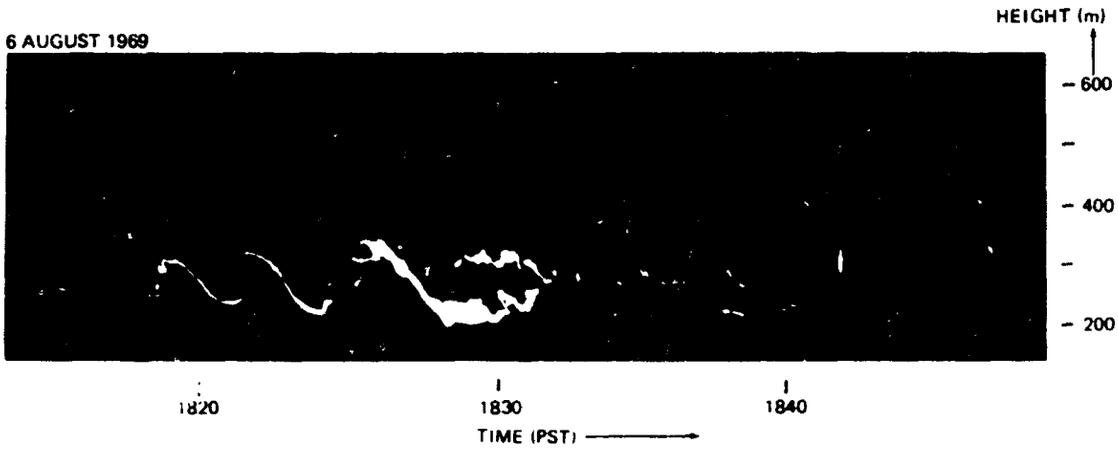

Figure 21. Breaking wave (intensity modulation).

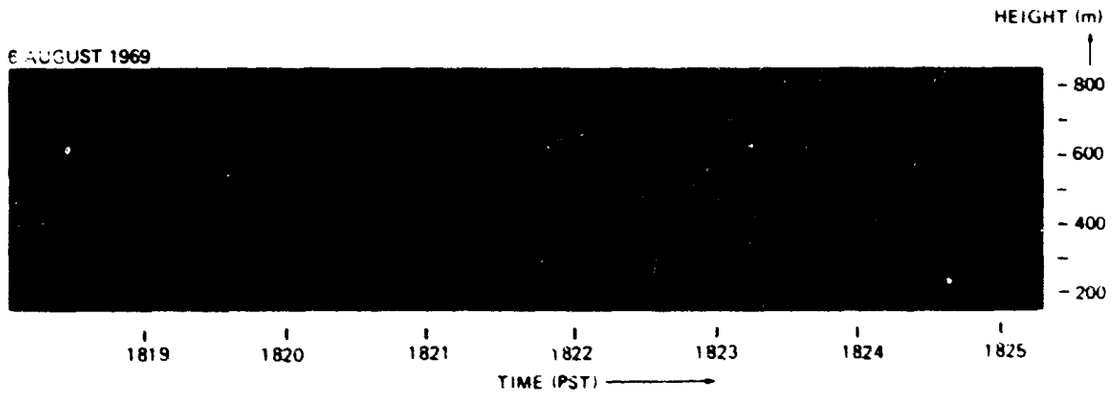

Figure 22. Breaking wave (A-I presentation).

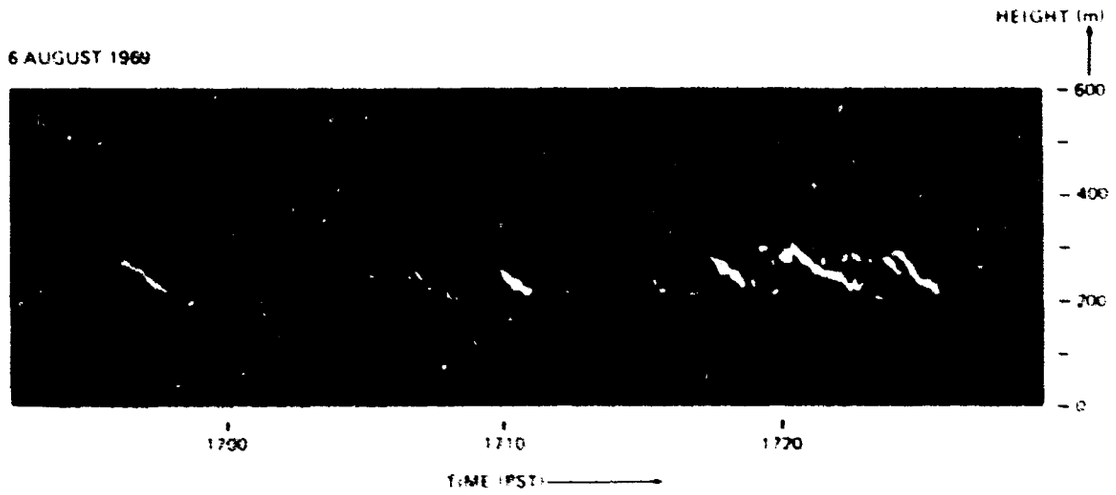

Figure 23. Breaking wave group bunched appearance

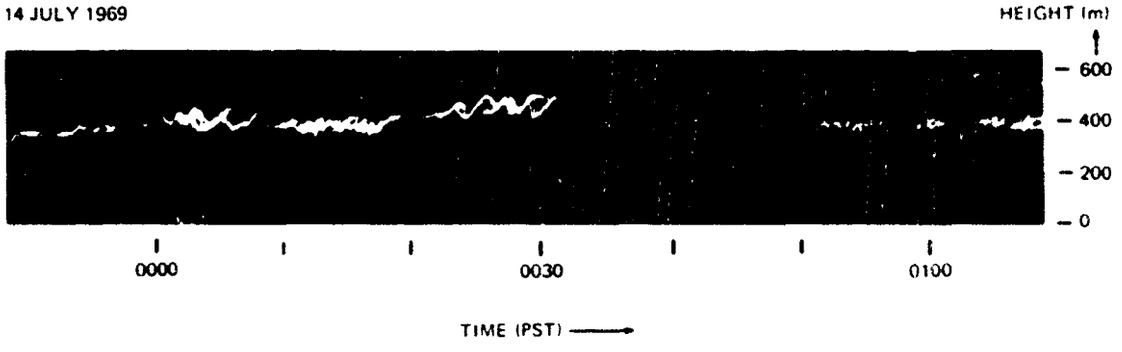

Figure 24. Repeated occurrence of wave trains.

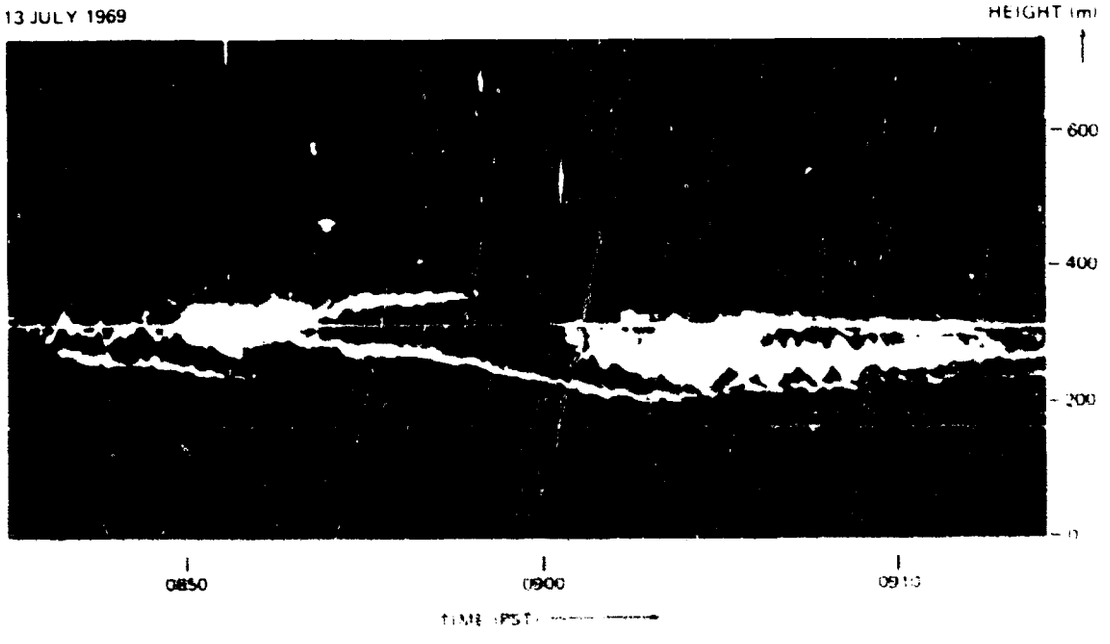

Figure 25. Splitting layer.

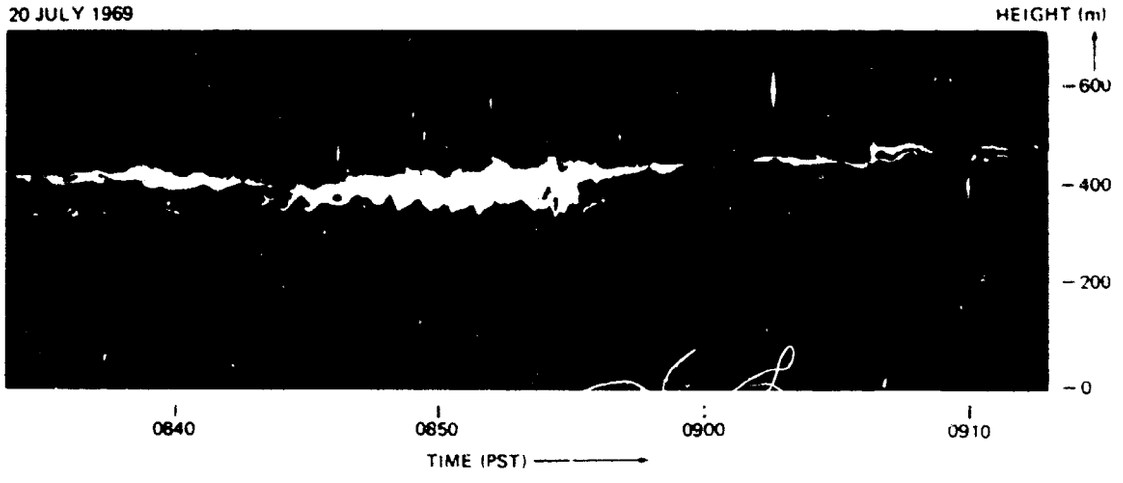

Figure 26. Breaking wave in multiple-layer structure.

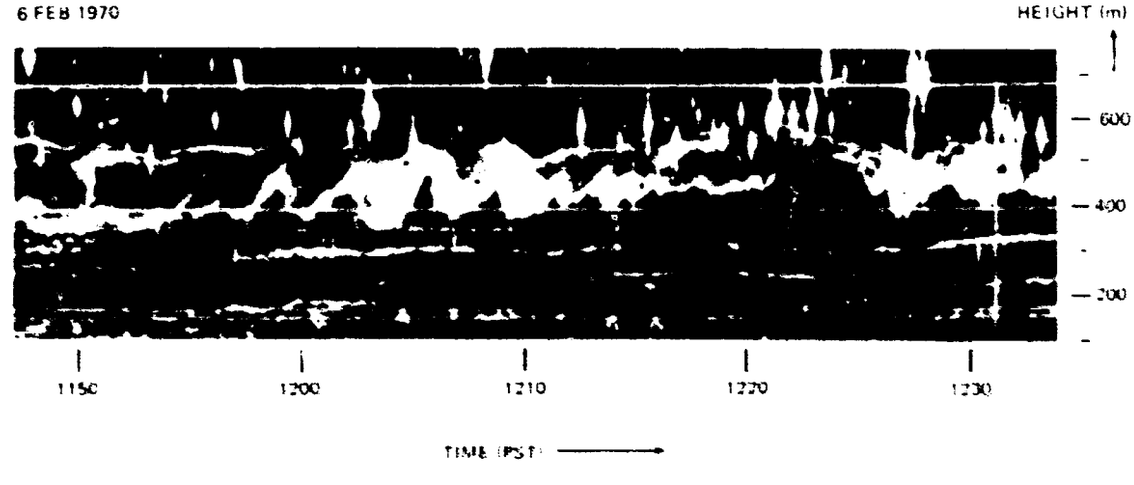

Figure 27. Wave structures

CONCLUSIONS

The FM/cw radar sounder represents a novel tool to investigate and study the structure of the troposphere. It has yielded significant results to date, in particular in the area of radar reflectivity and atmospheric wave motions. The sounder permits continuous monitoring of the vertical refractive index structure in the troposphere with range resolution as high as 1 meter. Layer structures are detected routinely. As they may change their height in short time intervals, a continuous knowledge--not only of their presence but also of their exact height—is necessary for accurate radio and radar propagation predictions. The study of dot echoes warrants further attention, as they may add information about atmospheric processes. The sounder is an excellent tool for the study of the structure of rain. The sounder already has played and will in the future play an important role in the field of mesoscale meteorology, in which conventional sounding techniques are extraordinarily difficult.

RECOMMENDATIONS

It is recommended that the present studies be intensified in two major areas: the study of the mechanism responsible for the reflection of electromagnetic energy, and atmospheric mesoscale structure. For the study of the reflection mechanism, an effort should be made to measure the refractive index fluctuations directly, perhaps with balloon soundings using spaced, fast-response humidity sensors. The phenomenology of waves warrants further study, as it appears that waves play a significant role in the energy distribution within the troposphere.

Finally, some improvements and extensions of the sounder hardware should be undertaken. Magnetic-tape recordings before the spectrum analysis could be used to analyze a wider height range and for digital processing. The feasibility of a second-generation FM/cw radar sounder for mobile use with a single antenna should be carefully studied.

REFERENCES

1. Richter, J. H., "High Resolution Tropospheric Radar Sounding," *Radio Science, New Series*, v. 4, p. 1261-1268, December 1969

2. Atlas, E. and Hardy, K. R., "Radar Analysis of the Clear Atmosphere: Angels," p. 401-478 in International Scientific Radio Union, *Progress in Radio Science 1963-1966: Proceedings During XVth General Assembly of URSI, Munich, September 5-15, 1966*, International Scientific Radio Union, 1967

3. Hardy, K. R. and others, "Multiwavelength Backscatter From the Clear Atmosphere," *Journal of Geophysical Research*, v. 71, p. 1537-1552, 15 March 1966

4. Hardy, K. R. and Katz, I., "Probing the Clear Atmosphere With High Power, High Resolution Radars," *Institute of Electrical and Electronics Engineers, Proceedings*, v. 57, p. 468-480, April 1969

5. Saxton, J. A. and others, "Layer Structure of the Troposphere," *Institution of Electrical Engineers, Proceedings*, v. 111, p. 275-283, February 1964

6. Fehlhaber, L. and Grosskopf, J., "An Investigation of the Structure of the Troposphere by Means of a Vertically-Directed Radar," *NTZ Communications Journal*, v. 4, No. 4, p. 185-190, 1965

7. Navy Electronics Laboratory Report 773, *The NEL T21 Microbarographic Recording System*, by C. T. Johnson and J. R. Chiles, 16 April 1957

8. Chicago. University. Laboratory For Atmospheric Probing Technical Report 13, *Waves, Turbulence and Insects as Seen by Ultra High Resolution Radar*, by D. Atlas, J. H. Richter and E. E. Gossard, 15 October 1969

9. Chicago. University. Laboratory For Atmospheric Probing Technical Report 17, *The Measurement of Point Target Speeds With Incoherent Non-Tracking Radar: Insect Speeds in Atmospheric Waves*, by D. Atlas, F. I. Harris and J. H. Richter, 1 April 1970

10. Gossard, E. E. and Munk, W., "On Gravity Waves in the Atmosphere," *Journal of Meteorology*, v. 11, p. 259-269, August 1954

11. Gossard, E. E., Richter, J. H. and Atlas, D., "Internal Waves in the Atmosphere From High Resolution Radar Measurements," *Journal of Geophysical Research* (In press)

12. Atlas, D., Metcalf, J. I., Richter, J. H. and Gossard, E. E., "The Birth of 'CAT' and Microscale Turbulence," *Journal of the Atmospheric Sciences* (In press)

13. Gossard, E. E. and Richter, J. H., "The Shape of Internal Waves of Finite Amplitude From High Resolution Radar Sounding of the Lower Atmosphere," *Journal of the Atmospheric Sciences* (In press)

APPENDIX: SIMULTANEOUS RADAR AND RADIOSONDE SOUNDINGS

In the following, all simultaneous radar and radiosonde soundings performed in the second half of 1969 are shown. All of them are presented in the same format; i.e., the intensity-modulated radar picture is shown to the same height scale as the plots of temperature and relative humidity measured by the sounding balloon. Potential temperature and $N = (n-1)\ 10^6$ (n = refractive index) are computed from these values. Wind speed and direction are also included in the plots. The individual figures do not need special explanation. The excellent agreement between heights of radar returns and refractive index gradients is evident. In several cases a signal is scattered back from the radiosonde, resulting in a slanted line right after launch. The signal is received via sidelobes of the antennas; the trace itself on the photograph does therefore not represent a correct height at the given time scale but is rather the radius vector between radiosonde and antenna. The difference between the actual height and the radius vector is dependent on horizontal wind velocity and rate of rise of the balloon. The various height ranges for the radar picture reflect the resolution used. The 720-meter height range corresponds to 2-meter resolution, the 360-meter range to 1-meter height resolution.

DATE 9 JULY 1969

RADIOSONDE RELEASE TIME 1332

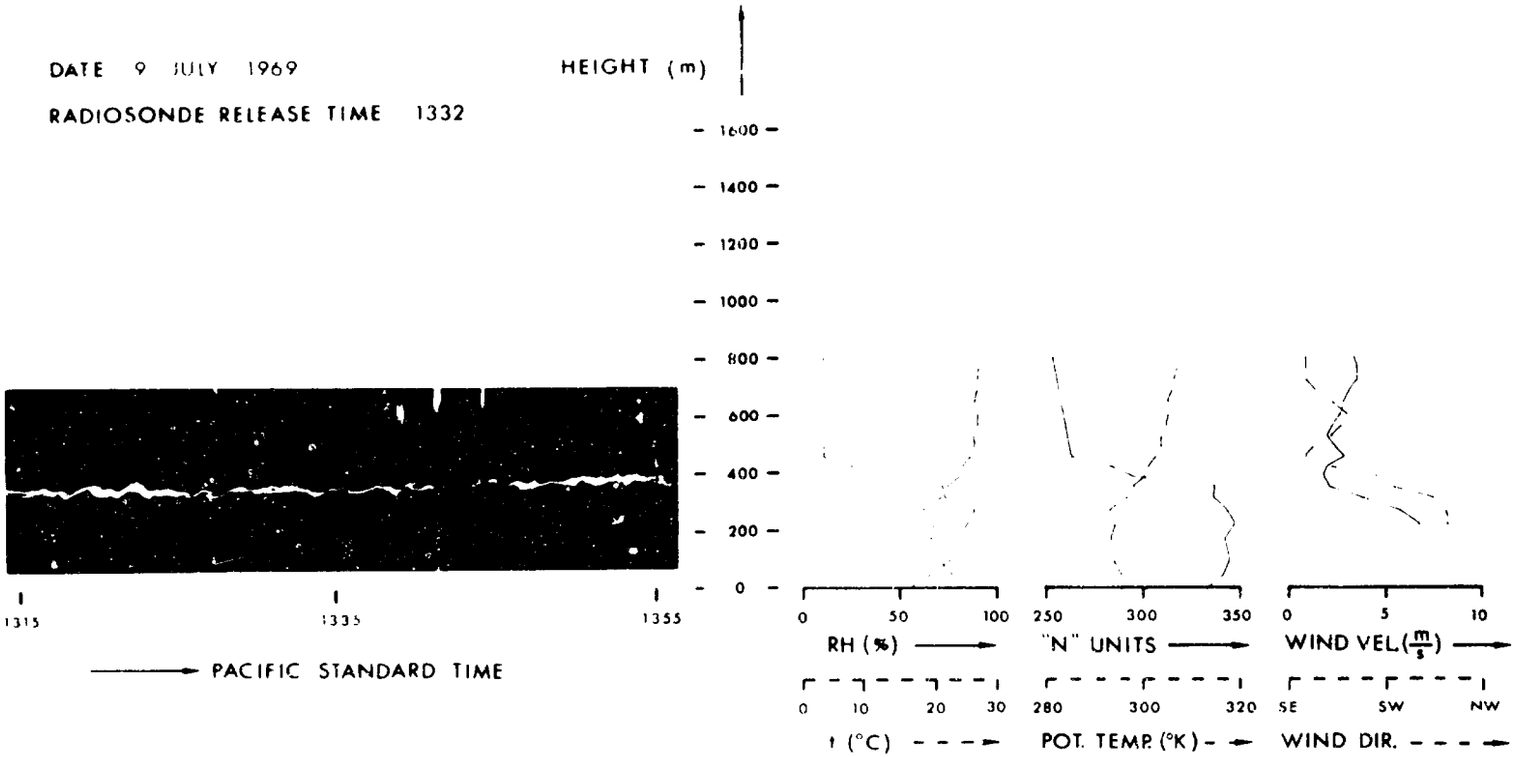

SIMULTANEOUS RADAR AND RADIOSONDE SOUNDINGS

LOCATION: 32°42' N. LAT., 117° 15' W. LONG., 31 m ABOVE MSL.

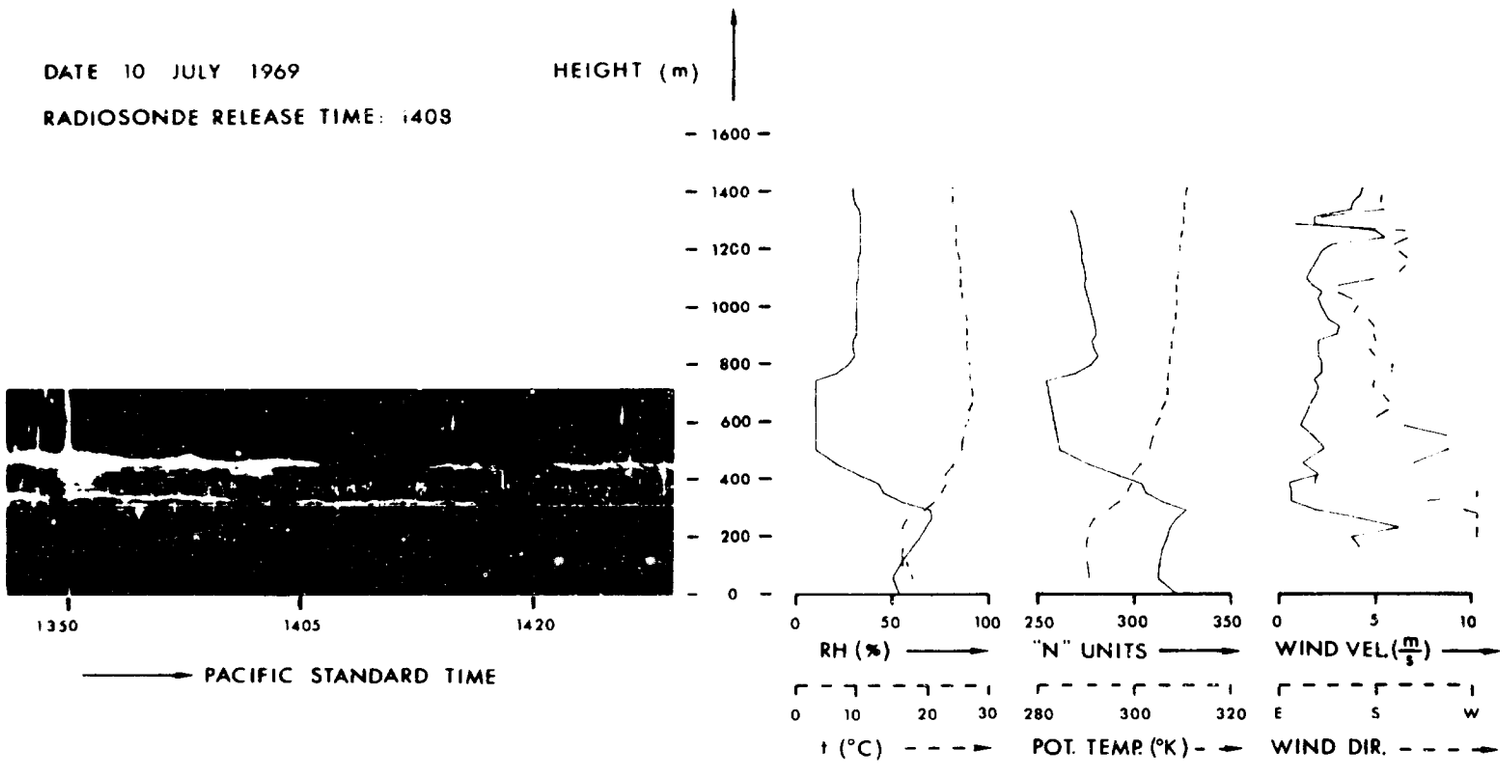

SIMULTANEOUS RADAR AND RADIOSONDE SOUNDINGS

LOCATION: 32°42' N. LAT., 117° 15' W. LONG., 31 m ABOVE MSL.

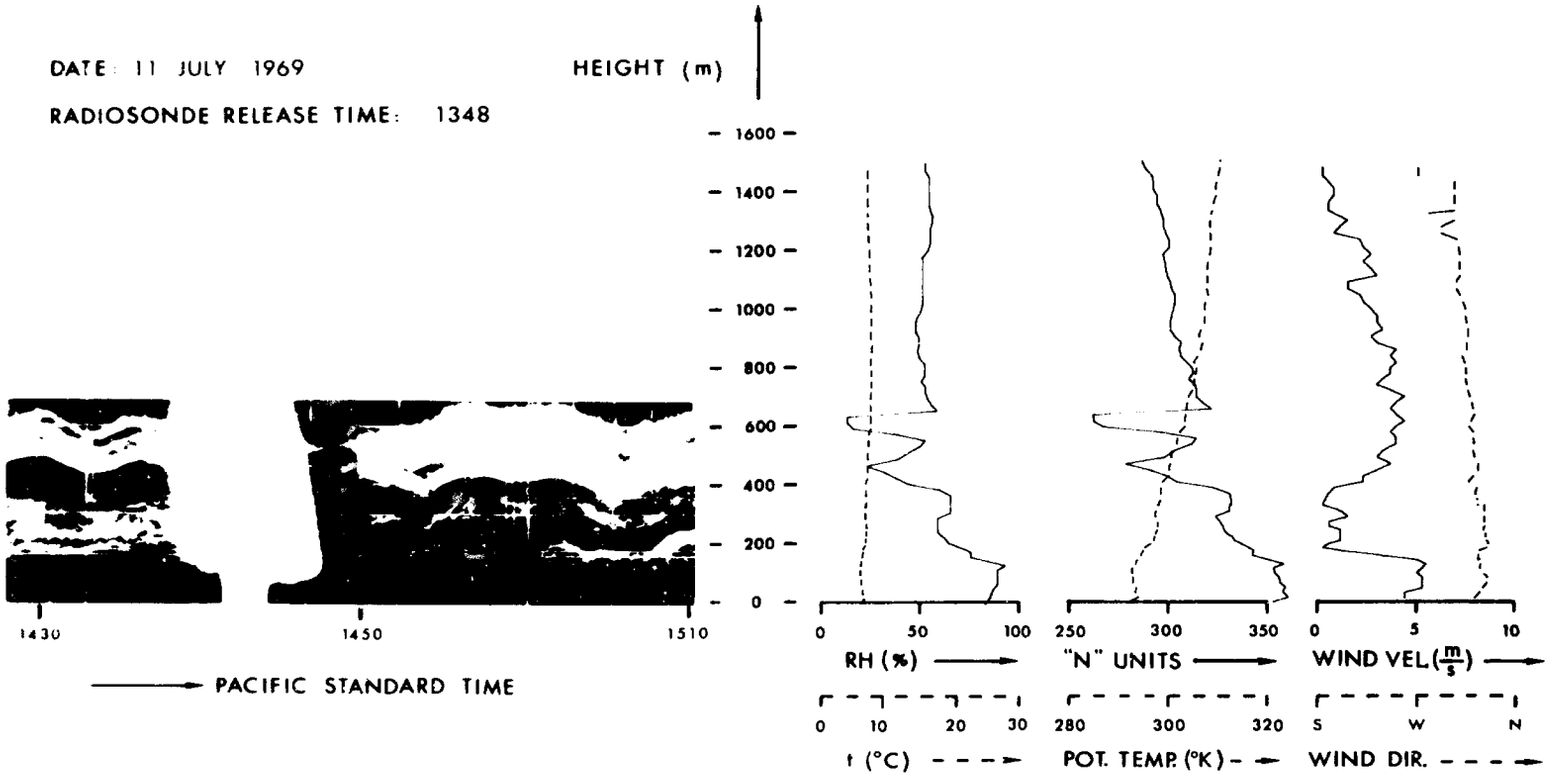

SIMULTANEOUS RADAR AND RADIOSONDE SOUNDINGS

LOCATION: 32°42′ N. LAT., 117° 15′ W. LONG., 31 m ABOVE MSL.

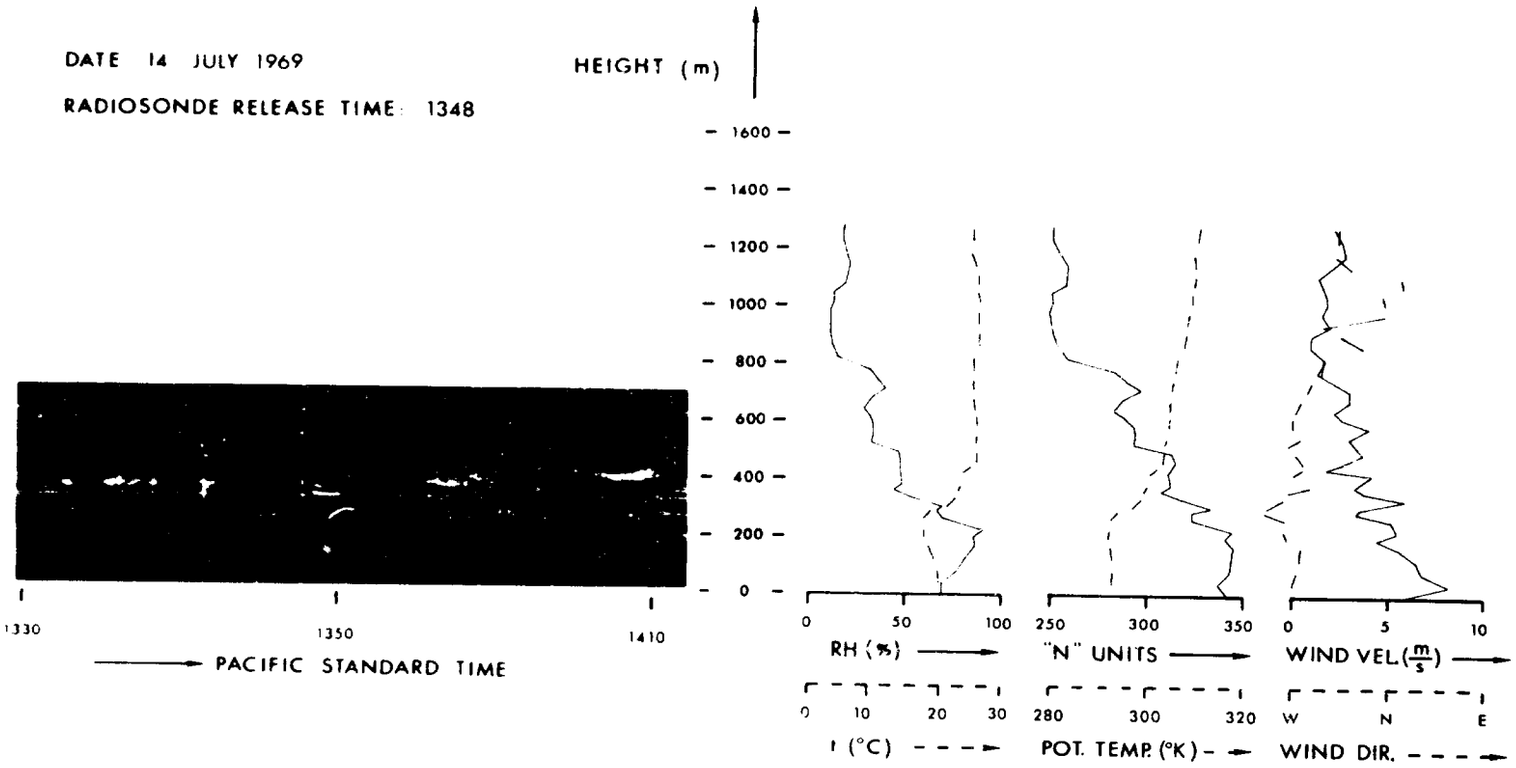

SIMULTANEOUS RADAR AND RADIOSONDE SOUNDINGS

LOCATION: 32°42′ N. LAT., 117° 15′ W. LONG., 31 m ABOVE MSL.

DATE 17 JULY 1969

RADIOSONDE RELEASE TIME 1331

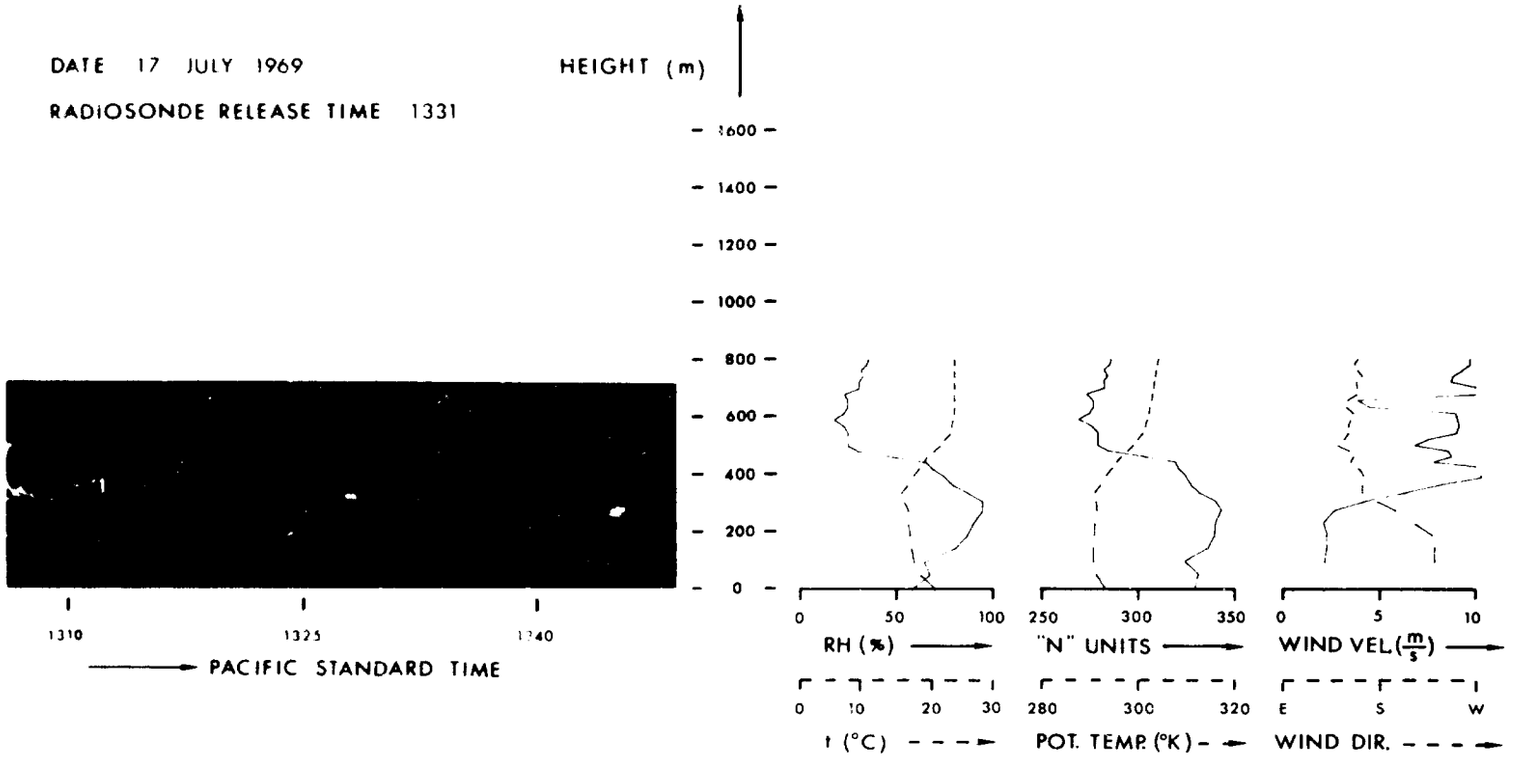

SIMULTANEOUS RADAR AND RADIOSONDE SOUNDINGS

LOCATION: 32°42' N. LAT., 117° 15' W. LONG., 31 m ABOVE MSL.

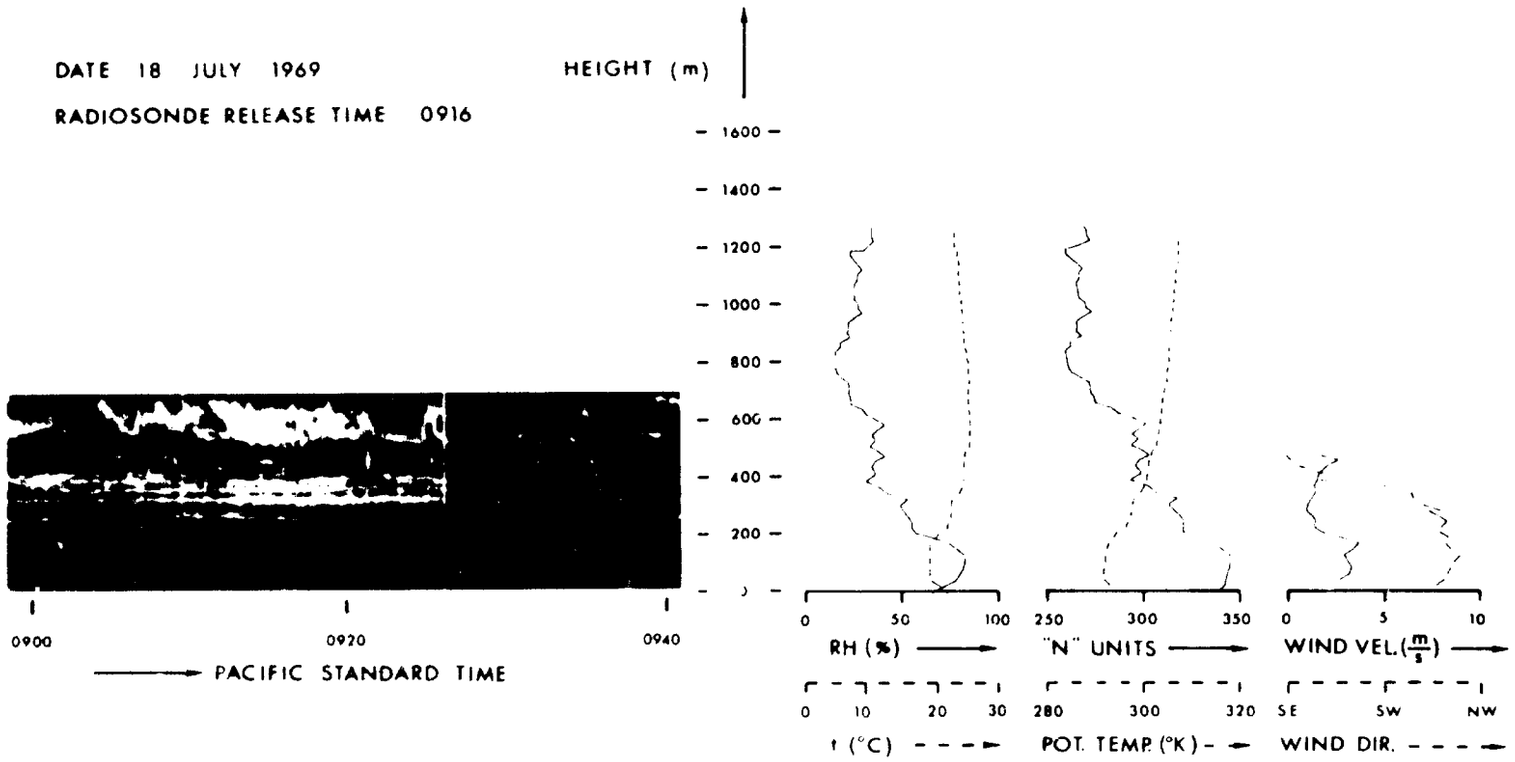

SIMULTANEOUS RADAR AND RADIOSONDE SOUNDINGS

LOCATION: 32°42' N LAT., 117° 15' W LONG., 31 m ABOVE MSL

8

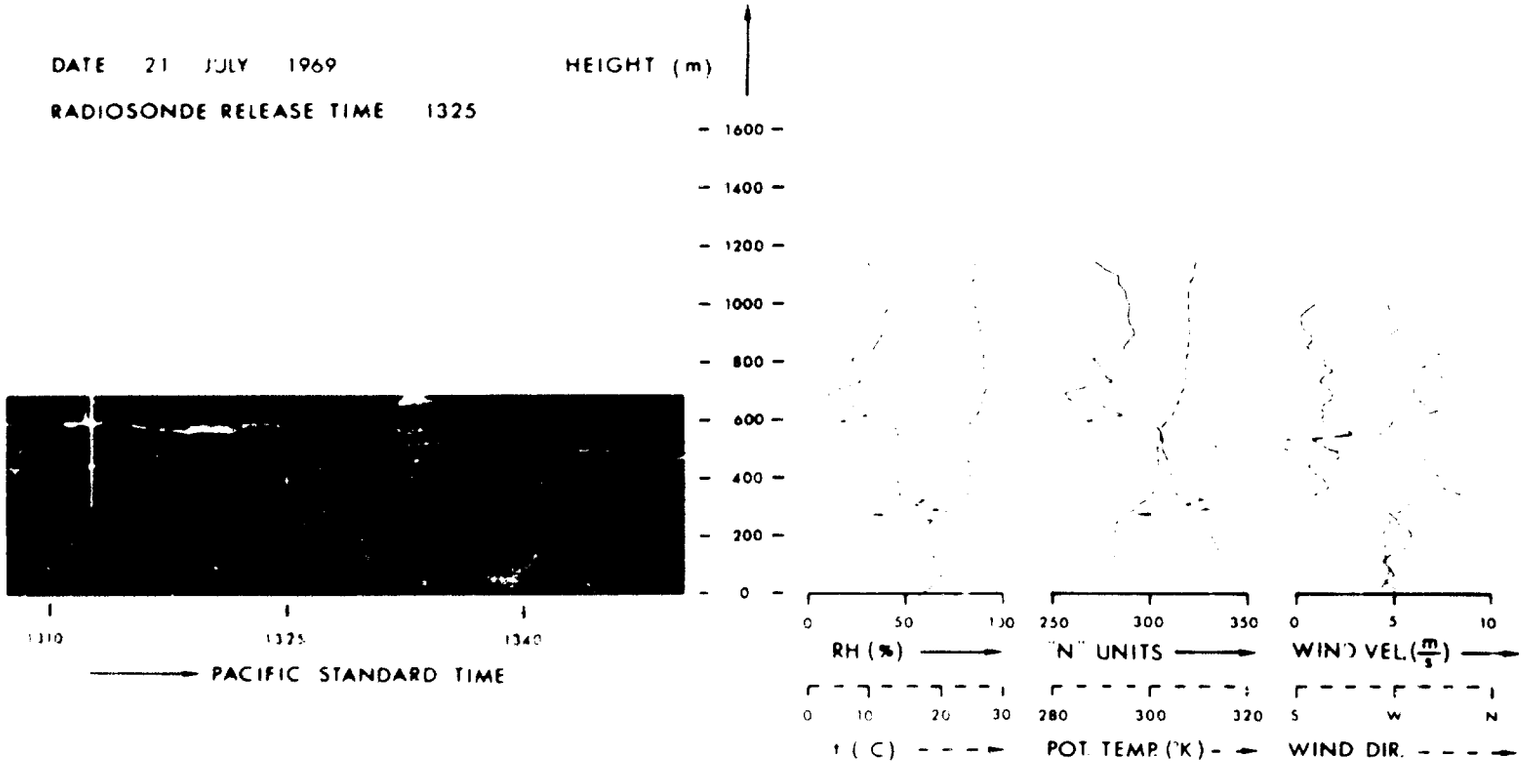

SIMULTANEOUS RADAR AND RADIOSONDE SOUNDINGS

LOCATION 32 42' N LAT., 117 15' W LONG., 31 m ABOVE MSL

DATE 23 JULY 1969

RADIOSONDE RELEASE TIME 1313

1300 1315 1330

PACIFIC STANDARD TIME

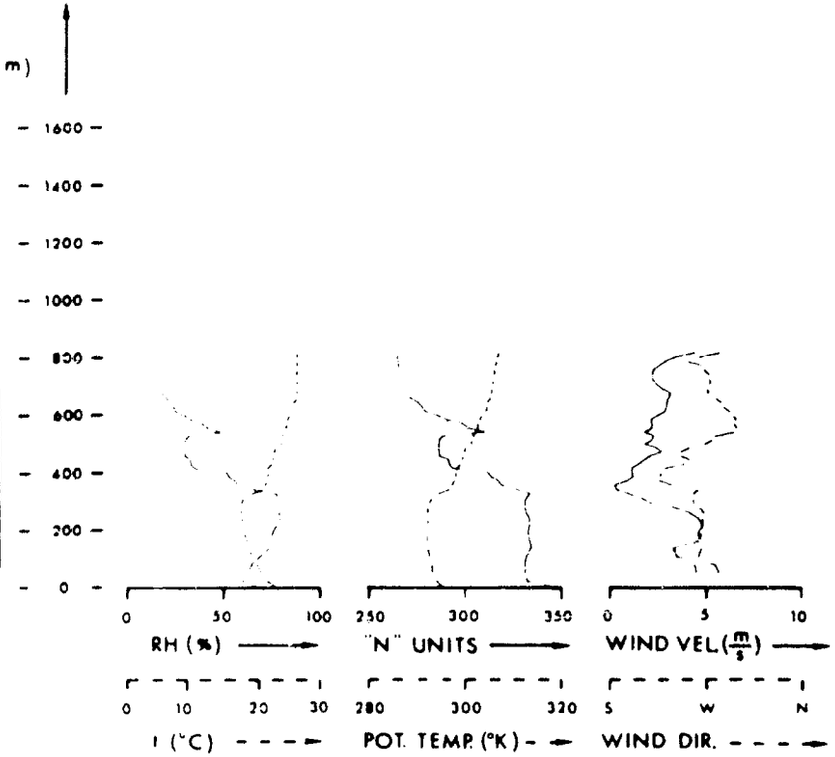

SIMULTANEOUS RADAR AND RADIOSONDE SOUNDINGS

LOCATION 32°42' N LAT., 117° 15' W LONG., 31 m ABOVE MSL.

DATE 24 JULY 1969

RADIOSONDE RELEASE TIME 1434

PACIFIC STANDARD TIME

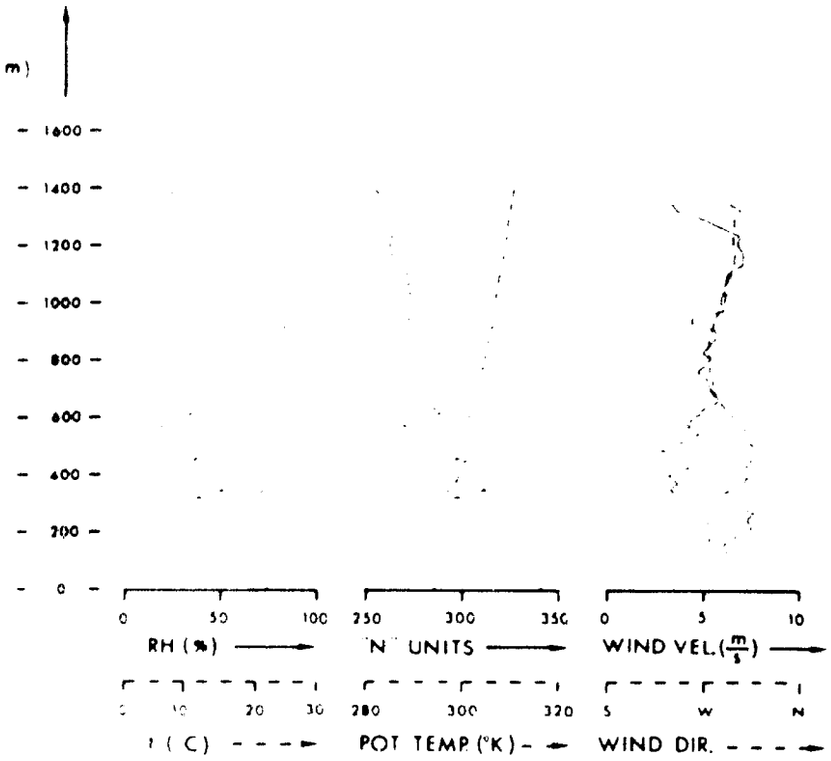

SIMULTANEOUS RADAR AND RADIOSONDE SOUNDINGS

LOCATION 32° 42' N LAT., 117° 15' W LONG., 31 m ABOVE MSL

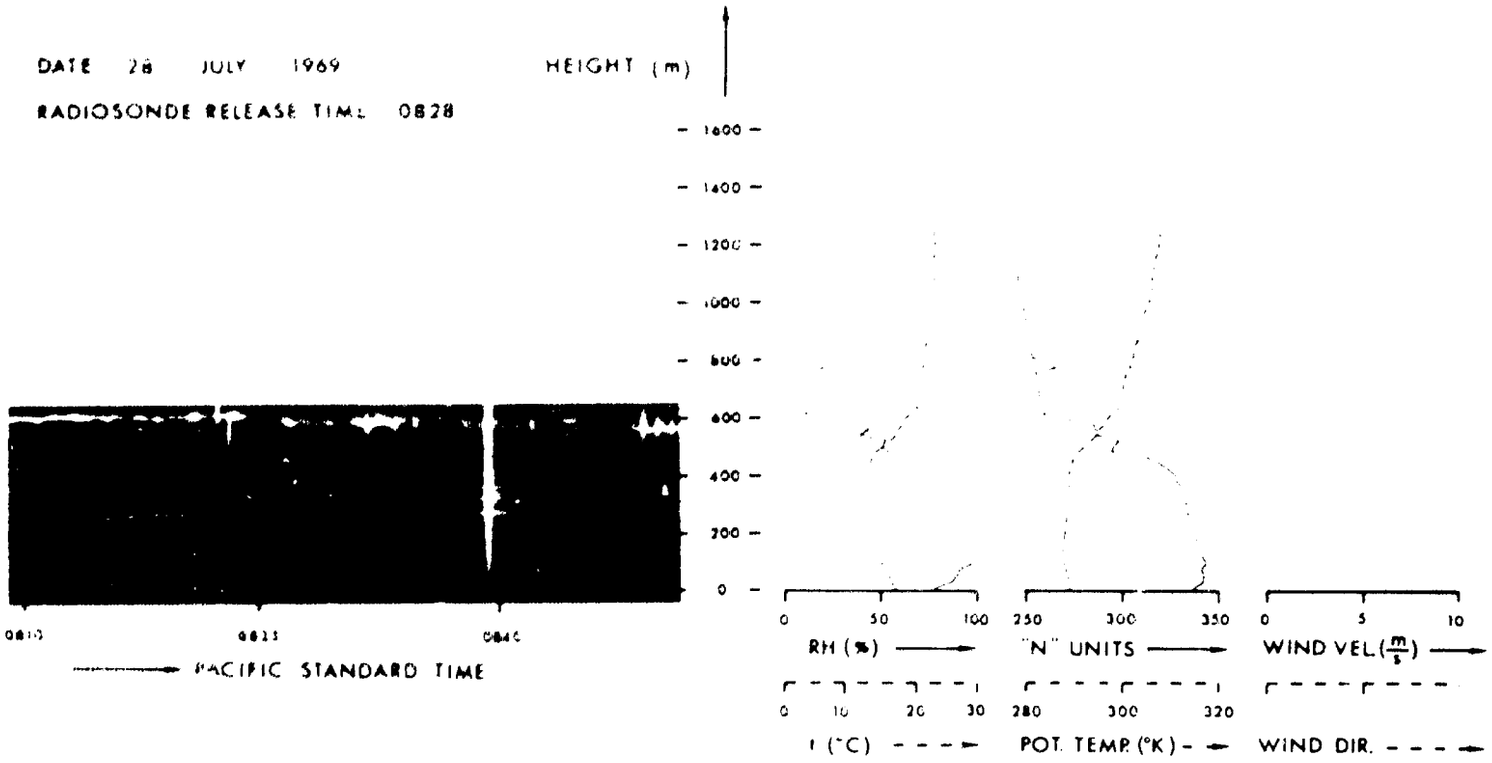

SIMULTANEOUS RADAR AND RADIOSONDE SOUNDINGS

LOCATION: 32°49' N LAT., 117° 15' W LONG., 31 m ABOVE MSL

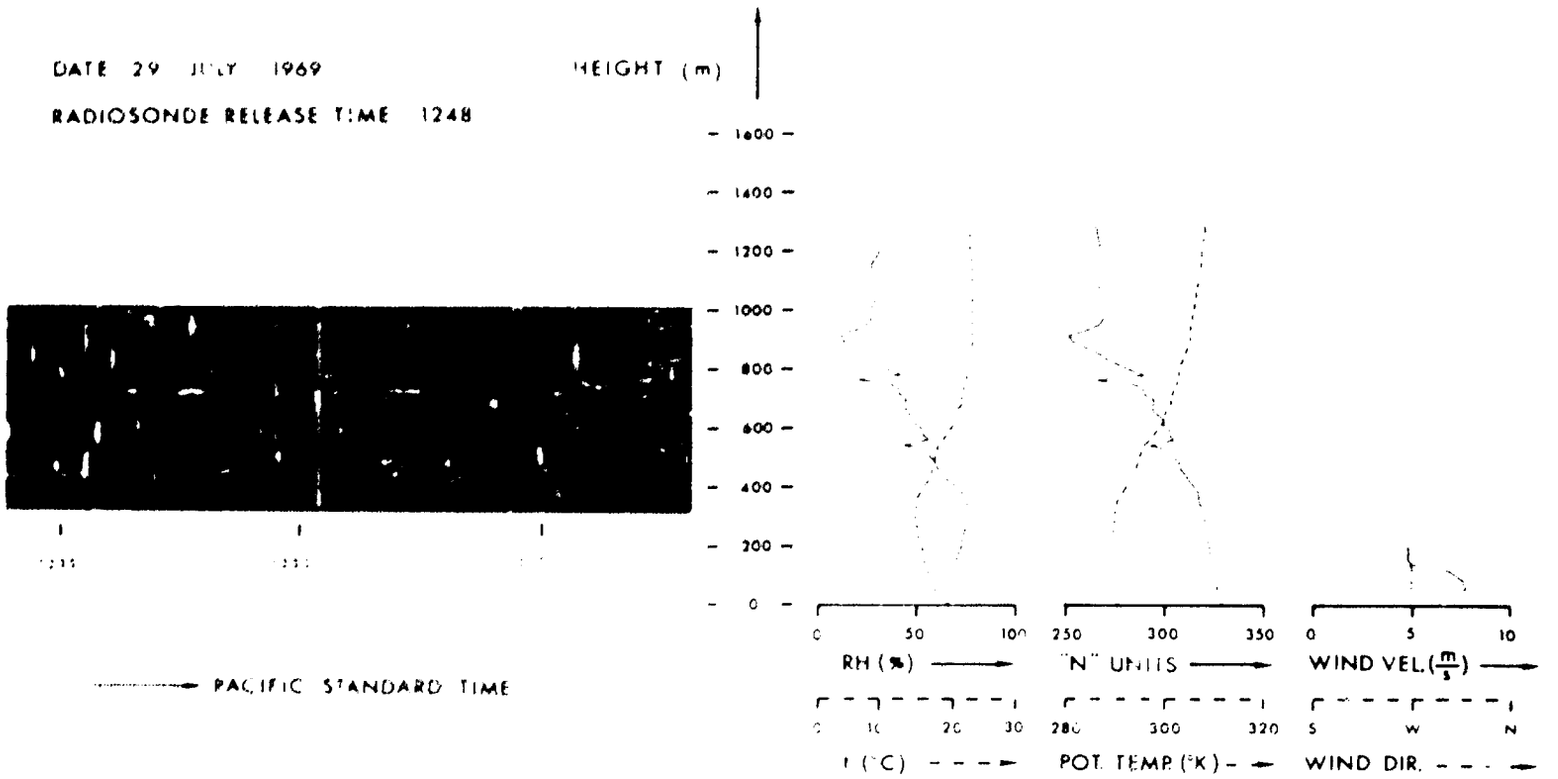

SIMULTANEOUS RADAR AND RADIOSONDE SOUNDINGS

LOCATION: 32° 42' N LAT, 117° 15' W LONG, 31 m ABOVE MSL

DATE 30 JULY 1969

RADIOSONDE RELEASE TIME: 0916

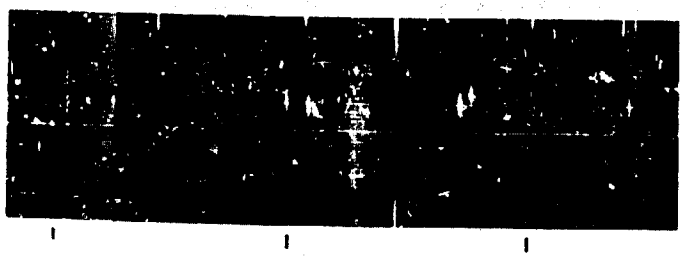

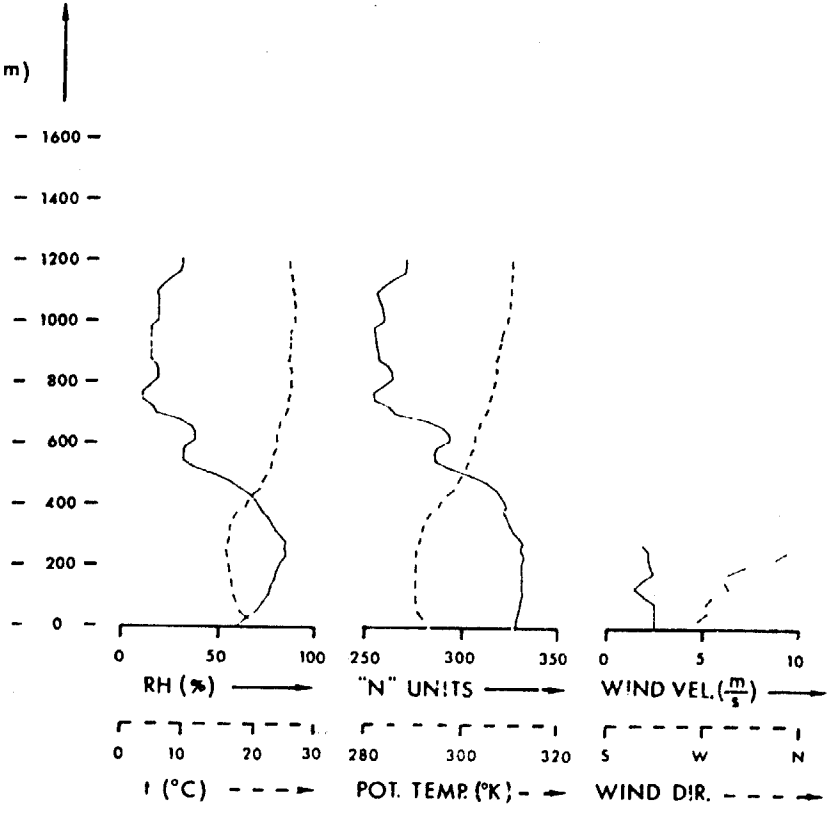

SIMULTANEOUS RADAR AND RADIOSONDE SOUNDINGS

LOCATION: 32°42' N. LAT., 117° 15' W. LONG., 31 m ABOVE MSL.

DATE: 31 JULY 1969

RADIOSONDE RELEASE TIME: 1238

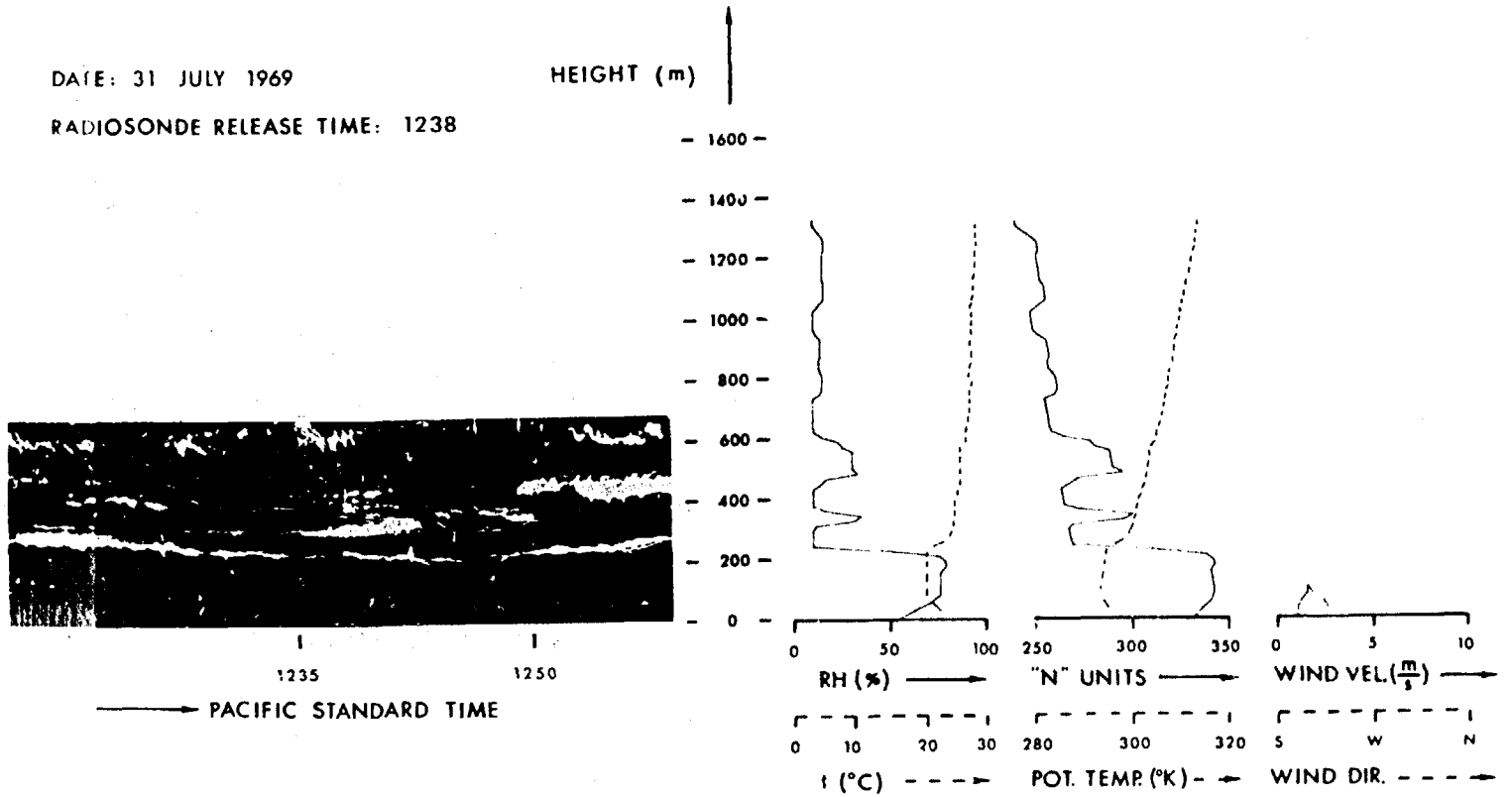

SIMULTANEOUS RADAR AND RADIOSONDE SOUNDINGS

LOCATION: 32°42' N. LAT., 117° 15' W. LONG., 31 m ABOVE MSL.

DATE: 1 AUG. 1969

RADIOSONDE RELEASE TIME: 1408

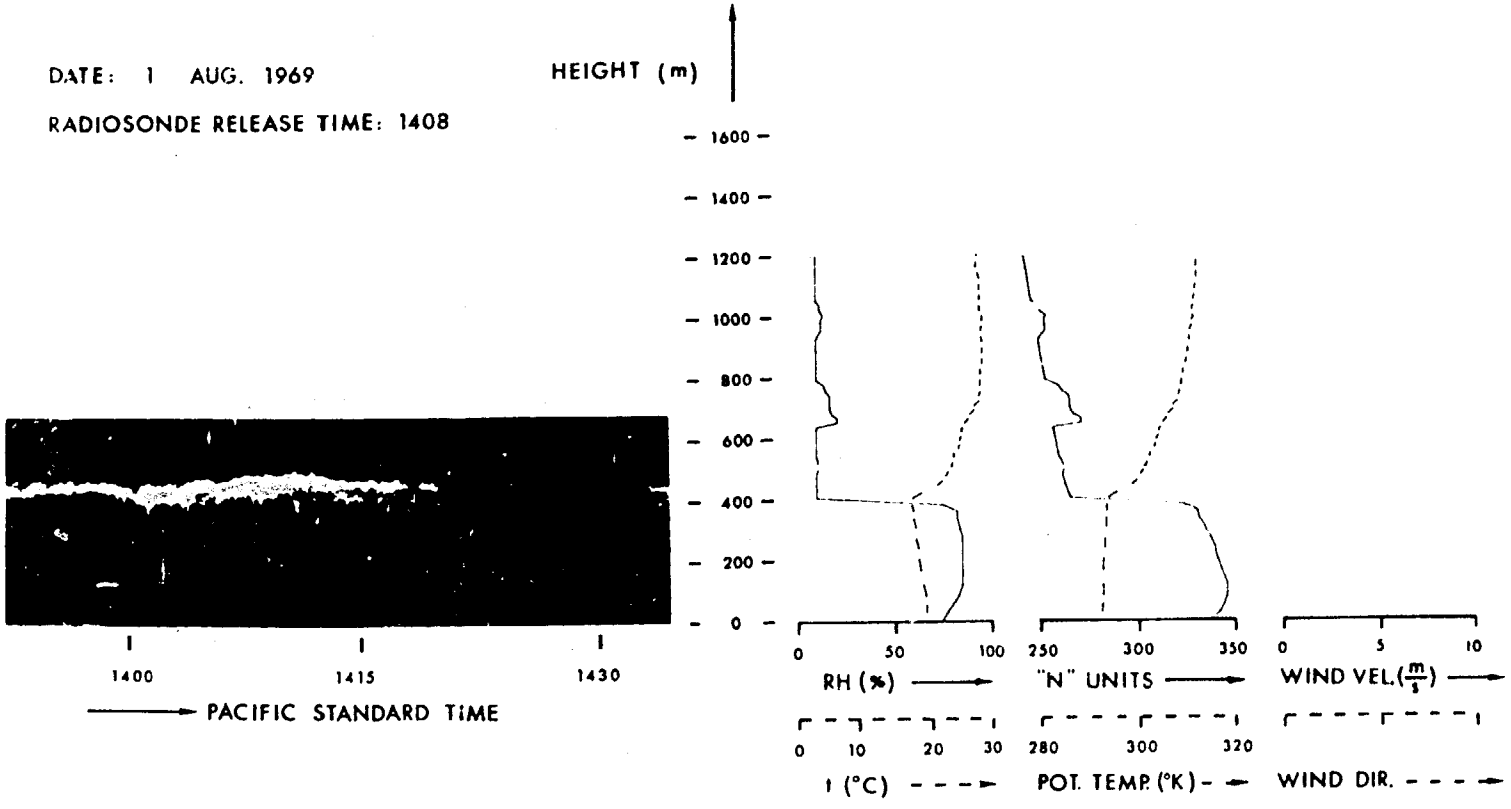

SIMULTANEOUS RADAR AND RADIOSONDE SOUNDINGS

LOCATION: 32°42' N. LAT., 117° 15' W. LONG., 31 m ABOVE MSL.

DATE: 4 AUG. 1969

RADIOSONDE RELEASE TIME: 1319

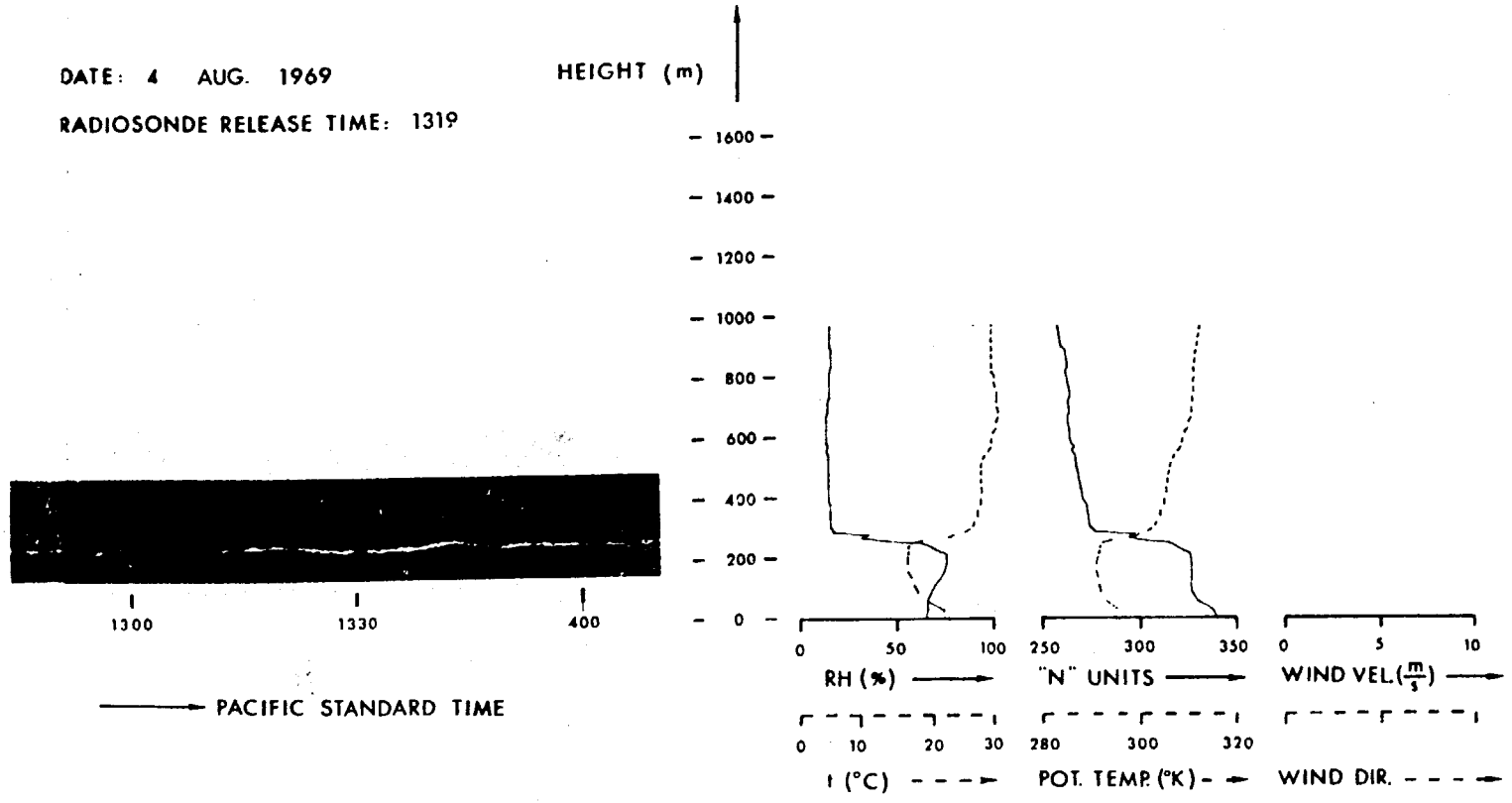

SIMULTANEOUS RADAR AND RADIOSONDE SOUNDINGS

LOCATION: 32°42' N. LAT., 117° 15' W. LONG., 31 m ABOVE MSL.

DATE: 5 AUG. 1969

RADIOSONDE RELEASE TIME: 1158

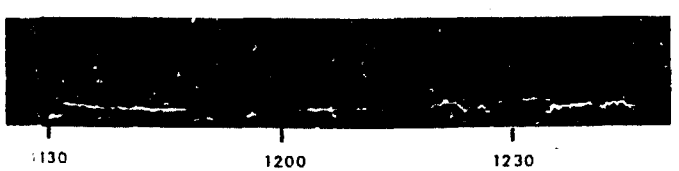

PACIFIC STANDARD TIME

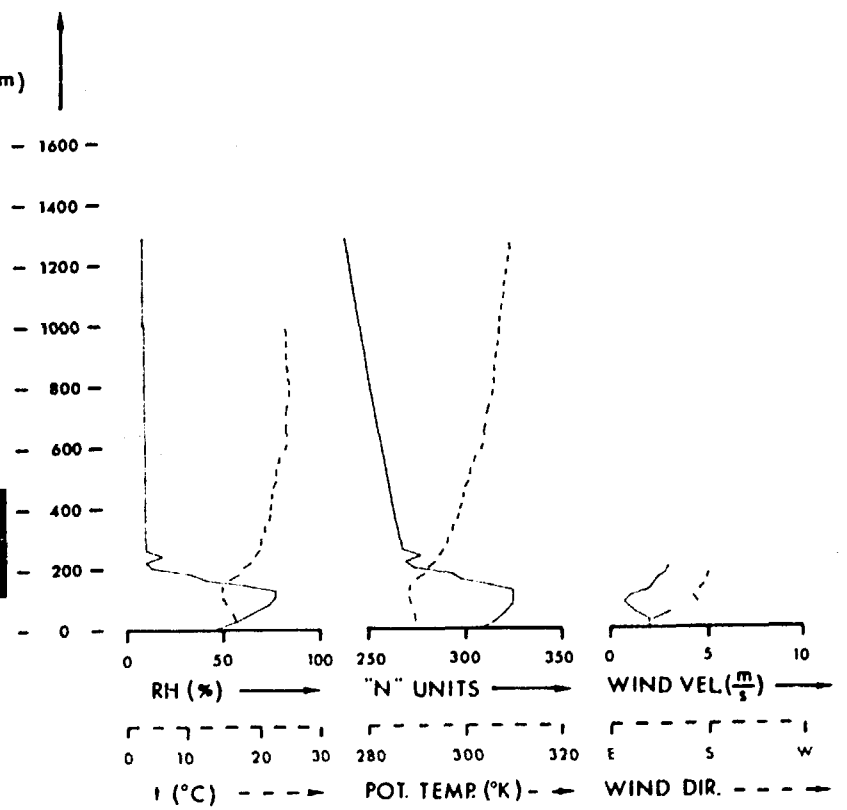

SIMULTANEOUS RADAR AND RADIOSONDE SOUNDINGS

LOCATION: 32°42' N. LAT., 117° 15' W. LONG., 31 m ABOVE MSL.

DATE: 6 AUG. 1969

RADIOSONDE RELEASE TIME: 1349

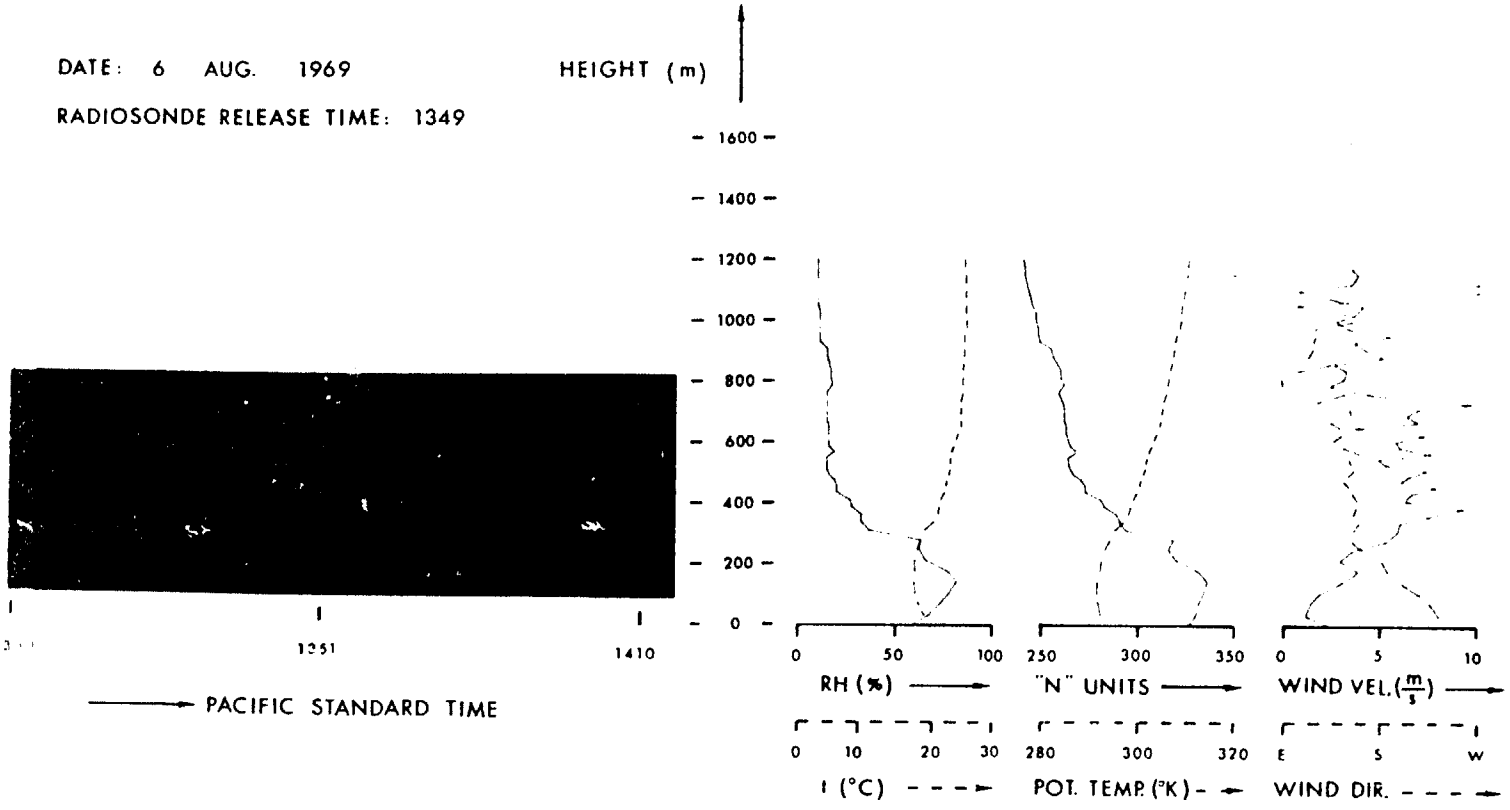

SIMULTANEOUS RADAR AND RADIOSONDE SOUNDINGS

LOCATION: 32°42' N. LAT., 117° 15' W. LONG., 31 m ABOVE MSL.

DATE: 7 AUG. 1969

RADIOSONDE RELEASE TIME: 1247

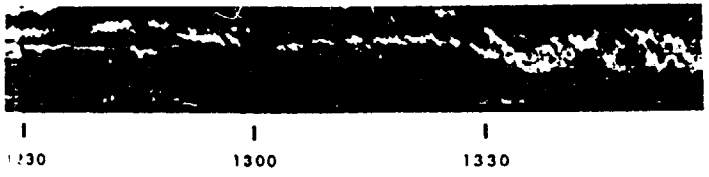

PACIFIC STANDARD TIME

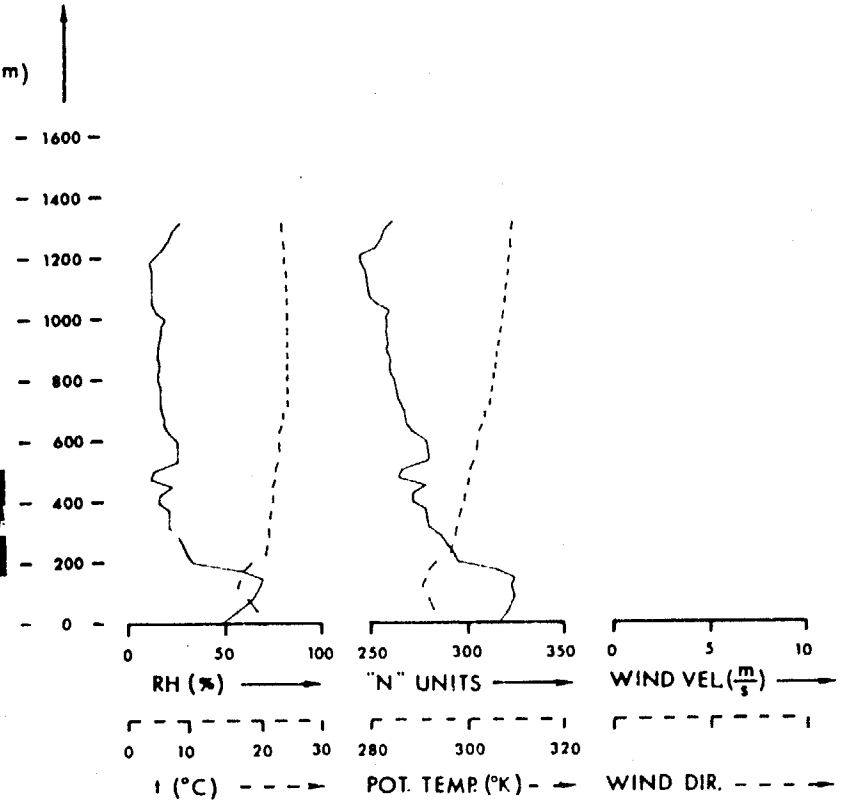

SIMULTANEOUS RADAR AND RADIOSONDE SOUNDINGS

LOCATION: 32°42' N. LAT., 117° 15' W. LONG., 31 m ABOVE MSL.

3

DATE: 14 NOV. 1969

RADIOSONDE RELEASE TIME: 1500

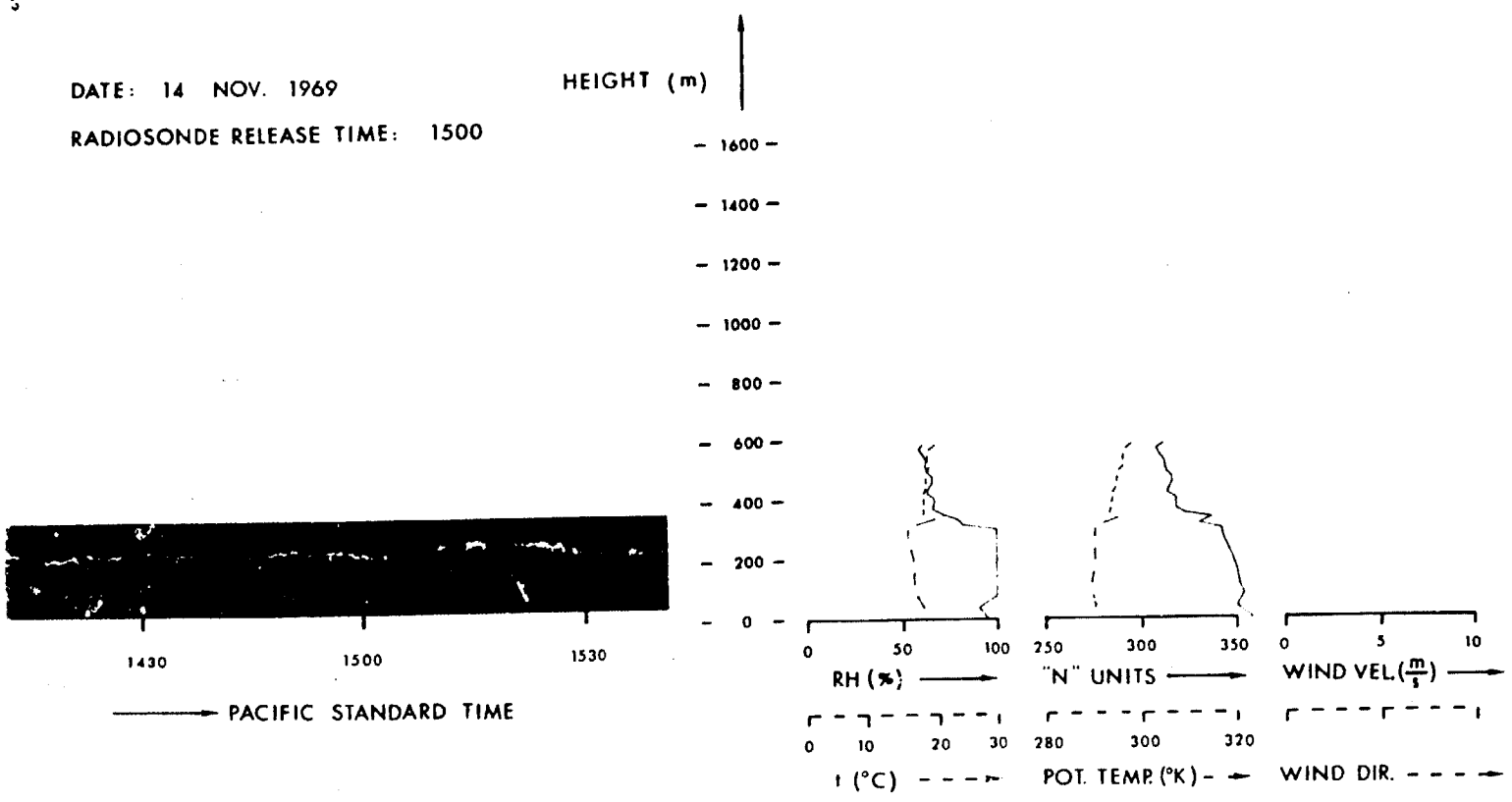

SIMULTANEOUS RADAR AND RADIOSONDE SOUNDINGS

LOCATION: 32°42' N. LAT., 117° 15' W. LONG., 31 m ABOVE MSL.

DATE: 18 NOV. 1969

RADIOSONDE RELEASE TIME: 1339

1300 1330 1400

PACIFIC STANDARD TIME

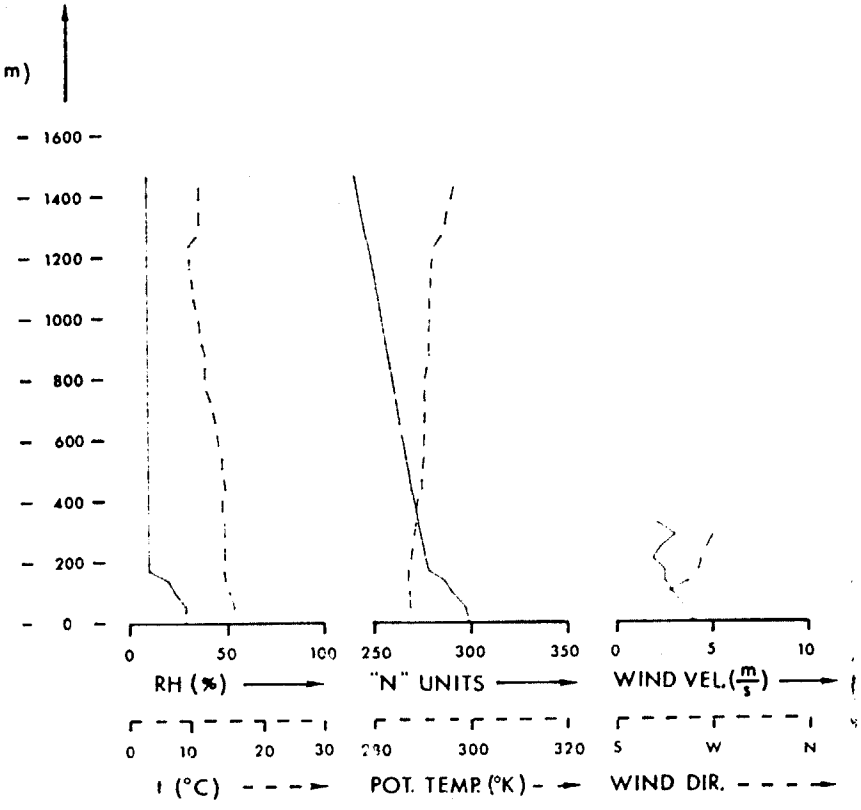

SIMULTANEOUS RADAR AND RADIOSONDE SOUNDINGS

LOCATION: 32°42' N.LAT., 117° 15' W. LONG., 31 m ABOVE MSL.

DATE: 19 NOV. 1969

RADIOSONDE RELEASE TIME: 1345

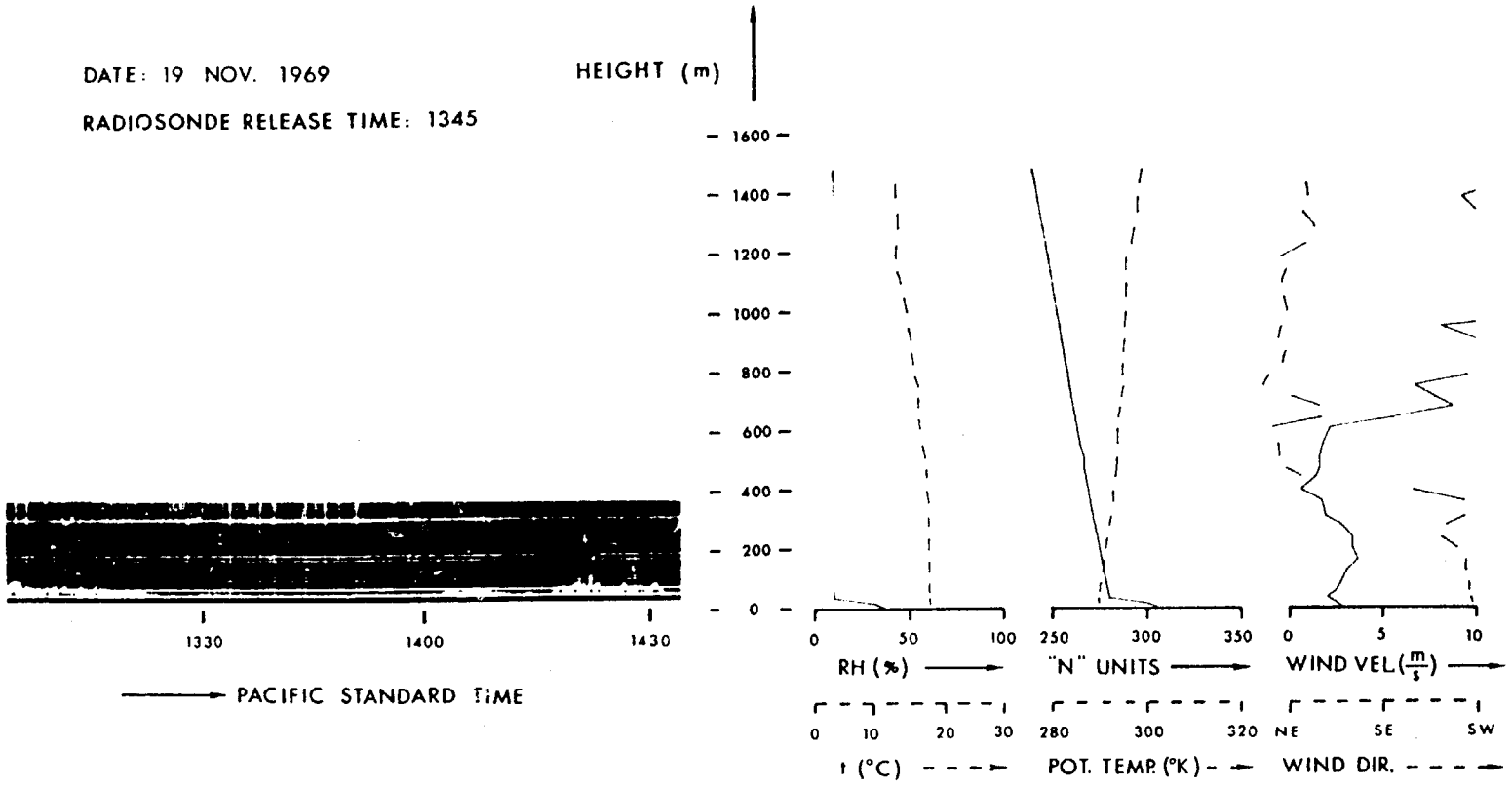

SIMULTANEOUS RADAR AND RADIOSONDE SOUNDINGS

LOCATION: 32°42' N. LAT., 117° 15' W. LONG., 31 m ABOVE MSL.

DATE: 24 NOV. 1969

RADIOSONDE RELEASE TIME: 1152

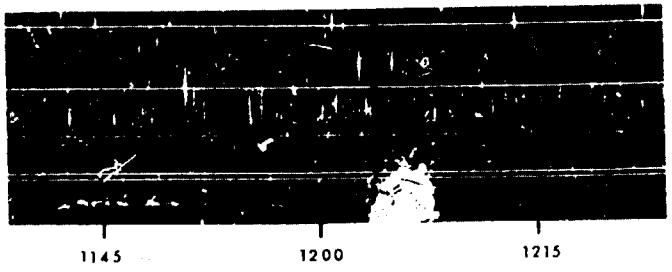

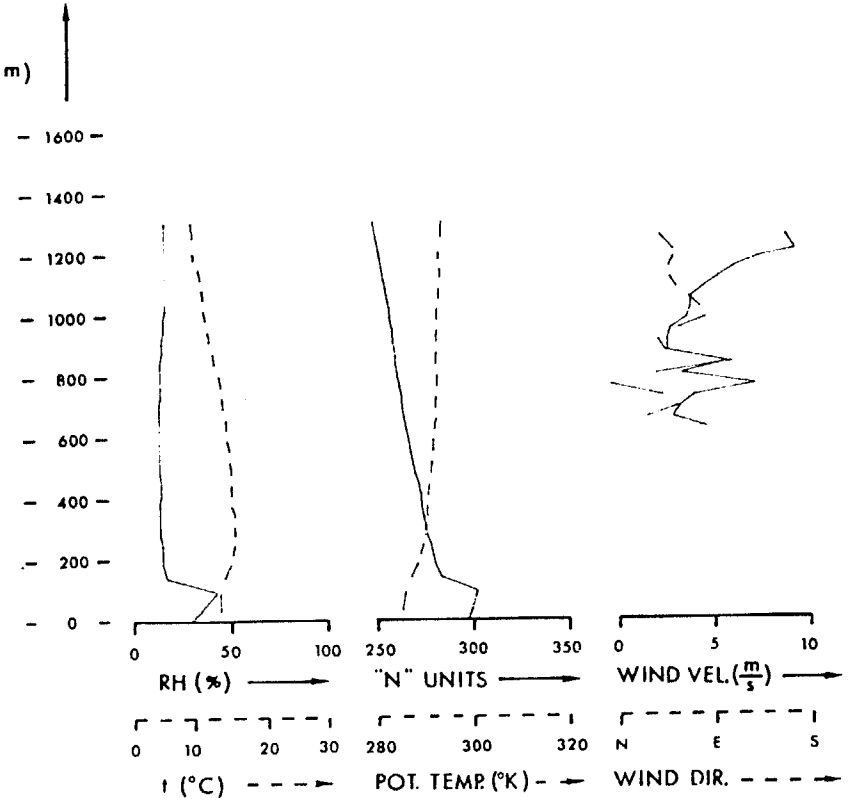

SIMULTANEOUS RADAR AND RADIOSONDE SOUNDINGS

LOCATION: 32°42' N. LAT., 117° 15' W. LONG., 31 m ABOVE MSL.

DATE: 12 DEC. 1969

RADIOSONDE RELEASE TIME: 1417

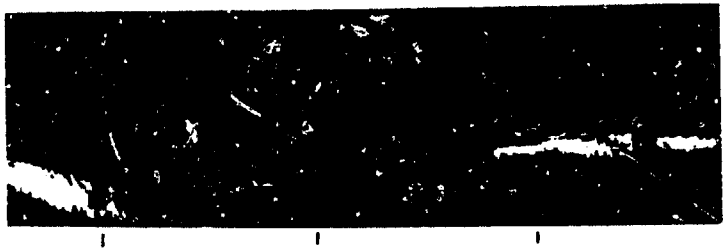

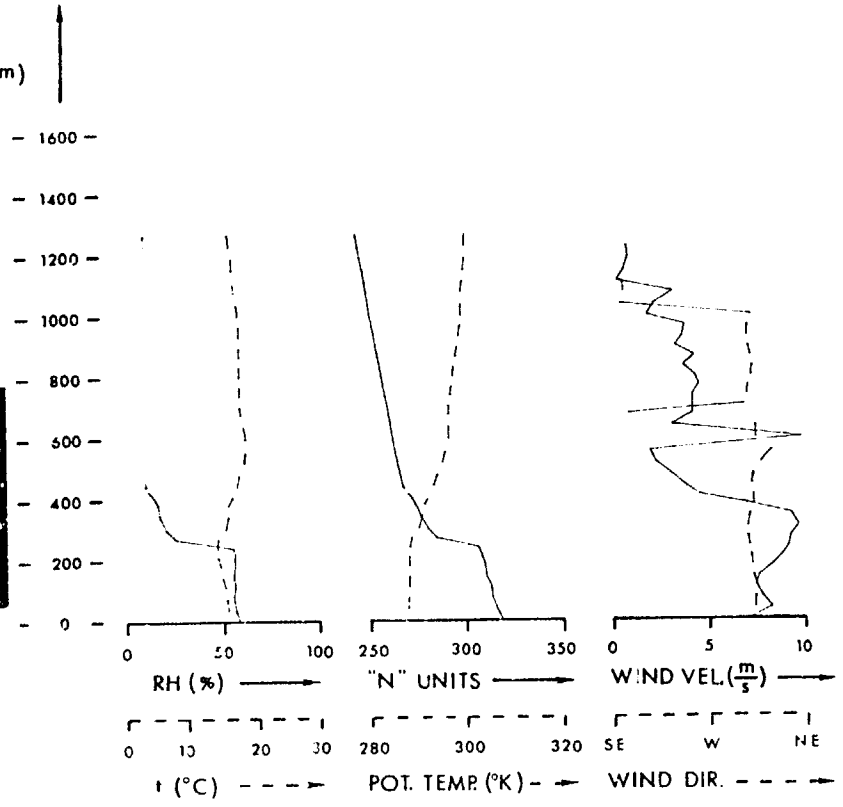

SIMULTANEOUS RADAR AND RADIOSONDE SOUNDINGS

LOCATION: 32°42' N.LAT., 117° 15' W.LONG., 31 m ABOVE MSL.

DATE: 15 DEC. 1969

RADIOSONDE RELEASE TIME: 1337

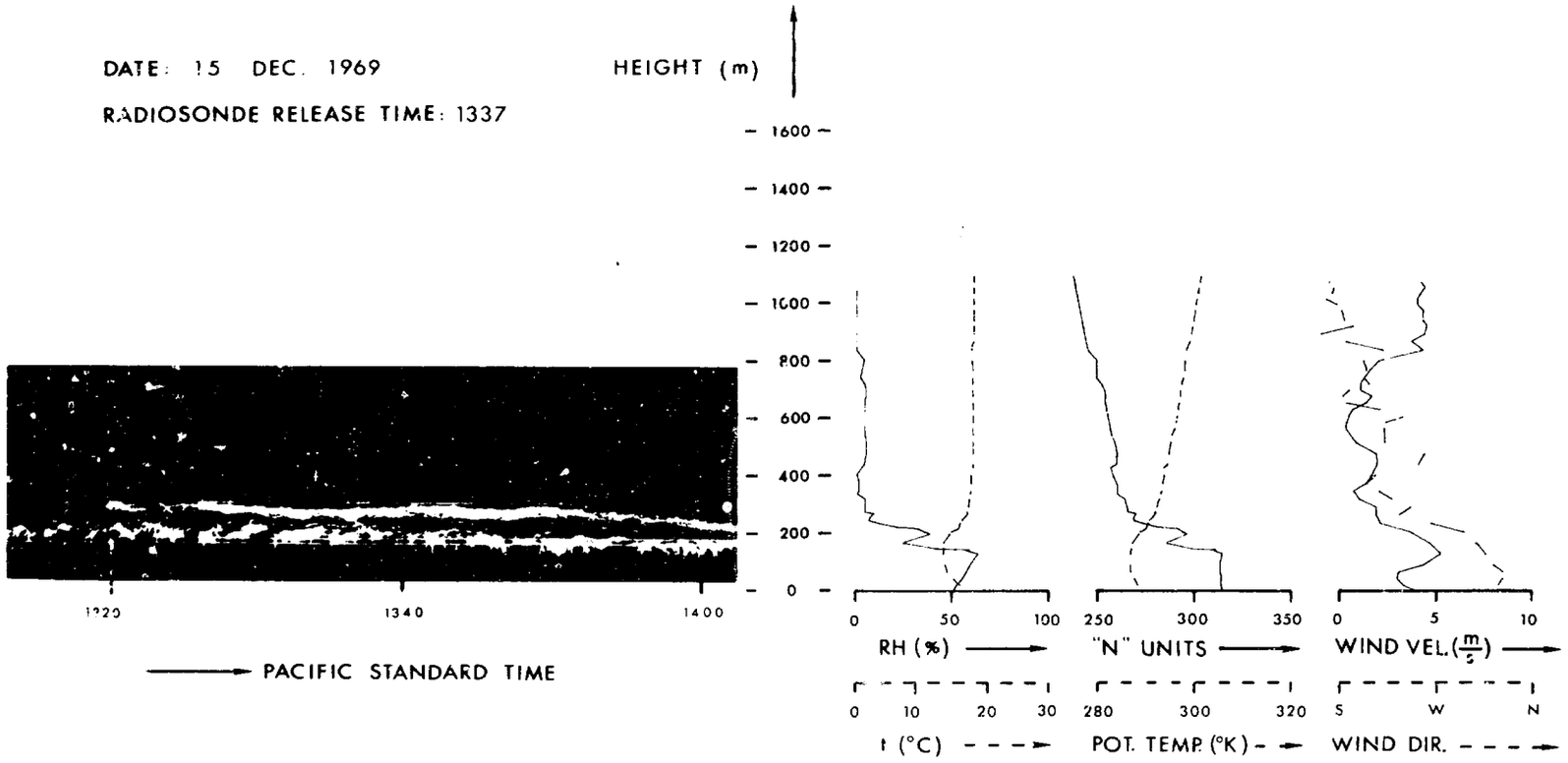

SIMULTANEOUS RADAR AND RADIOSONDE SOUNDINGS

LOCATION: 32°42′ N. LAT., 117° 15′ W. LONG., 31 m ABOVE MSL.

DATE: 16 DEC. 1969

RADIOSONDE RELEASE TIME: 1343

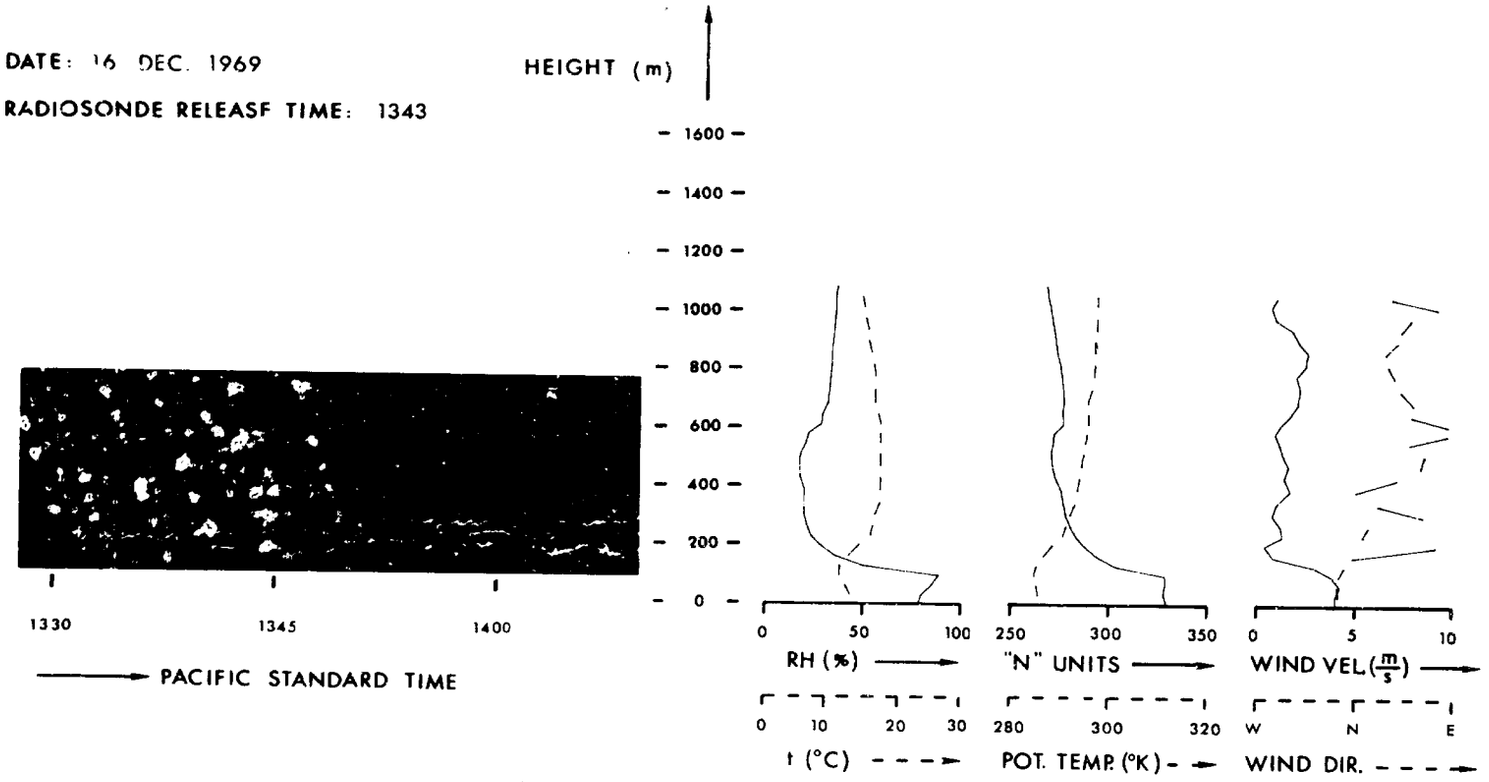

SIMULTANEOUS RADAR AND RADIOSONDE SOUNDINGS

LOCATION: 32°42′ N. LAT., 117° 15′ W. LONG., 31 m ABOVE MSL.

DATE: 17 DEC. 1969

RADIOSONDE RELEASE TIME: 1339

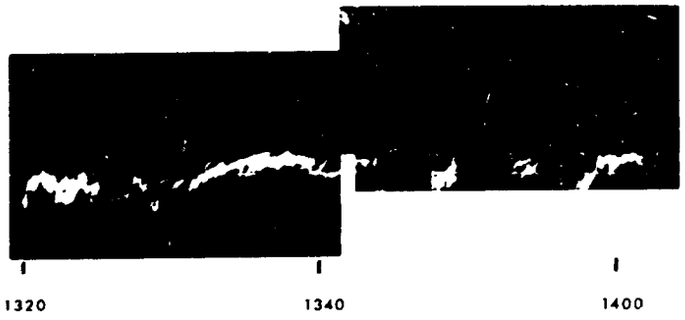

PACIFIC STANDARD TIME

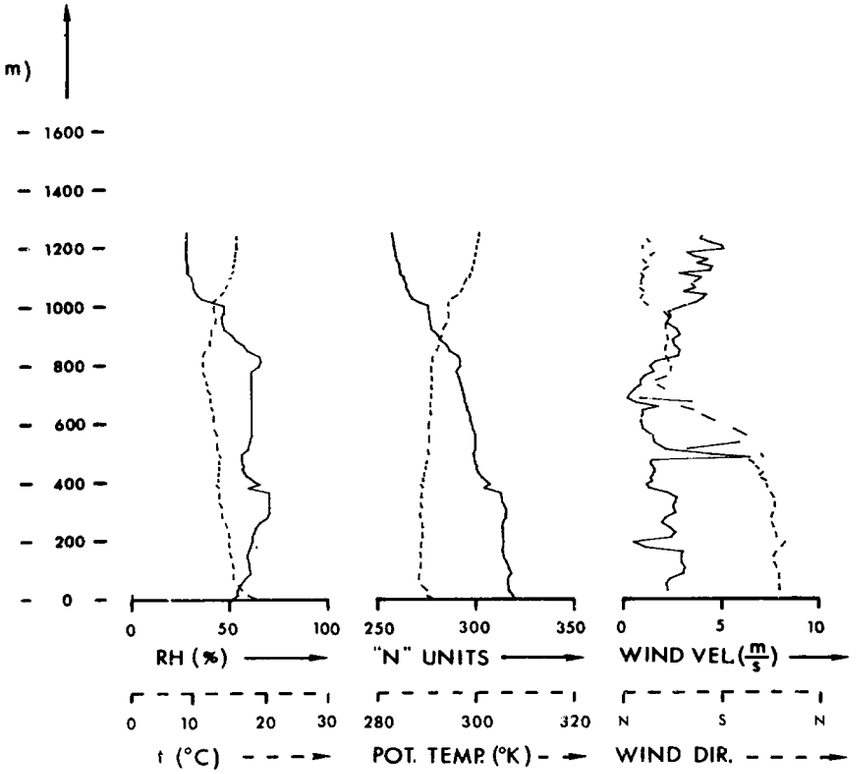

SIMULTANEOUS RADAR AND RADIOSONDE SOUNDINGS

LOCATION: 32°42' N. LAT., 117° 15' W. LONG., 31 m ABOVE MSL.

DATE: 18 DEC 1969

RADIOSONDE RELEASE TIME: 1430

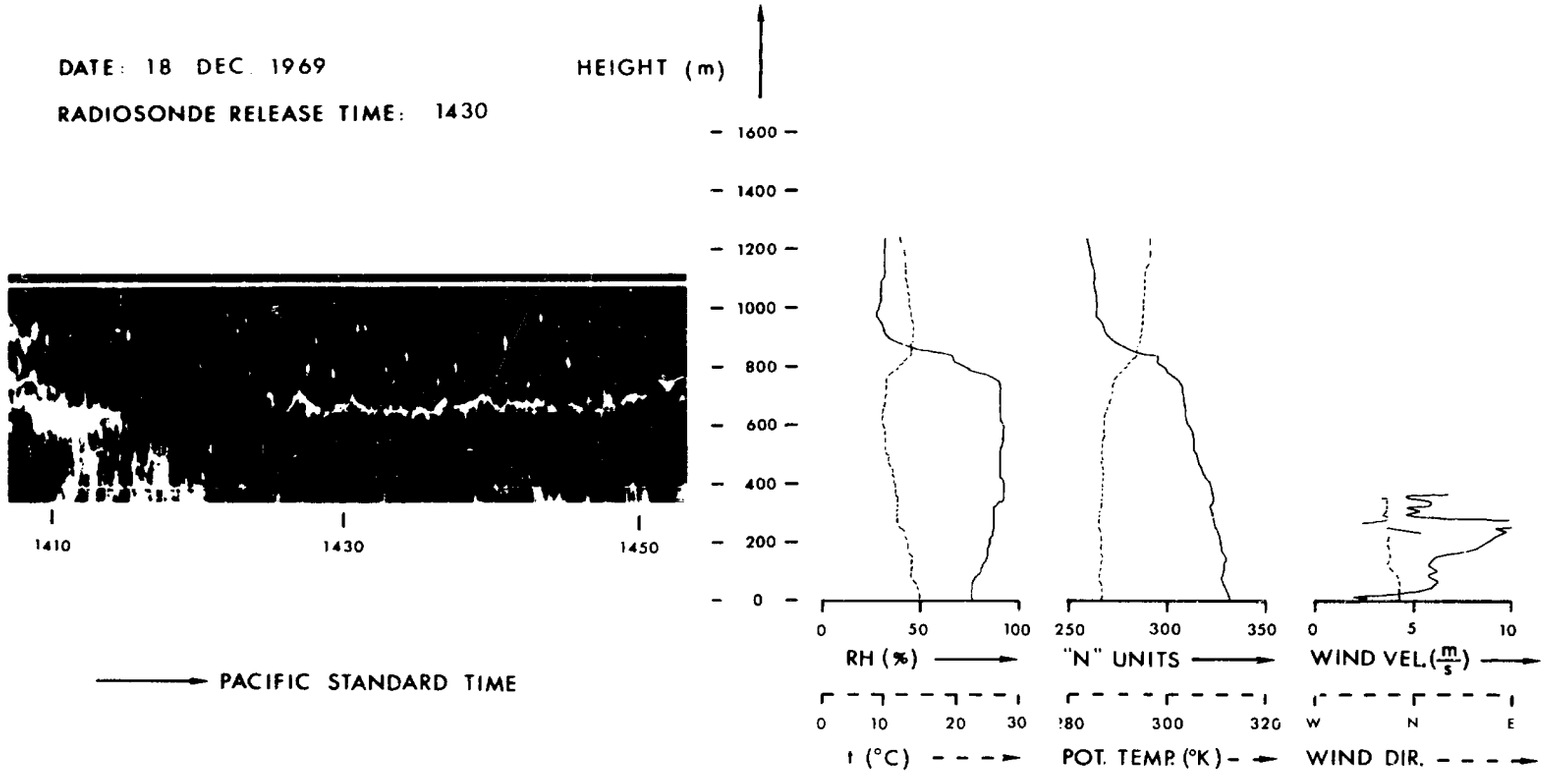

SIMULTANEOUS RADAR AND RADIOSONDE SOUNDINGS

LOCATION: 32°42′ N. LAT., 117° 15′ W. LONG., 31 m ABOVE MSL.

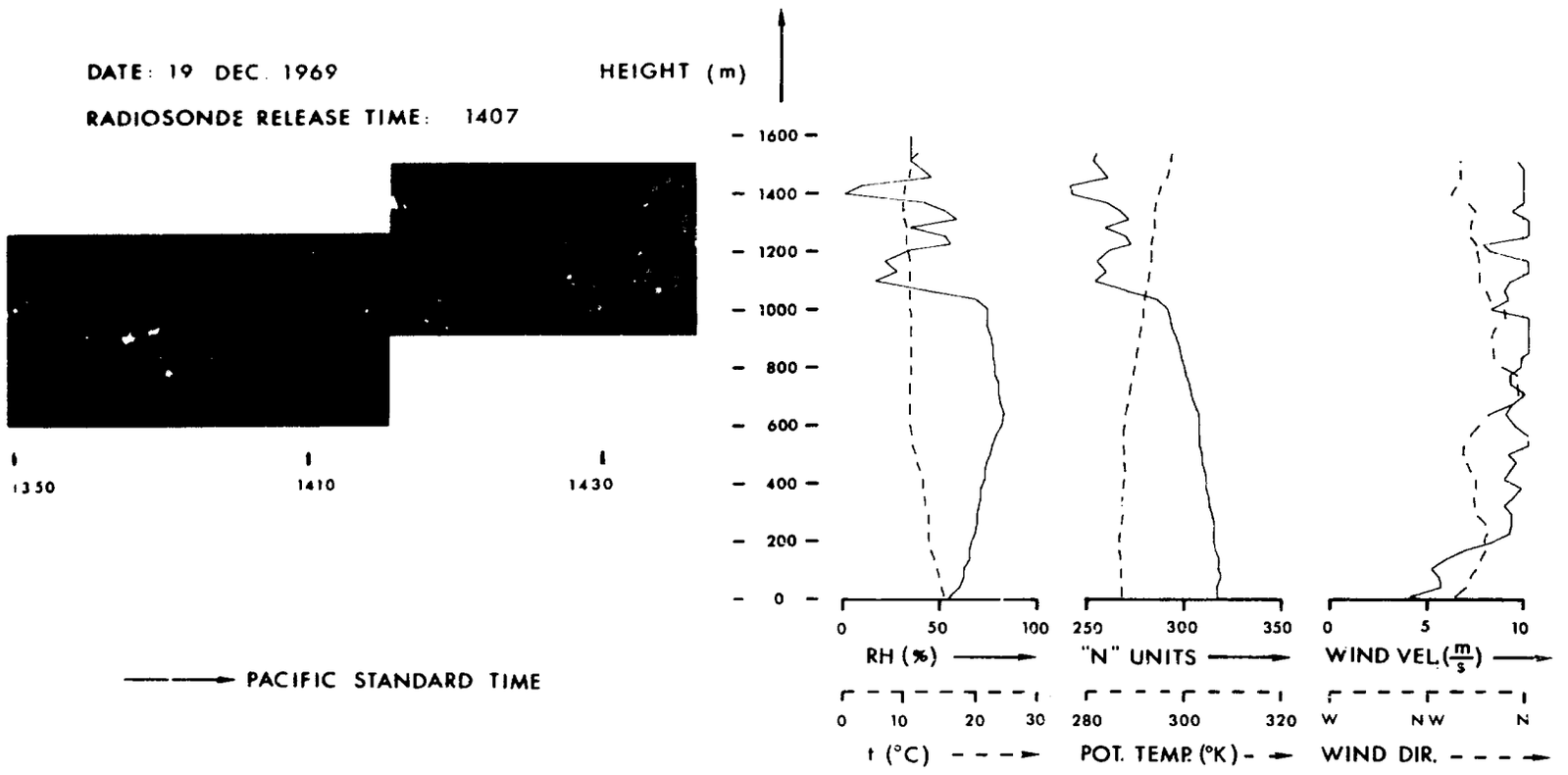

SIMULTANEOUS RADAR AND RADIOSONDE SOUNDINGS

LOCATION: 32°42′ N. LAT., 117° 15′ W. LONG., 31 m ABOVE MSL.

R

DATE: 23 DEC. 1969

RADIOSONDE RELEASE TIME: 1152

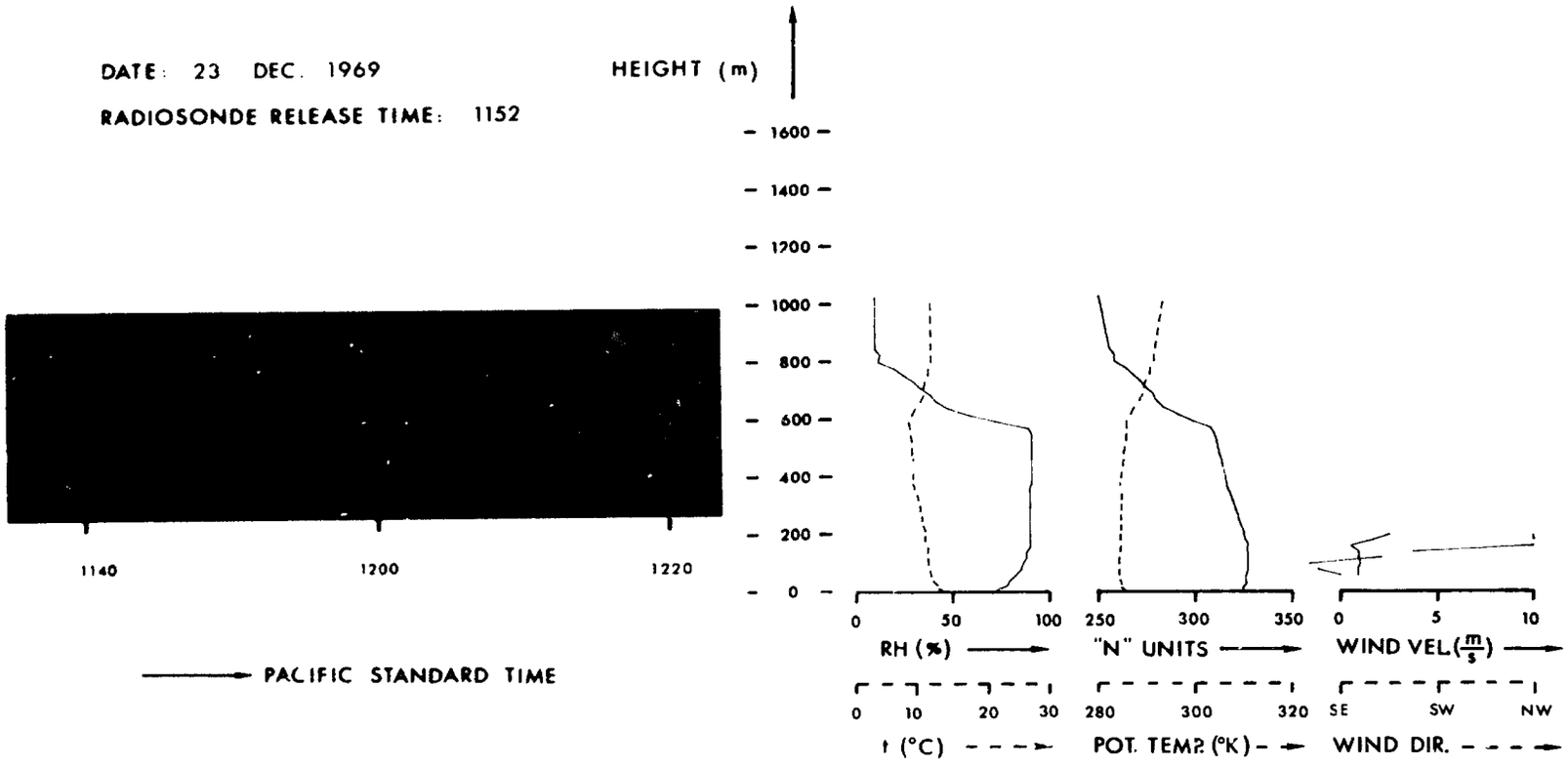

SIMULTANEOUS RADAR AND RADIOSONDE SOUNDINGS

LOCATION: 32°42′ N. LAT., 117° 15′ W. LONG., 31 m ABOVE MSL.

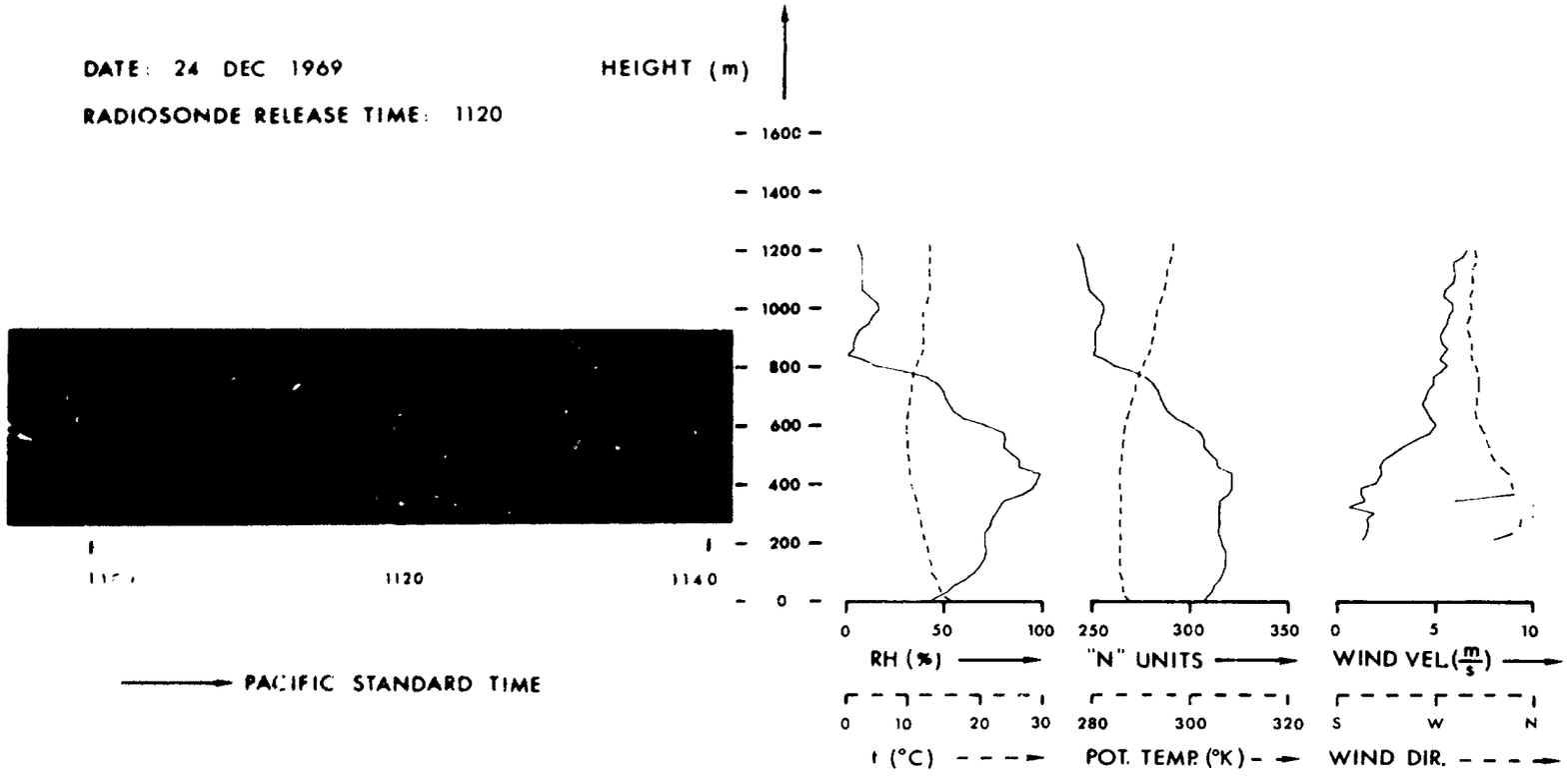

SIMULTANEOUS RADAR AND RADIOSONDE SOUNDINGS LOCATION: 32°42' N. LAT., 117° 15' W. LONG., 31 m ABOVE MSL.

DATE 29 DEC 1969

RADIOSONDE RELEASE TIME: 1130

1133 1155 1210

PACIFIC STANDARD TIME

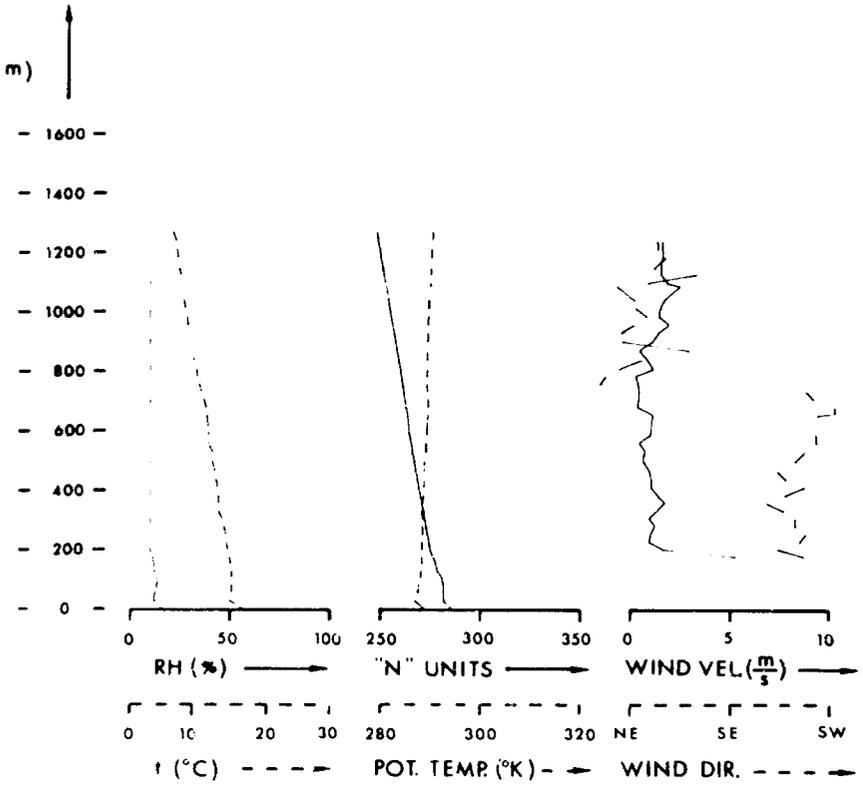

SIMULTANEOUS RADAR AND RADIOSONDE SOUNDINGS

LOCATION: 32°42' N. LAT., 117° 15' W. LONG., 31 m ABOVE MSL.

DATE 22 JAN 1970

RADIOSONDE RELEASE TIME 1052

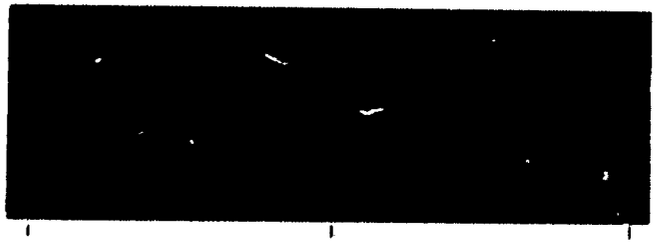

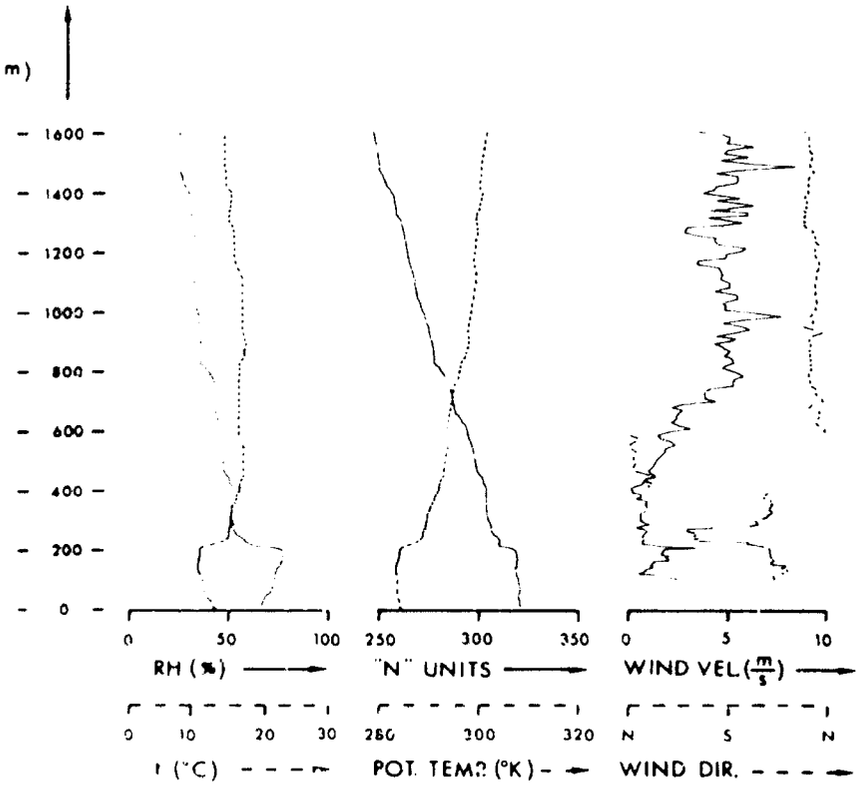

SIMULTANEOUS RADAR AND RADIOSONDE SOUNDINGS

LOCATION: 32°42' N. LAT., 117° 15' W. LONG., 31 m ABOVE MSL

DATE 23 JAN 1970

RADIOSONDE RELEASE TIME 1448

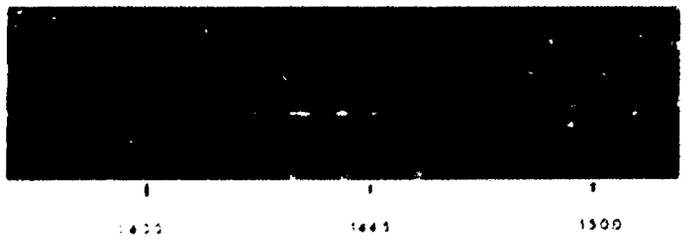

PACIFIC STANDARD TIME

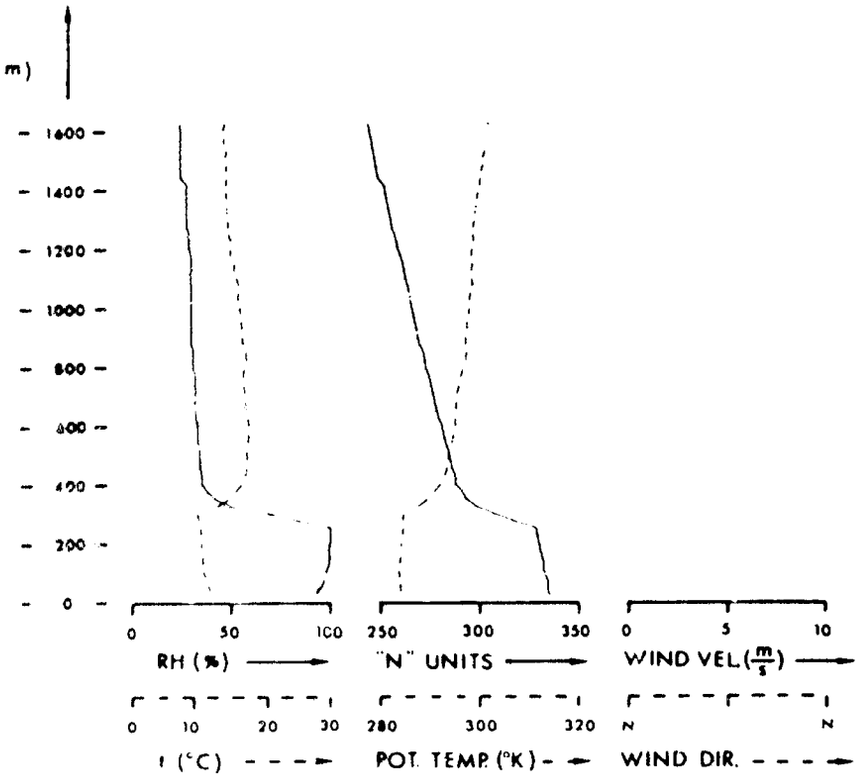

SIMULTANEOUS RADAR AND RADIOSONDE SOUNDINGS

LOCATION: 32°42' N. LAT., 117° 15' W. LONG., 31 m ABOVE MSL.

UNCLASSIFIED
Security Classification

DOCUMENT CONTROL DATA - R & D

(Security classification of title, body of abstract and indexing annotation must be entered when the overall report is classified)

1. ORIGINATING ACTIVITY (Corporate author) Naval Electronics Laboratory Center San Diego, California 92152	2a. REPORT SECURITY CLASSIFICATION UNCLASSIFIED 2b. GROUP

3. REPORT TITLE

LOWER TROPOSPHERIC STRUCTURE AS SEEN BY A HIGH-RESOLUTION RADAR

4. DESCRIPTIVE NOTES (Type of report and inclusive dates)
Research and Development January through December 1969

5. AUTHOR(S) (First name, middle initial, last name)
J. H. Richter and E. E. Gossard

6. REPORT DATE	7a. TOTAL NO. OF PAGES	7b. NO. OF REFS
26 June 1970	68	13

8a. CONTRACT OR GRANT NO	9a. ORIGINATOR'S REPORT NUMBER(S) 1718
b. PROJECT NO. XR 008 01 01, Task 7031 (NELC M103)	
c.	9b. OTHER REPORT NO(S) (Any other numbers that may be assigned this report)
d.	

10. DISTRIBUTION STATEMENT
This document is subject to special export controls and each transmittal to foreign governments or foreign nationals may be made only with prior approval of NELC.

11. SUPPLEMENTARY NOTES	12. SPONSORING MILITARY ACTIVITY
	Naval Electronic Systems Command

13. ABSTRACT

A radar sounder for the study of the refractive index structure in the troposphere is described. The specially built, high-sensitivity FM/cw radar has maximum range resolution of 1 meter. Design considerations and performance characteristics are given, and recordings obtained with the sounder are presented and discussed. Various meteorological measurements supporting the sounder data also are described. The emphasis of this report is on presentation of a wide cross section of data including various layer structures, dot echoes, precipitation, and wave motions. A large number of simultaneous radar and radiosonde soundings are described.

DD FORM 1 NOV 65 1473 (PAGE 1)
S/N 0101-807-6801

UNCLASSIFIED
Security Classification

14 KEY WORDS	LINK A		LINK B		LINK C	
	ROLE	WT	ROLE	WT	ROLE	WT
High resolution radar						
Refractivity						
Troposphere						
Tropospheric propagation						